SYNTHESIS, CHARACTERIZATION AND ANTIMICROBIAL PROPERTIES OF HETEROCYCLIC N, N'- BIDENTATE LIGANDS AND THEIR TRANSITION METAL (II) COMPLEXES

KEVIN NYARANGO OTAO

A Thesis Submitted to the Graduate School in Partial Fulfillment of the Requirements for Award of the Degree of Master of Science in Chemistry of Chuka University

CHUKA UNIVERSITY

OCTOBER, 2024

DECLARATION AND RECOMMENDATION

Declaration

This thesis is my original work and has not been previously *submitted for the award of a* diploma or conferment of a degree in any other institution.

Signature ..... Date ...12/10/2024

Kevin Nyarango Otao

SM11/63281/23

Recommendation

This thesis has been submitted for examination with our approval as the University supervisors.

Signature..... Date ...14/10/24.....

Prof. Joel Mwangi Gichumbi

Chuka University

Signature ..... Date...14/10/24.....

Prof. Eric Chomba Njagi

Chuka University

COPYRIGHT

© Chuka University @ 2024

All rights reserved. No part of this thesis may be reproduced, stored in a retrieval system or transmitted in any form or by any means, electronic, mechanical, photocopying, recording, or otherwise, without the prior permission in writing from the copyright owner or Chuka University.

DEDICATION

This research work is dedicated to my parents, Ronald and Ebisibah, my lovely wife Dianah and our son, Adrian, for love and patience during my studies. Thank you for everything.

ACKNOWLEDGEMENT

I am deeply grateful to the Almighty for the gift of life, mercy, and grace that made it possible for me to start and complete this MSc. program. I extend my heartfelt thanks to my supervisors, Prof. Joel Gichumbi and Prof. Eric Njagi, for their exceptional guidance, knowledge, and valuable insights throughout this research. Your simplicity, encouragement, and steadfast support have been truly appreciated.

I would also like to thank the laboratory technicians, Mr. Erick, Mr. Chrispin, and Madam Juliet, for their steadfast assistance in the lab. My gratitude extends to Mr. Mutembei from the Animal Science Department for his tireless help with the antibacterial tests. May you all be abundantly blessed.

To my fellow postgraduate students, I am grateful for the shared knowledge, countless hours spent in the lab, and the enjoyment we experienced together. Special thanks also go to the academic and non-academic staff members of the Department of Physical Sciences for their contributions to this MSc. program.

Finally, I want to express my deepest appreciation to my family—my parents, my wonderful wife, my son, my brother, my sisters—and everyone who encouraged, counseled, and supported me financially throughout this research and study. Thank you all so much.

ABSTRACT

Antimicrobial resistance has been named one of the greatest global threats to the health sector as many microbes are no longer susceptible to the drugs known to kill them, making diseases harder to treat or prevent. Efforts to develop new antibacterial agents with novel mechanisms of action, higher activity, and improved selectivity are crucial to address and counter antibiotic resistance. This study aimed at synthesizing and characterizing N, N'-bidentate ligands together with their copper and zinc complexes. The reaction of equimolar quantities of the selected hydrazinyl pyridazines with a diketone resulted in the formation of the expected pyrazolylpyridazines. The transition metal (II) complexes were obtained by the reaction of the metal chlorides with the synthesized ligands in the ratio 1:2. The synthesized ligands and the complexes were characterized using the melting point determination, molar conductivity measurements, FT-IR spectroscopy, UV-VIS spectroscopy, and ^{1}H-NMR spectroscopy. The ligands melted at lower temperatures compared to the complexes (72, 141 and 148 °C for L1, L2 and L3 respectively). It was observed that the complexes decomposed in the range of 268-320 °C and that decomposition temperature was dependent on the increase in the molecular weights of the complexes. Conductivity measurements revealed that all the compounds are non-electrolytes with their conductivities in the range 8 - 20 Ω^{-1} cm^2mol^{-1}. The spectral data revealed the presence of N, N'-donor groups in the aromatic rings due to the presence of –C=N- vibration bands at 1653cm^{-1}, 1660 cm^{-1} and 1624 $cm^{-1}$for L1, L2 and L3 respectively. Upon complexation, the bands shift to lower frequencies (1641, 1625 and 1598 cm^{-1} for zinc complexes of L1, L2 and L3 respectively, suggesting coordination through the N, N'-donor groups. An octahedral geometry of the complexes was proposed based on the presence of absorption bands in the wavelength range of 238 – 456 nm in the electronic spectra of the compounds. The ^{1}H NMR revealed the presence of –C=N- with resonance peaks at = 8.2, 8.1 and 7.8 ppm for L1, L2 and L3 respectively. Upon complexation, these peaks shift downfield (8.44, 8.57 and 7.89 ppm respectively) indicating that coordination to the metal is exclusively through the N, N' donor atoms in the ligands. Thereafter, the antimicrobial properties of the ligands and their corresponding complexes were tested using the disc diffusion method against the gram positive and gram negative bacterial strains (*Escherichia coli and staphylococcus aureus*) and the fungal strain (*candida albicans*). The diameter of inhibition was measured relative to that of the antibacterial standard (ampicillin) and the antifungal standard (fluconazole). Dimethyl sulfoxide was used as the negative control. The ligands L1, L2 and L3 had inhibition zones in the range 11-18 mm. for the complexes, inhibition zones were observed in the range 13-22 mm. The standards gave the highest inhibition zones in the range 22-28 mm. The evaluation results revealed that the transition metal (II) complexes exhibited higher antimicrobial activity than the free N, N'-donor bidentate ligands against the same bacterial strain. The increased activity of the complexes might be due to partial sharing of the positive charge of metal ion with the donor groups of the N, N'-donor bidentate ligand that increases the liposolubility of the complex across the microbial cell membrane. Based on the promising evaluation results, complexes in particular ZnL3 and CuL3 are recommended as lead compounds in the development of novel antimicrobials.

TABLE OF CONTENTS

DECLARATION AND RECOMMENDATION ..... **ii**
COPYRIGHT ..... **iii**
DEDICATION ..... **iv**
ACKNOWLEDGEMENT ..... **v**
ABSTRACT ..... **vi**
TABLE OF CONTENTS ..... **vii**
LIST OF TABLES ..... **x**
LIST OF FIGURES ..... **xi**
ACRONYMS ..... **xiii**
CHAPTER ONE: INTRODUCTION **1**
1.1 Background Information 1
1.2 Statement of the Problem 5
1.3 Objectives 5
1.3.1 General Objective 5
1.3.2 Specific Objectives 5
1.4 Research Questions 5
CHAPTER TWO: LITERATURE REVIEW **7**
2.1 The Rise of Antimicrobial Resistance from Different Pathogens 7
2.1.1 Drugs facing significant resistance from microbes 7
2.1.2 Most resistant microbial pathogens 8
2.1.3 Mode of resistance from microbes 10
2.1.4 Mode of action of some reported metal complexes 12
2.1.5 Pyridazine derivatives as N, N'-bidentate ligands 14
2.2 Synthesis and applications of Heterocyclic Ligands and Their Transition Metal Complexes 15
2.2.1 Synthesis of 3-chloro-6-(1H-pyrazol-1-yl) pyridazine 15
2.2.2 Synthesis of 3-chloro-6-(3, 5-dimethyl-1H-pyrazol-1-yl) pyridazine 16
2.2.3 Synthesis of 2, 2-bipyridine 17

2.2.4 Applications and Biological Significance of Metals and their Organic Complexes 18
2.3 Common Methods of Characterization of Compounds 27
2.3.1 Melting Point Determination 27
2.3.2 Molar Conductivity Measurement 27
2.3.3 Fourier Transform Infrared Spectroscopy (FT-IR) 28
2.3.4 UV-VIS Spectroscopy 30
2.3.5 Nuclear Magnetic Resonance 30
2.3.6 Elemental Analysis 32
2.3.7 Mass Spectrometry 34
2.4 Antimicrobial Susceptibility Testing 36
2.4.1 Preparation and Application of Mueller Hinton Agar Media 36
2.4.2 Application of Mueller Hinton Agar 37
CHAPTER THREE: RESEARCH METHODOLOGY 39
3.1 Study Sites 39
3.2 Materials and Reagents 39
3.3 Synthesis of Heterocyclic Ligands and their Transition Metal Complexes 39
3.3.1 Synthesis of 3-chloro-6-(1H-pyrazol-1-yl) pyridazine 39
3.3.2 Synthesis of 3-chloro-6-(3, 5-dimethyl-1H-pyrazol-1-yl) pyridazine 40
3.3.3 Synthesis of Zinc Complex Derived from 2, 2-Bipyridine 40
3.3.4 Synthesis of Copper Complex Derived from 2, 2-Bipyridine 41
3.3.5 Synthesis of Zinc Complex Derived from 3-chloro-6-(1H-pyrazol-1-yl) pyridazine 42
3.3.6 Synthesis of Copper Complex Derived from 3-chloro-6-(1H-pyrazol-1-yl) pyridazine 42
3.3.7 Synthesis of Copper Complex Derived from 3-chloro-6-(3, 5-dimethyl-1H-pyrazol-1-yl) pyridazine 43
3.3.8 Synthesis of Zinc Complex Derived from 3-chloro-6-(3, 5-dimethyl-1H-pyrazol-1-yl) pyridazine 44
3.4 Characterization of the Synthesized Compounds 44
3.4.1 Melting Point Determination 44

3.4.2 Molar Conductance Measurements 45
3.4.3 FT-IR Spectroscopy 45
3.4.4 UV-VIS Spectroscopy 45
3.4.5 ^{1}H NMR Spectroscopy 46
3.6 Antimicrobial Screening 46
3.6.1 Preparation of Inoculums 46
3.6.2 Preparation of the Test Solution 47
3.6.3 Procedure for Antimicrobial Screening 47
3.6 Data Analysis 47
3.7 Ethical Consideration 47
CHAPTER FOUR: RESULTS AND DISCUSSION 48
4.1 Melting Point Determination 48
4.2 FTIR Spectroscopy Analysis 49
4.3 UV/Vis spectroscopy analysis 52
4.4 ^{1}H-NMR spectroscopy analysis 54
4.5 Molar conductivity measurements 55
4.6 Antimicrobial Activity of Different Synthetic Compounds and their Copper and Zinc Complexes against *C. albicans*, *E. coli*, and *S. aureus* 56
4.7.1 Antimicrobial Activity of Compound L1 and its Copper and Zinc Complexes 56
4.7.2 Antimicrobial Activity of Compound L2 and its Copper and Zinc Complexes 62
4.7.3 Antimicrobial Activity of Compound L3 and its Copper and Zinc Complexes against *C. albicans*, *E. coli* and *S. aureus* 67
4.7.4 Comparison of Compound Complexes 71
4.7.5 Inhibition of Microorganisms at 1000 µg/ml of Compound ZnL3 75
CHAPTER FIVE: CONCLUSIONS AND RECOMMENDATIONS 77
5.1 Summary 77
5.2 Conclusion 77
5.2 Recommendations of the study 77
REFERENCES 79
APPENDICES 96

LIST OF TABLES

Table 4.1: Melting Points of the Selected Ligands and Their Copper and Zinc Complexes 48

Table 4.2: Selected FT-IR absorption bands (cm^{-1}) of the heterocyclic N, N' donor bidentate ligands and their copper and zinc complexes 49

Table 4.3: Assignment of the observed λ_{max} (nm) of the N, N' donor bidentate ligands and their transition metal (II) complexes 52

Table 4.4: Molar conductivity measurements of the synthesized ligands (L1-L3) and their complexes 56

Table 4.5: Antimicrobial Activity of Compound L1 against *Candida albicans, Escherichia coli,* and *Staphylococcus aureus.* 57

Table 4.6: Antimicrobial Activity of Compound CuL1 against *Candida albicans, Escherichia coli,* and *Staphylococcus aureus.* 58

Table 4.7: Antimicrobial Activity of Compound ZnL1 against *Candida albicans, Escherichia coli,* and *Staphylococcus aureus* 60

Table 4.8: Antimicrobial Activity of L2 against *Candida albicans, Escherichia coli,* and *Staphylococcus aureus* 63

Table 4.9: Bioactivity of Compound ZnL2 against *C. albican, E. coli* and *S. aureus* 64

Table 4.10: Bioactivity of Compound CuL2 against *C. albican, E. coli* and *S. aureus* ... 65

Table 4.11: Antimicrobial activity of Compound L3 against *C. albican, E. coli* and *S. aureus* 68

Table 4.12: Antimicrobial activity of Compound ZnL3 against *C. albican, E. coli and S. aureus* 69

Table 4.13: Antimicrobial activity of Compound CuL3 against *C. albican, E. coli and S. aureus* 69

LIST OF FIGURES

Figure 1: General mechanism for the reaction of hydrazine with carbonyl compounds. ... 2
Figure 2: commonly used antimicrobials with the pyrazole ring (Monteiro *et al.,* 2014).. 4
Figure 3: substitution of a halogenated pyridazine 16
Figure 4: Synthesis of 3-chloro-6-(1H-pyrazol-1-yl) pyridazine..... 16
Figure 5: Synthesis of 3-chloro-6-(1H-pyrazol-1-yl) pyridazine..... 17
Figure 6: Synthesis of 2, 2-bipyridine..... 18
Figure 7: 3-chloro-6-(1H-pyrazol-1-yl) pyridazine complex formation..... 27
Figure 8: Synthesis of 3-chloro-6-(1H-pyrazol-1-yl) pyridazine using 3-chloro-6-hydrazinylpyridazine and malonaldehyde 40
Figure 9: Synthesis of 3-chloro-6-(3, 5-dimethyl-1H-pyrazol-1-yl) pyridazine..... 40
Figure 10: Predicted structure of zinc complex derived from 2,2-bipyridine..... 41
Figure 11: Predicted structure of copper complex derived from 2,2-bipyridine 41
Figure 12: Structure of zinc complex derived from 3-chloro-6-(1H-pyrazol-1-yl) pyridazine..... 42
Figure 13: Structure of expected copper complex derived from 3-chloro-6-(1H-pyrazol-1-yl) pyridazine 43
Figure 14: Predicted structure of copper complex derived from 3-Chloro-6-(3, 5-dimethyl-1H-pyrazol-1-yl) pyridazine..... 43
Figure 15: Predicted structure of zinc complex derived from 3-Chloro-6-(3, 5-dimethyl-1H-pyrazol-1-yl) pyridazine 44
Figure 16: FTIR spectrum of L2 50
Figure 17: FTIR spectrum of CuL2 51
Figure 18: UV/VIS spectrum of L1 53
Figure 19: UV/VIS spectrum of ZnL1..... 53
Figure 20: NMR spectrum of CuL1..... 54
Figure 21: NMR spectrum of ZnL3..... 55
Figure 22: Bioactivity of different complexes compounds against S. aureus..... 72
Figure 23: Bioactivity of different compounds against *E. coli*..... 73
Figure 24: Inhibition of different compounds against microorganisms at 1000 µg/ml of Compound ZnL3..... 74

Figure 25: Inhibition of different compounds against microorganisms at 1000 μg/ml of Compound ZnL3 75

ACRONYMS

^{1}H-NMR	Proton Nuclear Magnetic Resonance
DMSO	Dimethyl Sulfoxide
FT-IR	Fourier Transform Infrared
KEMRI	Kenya Medical Research Institute
MHz	Mega Hertz
MIC	Minimum Inhibitory Concentration
MLCT	Metal-Ligand Charge Transfer
MRSA	Methicillin Resistant *Staphylococcus Aureus*
NACOSTI	National Commission for Science, Technology and Innovation
PPM	Parts Per Million
STEC	Shiga Toxin-Producing *Escherichia Coli*
TMS	Tetra Methyl Silane
UPEC	Uropathogenic *Escherichia Coli*
UTI	Urinary Tract Infection
UV-VIS	Ultraviolet-Visible
WHO	World Health Organization

CHAPTER ONE: INTRODUCTION

1.1 Background Information

Nitrogen-containing heterocyclic compounds have attracted significant attention because they constitute an important class of pharmacologically active molecules that exhibit a broad spectrum of biological activities (Park *et al.,* 2005). N, N-bidentate ligands like 2, 2-bipyridine, 1, 10-phenanthroline and tridentate ligands like terpyridine have been used to synthesize transition and non-transition metal complexes. This is because the ligands provide a soft site for metal coordination. After all, they are very good pi-acceptors (Paira *et al.,* 2007).

When methylene group is incorporated between the rings, the electronic communication between these two heterocyclic is prevented and the complexes of such ligands give rise to significantly different electronic properties (Takfaoui *et al.,* 2014). The design of such ligands is an important factor influencing the stability and molecular geometry of the complexes. Pyrazole is an organic compound with a simple aromatic five-member ring structure comprising three carbon and two nitrogen atoms at adjacent positions. The aromatic nature arises from the four π-electrons and the unshared pair of electrons on the –NH nitrogen that takes part in resonance and completes 6π electrons (Eicher *et al.,* 2013).

Derivatives of pyridine, pyridazine and pyrazole exhibit a broad spectrum of pharmacological and biological activities like antibacterial (Malladi *et al.,* 2012), antifungal (Ouyang *et al.,* 2008), antiviral, anticonvulsant, anticancer, analgesic, anti-inflammatory, antitubercular, cardiovascular, antidepressant and hypoglycaemic agent (Vijesh *et al.,* 2013). Pyrazoles and pyridazines are prepared by the acid-catalyzed addition of hydrazine to a diketone like acetylacetone (Aljamali *et al.,* 2019). The reaction follows the same mechanism as that of nucleophilic attack of the amino group at the carbonyl carbon. The general mechanism is illustrated in Figure 1.

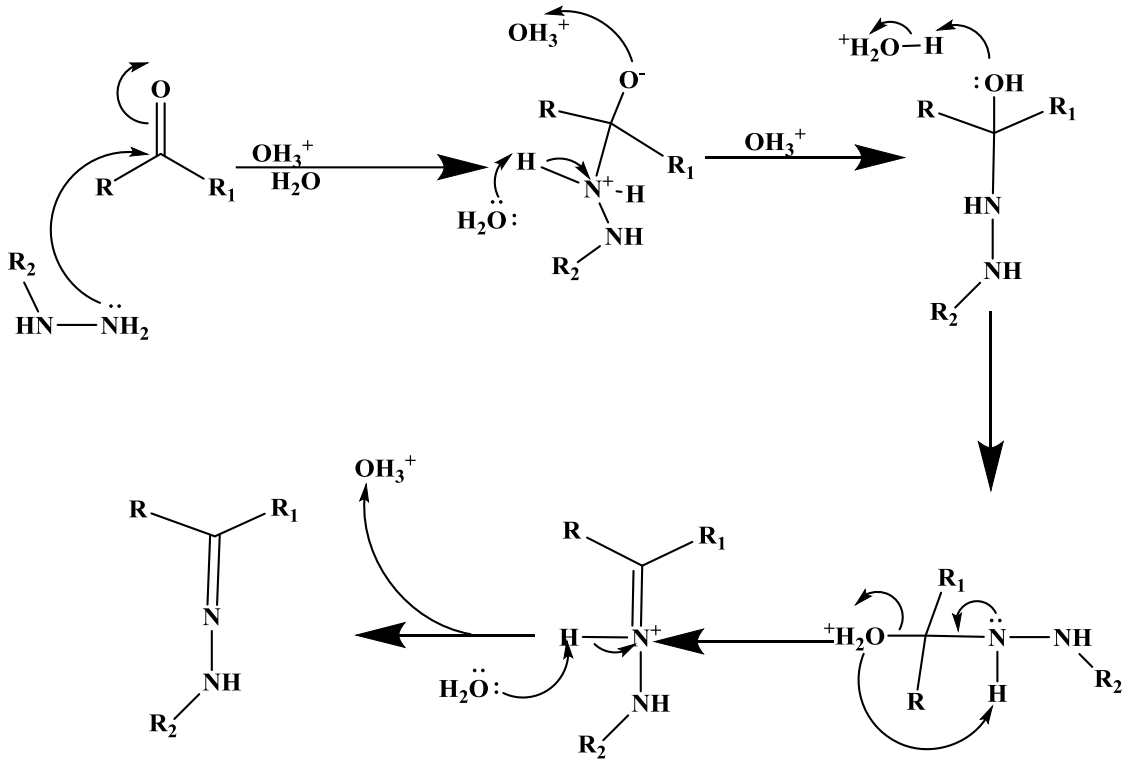

Figure 1: General mechanism for the reaction of hydrazine with carbonyl compounds.

To obtain the pyrazole ring, both amino groups in hydrazine attack the carbonyl carbon atoms of the diketone leading to cyclization to form a five-membered ring. According to Pervaiz and coworkers, the complexation of ligands with metals generally leads to enhanced antibacterial and antifungal effects in comparison with free ligands (Pervaiz *et al.,* 2021; Khalid *et al.,* 2020; Ommenya *et al.,* 2021). Heterocyclic compounds are among the most promising molecules in developing new drugs. Bipyridine, pyrazoles, and pyridazines are readily complexed with several metals that act as bidentate ligands (Safaa *et al.,* 2013). These ligands together with their complexes can be used in the development of antimicrobial agents.

Antimicrobials are medicines used to treat or prevent infections. The decrease in the effectiveness of these antimicrobials has been reported and linked to the rise in antimicrobial resistance (Vicente *et al.,* 2019; Bax *et al.,* 2000; Hu *et al.,* 2019). Antimicrobial resistance arises when pathogens (bacteria, viruses, fungi, and parasites) become resistant, and their response to medicines that they were once susceptible to stops, making treatment and prevention of diseases harder (Bush *et al*., 2011).

Antimicrobial resistance can occur due to overuse of existing drugs (Catalano *et al.*, 2021). Drug-resistant microbes can be found in the soil, air, or water. Antibiotics are often applied in the treatment of livestock and other animals indiscriminately which may lead to the development of resistance. Drugs can kill up to 99.9% of the bacteria or fungus causing the infection. According to Jarvis (2019), there is a possibility that the 0.01% survive due to resistance to the drug used and will later multiply and become dominant or infect other people or the original host. The wide occurrence of antibacterial resistance in bacterial infections has forced humans to develop new and more potent molecules with desired properties that could resolve this resistance (Davis *et al*., 2010). A successful technique is the use of metallodrugs with the potential to treat multidrug-resistant infections more efficiently, due to the synergistic effects coupled from both the ligand and the metal (Dickey *et al*., 2017).

Currently, fluconazole, ketoconazole, miconazole, and clotrimazole (Figure 2) are the most used antifungal drugs in the treatment of many fungal infections like tinea capitis, athlete's foot, ringworm and candida infections (Tonglairoum *et al*., 2014; Trivedi *et al*., 2005; Valerio *et al*., 2013; Vanic & Skalko-Basnet, 2013). The similarity in these drugs is that they all contain the functionalized pyrazole or the pyridine ring in their structures. Their effectiveness has been reported to decrease in recent years due to the suspected resistance of fungal pathogens (Sanguinetti *et al.*, 2005). Clotrimazole has been extensively used in the treatment of fungal infections (Weig & Brown, 2007). The drawbacks of this drug are serious side effects and drug resistance from immunocompromised patients (Monteiro *et al.*, 2014). The above preparation comprises some of the antibiotics that have the pyrazole ring includes sulfaphenazole, sulfamethizole and aminophenazone. Aminophenazone is a carbonyl containing analgesic belonging to phenazone having a pyrazole ring. Up until recently, it had been prescribed for many infections as an antipyretic and an anti-inflammatory. Because of the related side effects and microbial resistance the use has declined since it was banned (Caubet *et al.*, 2002).

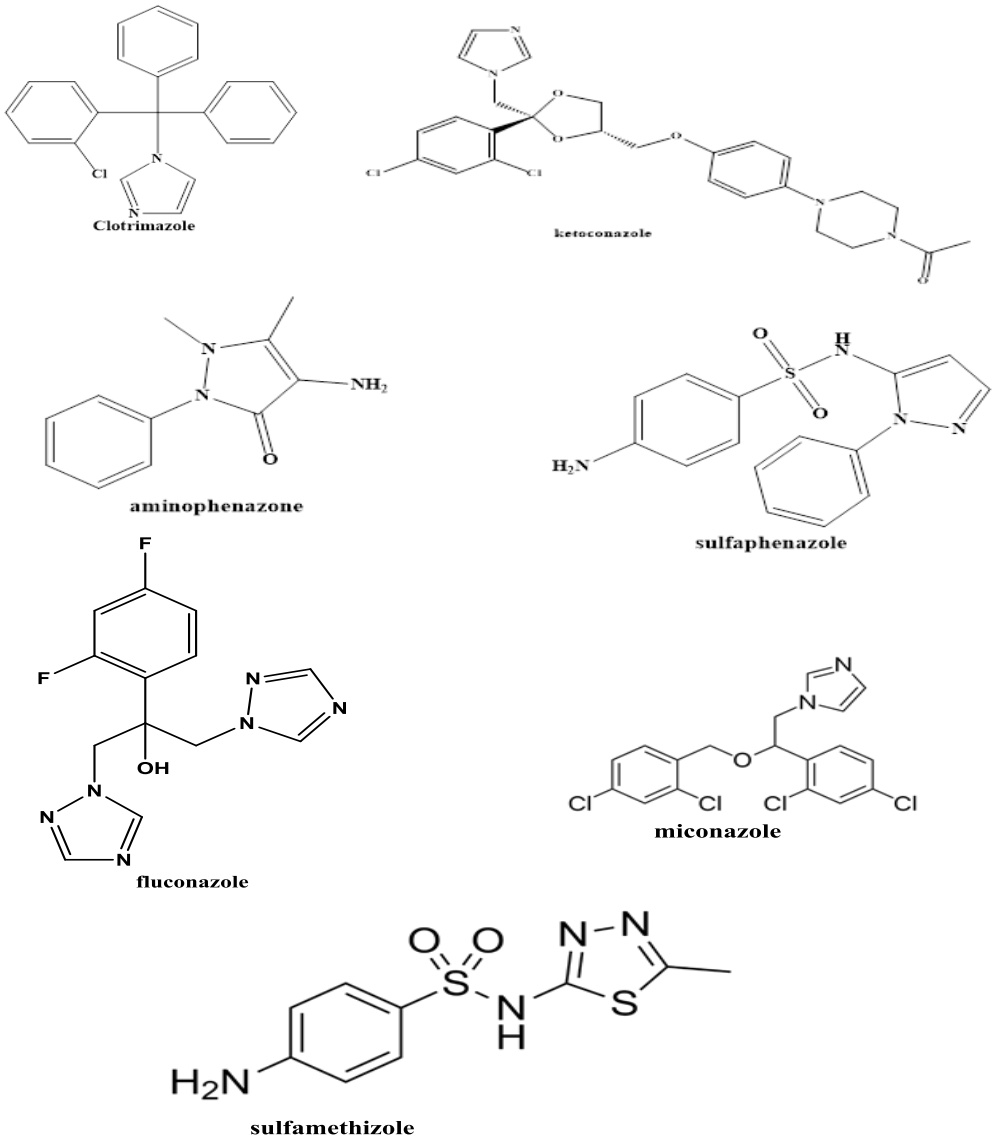

Figure 2: commonly used antimicrobials with the pyrazole ring (Monteiro *et al.,* 2014)

Copper and zinc have shown multifunctional biological activities and thus are essential elements in the development of drugs. Copper complexes have been used for their microbial, neoplastic, and other biological efficacy uses. For instance, protracted copper compounds have been found to possess good efficacy against drug resistant bacteria and exhibit antitumor effects through diverse regulations (Mulani *et al.,* 2019). Like with other trace elements, zinc is credited with participation in many enzymatic reactions together with immune system performance. Organometallic zinc has gained potentiality regarding application in some fields like antiviral treatment and in the management of

neurodegenerative diseases (Tardito *et al.,* 2018; Szewczuk *et al.,* 2017). The utilization of copper and zinc complexes as the drug seekers gives hints about the expansion of new therapeutic approach.

1.2 Statement of the Problem

As the prevalence of antimicrobial resistance increases as reflected in such pathogens as *Escherichia coli, Staphylococcus aureus* and *Candida albicans*, there is need to find new and more effective solutions to deal with microbial threats. The synthesis, determination of structural properties, and evaluation of the antimicrobial properties of heterocyclic ligands and their heteroleptic transition metal complexes present a timely and vital research focus. Understanding the molecular structures and properties of these ligands as well as the effect of the metal ions in relation to lipid membrane permeability and microbial cell survival is essential for advancing our knowledge of their potential applications. This investigation aimed at addressing the urgent challenge of developing novel compounds that can effectively counter the rising resistance exhibited by pathogens.

1.3 Objectives

1.3.1 General Objective

The general objective of this research was to synthesize, characterize and test the antimicrobial activity of N, N' bidentate ligands and their transition metal (II) complexes.

1.3.2 Specific Objectives

i. To synthesize and characterize heterocyclic N, N'- bidentate ligands.
ii. To synthesize and characterize copper and zinc complexes derived from heterocyclic N, N'- bidentate ligands.
iii. To determine the antimicrobial activity of the synthesized heterocyclic N, N'- bidentate ligands and their copper and zinc complexes.

1.4 Research Questions

The research was guided by the following questions:

i. What methods can be used to synthesize and characterize heterocyclic N, N'- bidentate ligands?
ii. What methods can be employed to synthesize and characterize copper and zinc complexes derived from heterocyclic N, N'- bidentate ligands?
iii. Do transition metal (II) complexes derived from the synthesized heterocyclic N, N'- bidentate ligands possess antimicrobial activity?

1.5 Justification of the Research

It is very important to develop new strategies for management of diseases caused by infectious agents due to emergence of drug resistant microbes (Vicente *et al.*, 2019). In 2013 WHO recognized the antimicrobial resistance as the case for health sector that is a challenge to the achievement of the Sustainable Development Goals (SDGs). These resistant microbes claim about 700000 lives in the world and projected to kill 10,000,000 people annually by the year 2050 (Shankar, 2016). They are probably short lived at the present since microbes appear to evolve from time to time making them develop structures that can heg children from the activity of the existing drugs. Consequently, this has promoted the morbidity and mortality rate of the world and increased at a higher degree than before (Bax *et al.*, 2000). Thus, there is a need to design new chemotypes as substitutes for existing organic molecules for the treatment of infections as well as increased mechanisms and structural activities.

Complexes of metal ions have shown mild to good levels of inhibition against microbes, but he potential of metals as antimicrobial agents is far from being realized. Through the proposed research leaning toward the synthesis of antimicrobial complexes, there will be an opportunity to advance new mechanisms in the treatment of diseases by inhibiting microbes' growth and reduce microbial resistance and improve public health outcomes (Hu *et al.*, 2019). N, N bidentate ligands such as pyrazole, pyridine and pyridazine derivatives have gained importance for novel antibacterial agents. These ligands can complex with many transition metals, coordinate with different centers of coordination, and withstand the formation of metal complexes. These compounds can form with metals and can result in complex with potent antibacterial system (Ang *et al.*, 2011).

CHAPTER TWO: LITERATURE REVIEW

2.1 The Rise of Antimicrobial Resistance from Different Pathogens

The problem of antibiotic resistance similarly poses a great threat to the global public health since many productions fail to work against microbiological diseases. Antimicrobial resistance is currently one of the largest threats to global health because it reduces the effectiveness of existing treatments for diseases and hampers the ability to prevent the spread of the diseases. A combination approach is necessary to address the health threat posed by antimicrobial resistance namely the responsible use of antimicrobial drugs the development of new antimicrobial drugs and treatment approaches and development of surveillance and stewardship programs. These are the drugs experiencing high hurdles from microbes and which mechanisms of motorists are being advanced, health care providers and policy makers can jointly stop the effects of antimicrobial resistance and protect people's health.

2.1.1 Drugs facing significant resistance from microbes

The several classes of drugs that are experiencing higher levels of resistance from microbes such as bacteria, fungi, viruses, and parasites are elaborated as follows. Understanding the challenges posed by antimicrobial resistance is crucial for developing strategies to combat this global health crisis (Spellberg *et al.*, 2013).

2.1.1.1 Antibiotics

This work explains that antibiotics used for the last fifty years in treating bacterial infections are falling prey to resistance from pathogenic bacteria. As pointed out by Spellberg and coworkers (2013), bacterial strains such as *Staphylococcus aureus* and *Enterococcus faecium* have developed resistance to antibiotics ranging from beta-lactams to vancomycin making infections hard to control. The abuse of antibiotics in healthcare and especially in livestock production has a led to emergence of resistance mechanisms of bacteria, which require new forms of antimicrobial drugs (Spellberg *et al.,* 2013).

2.1.1.2 Antifungal Drugs

Systemic fungal infections culminating from Candida species and *Aspergillus fumigatus* are increasingly proving difficult to treat due to resistance to antifungal agents. Denning and Bromley, 2015 have pointed out that a new species of multidrug-resistant yeast *Candida auris* which has been identified causes invasive infections with high mortality. The emergence of azole antifungals resistance for instance fluconazole among Candida species is well reported, calling for better antifungal stewardship and new therapeutic options (Denning & Bromley 2015).

2.1.1.3 Antiviral Drugs

Antiviral resistance poses challenges in the management of viral infections, including influenza, HIV, and hepatitis. Hayden and Shindo (2019) report that influenza viruses, particularly influenza A and influenza B, have developed resistance to neuraminidase inhibitors such as oseltamivir and zanamivir, reducing the effectiveness of these drugs in controlling seasonal influenza outbreaks. Additionally, resistance to antiretroviral drugs among HIV strains is a growing concern, underscoring the importance of adherence to treatment regimens and the development of new antiviral agents.

2.1.1.4 Antiparasitic Drugs

Antiparasitic resistance is observed in protozoal and helminthic infections, posing difficulties in treating illnesses such soil-transmitted helminthiasis, leishmaniasis, and malaria. Global attempts to control and eradicate malaria are at risk due to the evolution of resistance to artemisinin-based combination treatments (ACTs) in Southeast Asia's Plasmodium falciparum, the disease's causal agent, according to Keiser and Utzinger (2019). Furthermore, the efficacy of mass deworming efforts in endemic areas is jeopardized by soil-transmitted helminths like Ascaris lumbricoides and Trichuris trichiura developing resistance to anthelmintic medications.

2.1.2 Most resistant microbial pathogens

Among the microbial strains developing noticeable resistance the following among others; Methicillin-Resistant *Staphylococcus aureus* (MRSA), Extended-Spectrum Beta-

Lactamase (ESBL)-Producing Enterobacterales, Carbapenem-Resistant Enterobacterales (CRE) and Vancomycin-Resistant Enterococci (VRE).

2.1.2.1 Methicillin-Resistant Staphylococcus aureus (MRSA)

MRSA is a leading cause of healthcare-associated and community-acquired infections worldwide. This bacterium has acquired resistance to multiple classes of antibiotics, including beta-lactams, through the acquisition of a gene that encodes a modified penicillin-binding protein (PBP2a) with reduced affinity for beta-lactam antibiotics (Tacconelli *et al.,* 2018). MRSA infections are associated with increased morbidity, mortality, and healthcare costs, emphasizing the importance of effective infection control measures and antimicrobial stewardship programs. The gram-positive *staphylococcus aureus* is another major bacterial strain causing several infections including septicemia, pneumonia, food poisoning, and endocarditis. Staphylococcus pneumonia is responsible for deaths of up to 50% of total pneumonia deaths (Hookey & Richardson, 1998).

2.1.2.3 Extended-Spectrum Beta-Lactamase (ESBL)-Producing Enterobacterales

ESBL-producing Enterobacterales, such as *Escherichia coli* and *Klebsiella pneumoniae*, pose a significant threat in healthcare settings due to their ability to hydrolyze extended-spectrum beta-lactam antibiotics, including third-generation cephalosporins and monobactams (Livermore *et al.*, 2021). The gram-negative *Escherichia coli* is a normal inhabitant of the human large intestine. Virulent strains are responsible for urinary tract infections, septicemia, and diarrheal infections. The route of infection is predominantly through contaminated food and water. UPEC often resides in the colon and can be introduced into the urethra. UPEC strains are responsible for more than 70% of reported UTIs. Its growth is associated with blockage of the urinary tract, leading to pools of stagnant urine (Makvana & Krilov, 2015). ESBL genes are often carried on mobile genetic elements, facilitating their dissemination among bacterial populations. Infections caused by ESBL-producing Enterobacterales are associated with higher rates of treatment failure and mortality, highlighting the need for rapid detection methods and alternative treatment options.

2.1.2.3 Carbapenem-Resistant Enterobacterales (CRE)

Carbapenem antibiotics, which are frequently seen as the last resort when dealing with multidrug-resistant bacteria, do not work on CRE, including carbapenem-resistant E. coli and K. pneumoniae. The development of carbapenemase genes, which produce enzymes that can hydrolyze carbapenem antibiotics, is the main cause of carbapenem resistance (Logan & Weinstein, 2017). The high fatality rates and lack of available treatments for CRE infections highlight the urgent need for new antimicrobial drugs and infection control measures.

2.1.2.4 Vancomycin-Resistant Enterococci (VRE)

VRE, particularly *Enterococcus faecium*, has resisted vancomycin, a glycopeptide antibiotic commonly used to treat serious infections caused by gram-positive bacteria. The acquisition of vancomycin resistance genes, results in alterations to the bacterial cell wall, preventing the binding of vancomycin (Arias & Murray, 2012). VRE infections are challenging to treat due to limited therapeutic options and are associated with increased lengths of hospital stay and healthcare costs.

2.1.3 Mode of resistance from microbes

Different microbes resist the action of drugs through various ways. These modes of resistance include genetic mutations, horizontal gene transfer, biofilm formation and efflux pumps. The mode of resistance depends on the structure of the microbe and the nature of the drug.

2.1.3.1 Genetic Mutations

Genetic mutations play a fundamental role in microbial resistance by altering the structure or function of antimicrobial targets, thereby reducing the efficacy of antimicrobial agents. For example, bacteria can acquire mutations in genes encoding target proteins such as penicillin-binding proteins (PBPs) or ribosomal subunits, rendering antibiotics such as beta-lactams or macrolides ineffective (Blair *et al.*, 2015). Similarly, mutations in viral genes encoding viral polymerases or proteases can confer

resistance to antiviral drugs, as observed in influenza viruses and human immunodeficiency virus (HIV) (Sallusto *et al.*, 2019).

2.1.3.2 Horizontal Gene Transfer

Horizontal gene transfer (HGT) is a key mechanism by which microorganisms acquire resistance genes from other organisms, including bacteria, fungi, and viruses. HGT can occur through processes such as conjugation, transformation, and transduction, allowing bacteria to acquire resistance determinants, such as plasmids, integrons, or transposons, from their environment or neighboring bacteria (Frost *et al.*, 2005). This dissemination of resistance genes contributes to the rapid spread of antimicrobial resistance within microbial populations and across different species.

2.1.3.3 Biofilm Formation

Biofilms, complex microbial communities encased in a self-produced matrix of extracellular polymeric substances (EPS), provide a protective environment for microorganisms to resist antimicrobial agents and host immune defenses. The EPS matrix acts as a physical barrier that prevents antimicrobial agents from reaching their target cells, while also facilitating the exchange of genetic material through HGT (Hall-Stoodley *et al.*, 2004). Moreover, biofilm-associated microorganisms often exhibit altered metabolic states and reduced growth rates, further enhancing their resistance to antimicrobial agents.

2.1.3.4 Efflux Pumps

Efflux pumps are specialized transport proteins found in the cell membranes of bacteria, fungi, and other microorganisms, which actively pump antimicrobial agents out of the cell, thereby reducing intracellular drug concentrations and conferring resistance. These efflux pumps can be constitutively expressed or upregulated in response to antimicrobial exposure, allowing microorganisms to expel a wide range of antimicrobial agents, including antibiotics, antifungals, and antiseptics (Fernandez & Hancock, 2012). Efflux pump-mediated resistance is a significant contributor to multidrug resistance in many clinically relevant pathogens.

2.1.4 Mode of action of some reported metal complexes

Heterocyclic compounds and their metal complexes have demonstrated potential in the fight against the escalation of antibiotic resistance. The ability of metal complexes to covalently bind to biomolecules (such as the formation of a DNA adduct with cisplatin), the inhibition of important enzymes through substrate/metal ion mimicry, redox-active or catalytically active drugs (such as metals that produce reactive oxygen species (ROS)), or photoactivatable metal complexes (such as for photodynamic therapy (PDT)) are examples of metal-specific modes of action (Boros *et al*., 2020).

Many research teams have investigated metal complexes and their potential as new antibacterial agents in recent years. Fewer instances have been shown to be able to inhibit Gram-negative bacteria, but a wide range of compounds have been reported to be active against Gram-positive bacteria, particularly against Staphylococcus aureus (S. aureus) and the clinically relevant methicillin-resistant S. aureus (MRSA) strain. Morphological factors are one cause of this imbalance. While Gram-negative bacteria have a peptidoglycan layer encased between two membranes, Gram-positive bacteria have both a single-cell membrane and a peptidoglycan layer. This indicates that an antibacterial agent usually has an easier time entering Gram-positive bacteria. Ude *et al*. created compounds with copper (II) in conjunction with phenanthroline or phenazine and the clinically authorized antibiotic ciprofloxacin (Ude *et al.,* 2019).

When compared to ciprofloxacin alone, to which MRSA is extremely resistant, the complexes showed good effectiveness against MRSA. Although the authors state that ciprofloxacin has a 95% minimum inhibitory concentration of 125 μM against MRSA, their compounds have MIC values ranging from 16 to 32 μM (Murray *et al.,* 2022). Antibiotic coordination with a metal center may therefore offer a fresh strategy to fight antibiotic resistance. There have been several gold (I) and gold (III) compounds claimed to exhibit anti-MRSA and anti-Bacillus subtilis (B. subtilis) properties (Büssing *et al.*, 2019). Büs sing *et al.* found that the N-heterocyclic carbene (NHC) complexes of gold (I) and gold (III) effectively inhibit bacterial thioredoxin reductase (TrxR), with half-maximal inhibitory concentrations (IC50) ranging from 0.18 to 0.55 μM. TrxR, a

disulphide reductase, is essential for maintaining intracellular redox homeostasis (Ude *et al*., 2019).

According to Büssing *et al.* (2019), inhibition may result in oxidative damage and, eventually, cell death. Numerous rhenium (I) di- and tricarbonyl compounds and their anti-MRSA properties have been investigated by the Zobi group. They identified the positive charge of the rhenium complexes as a crucial feature for antibacterial activity. Only cationic compounds exhibited any activity against MRSA (MICs from 0.8 to 25 μM), while overall neutral complexes remained mostly inactive (MICs > 50 μM) (Sovari *et al.,* 2020). They determined that a key component of the rhenium compounds' antibacterial action is their positive charge. Neutral complexes remained generally inert (MICs > 50 μM), while only cationic compounds showed any efficacy against MRSA (Sovari *et al.,* 2020). Cooper *et al.* looked at another class of rhenium compounds. A number of bis(diphosphine)–rhenium(V)–dioxo complexes were found to have low toxicity to human cells and strong activity (MIC ≤ 0.25 μg mL-1) against MRSA (Cooper *et al.,* 2022).

Wang, Chun Yan, and their colleagues discovered that ruthenium (II) polypyridyl complexes are strong anti-S. aureus agents (MICs ranging from 1.3 to 5.6 μM). Their mode of action investigation showed that they effectively inhibited the growth of bacteria and quickly killed them by disrupting their membranes (Wang *et al.,* 2022; ChunYan *et al.,* 2022). The piano-stool structure is a motif frequently found in bioactive metal complexes. According to DuChane *et al.* (2019), ruthenium (II) and iridium (III) piano-stool complexes are effective against Gram-positive bacteria. DNA was shown to be a possible target for Navale *et al*.'s ruthenium (II) complexes after conducting mechanistic studies. Given that cationic compounds have a strong interaction with the negatively charged phosphate backbone, they emphasized the positive charge of their compounds as a crucial component in DNA binding (Navale *et al.,* 2022).

Busto *et al.* (2022) studied polypyridyl complexes of iridium (III) and discovered that they were active against MRSA (MICs ranging from 0.6 to 40 μM). Additional tests showed that when the biological reductant glutathione was present, their complexes could break DNA in a concentration-dependent manner. Accordingly, ROS-induced oxidative

cell damage was suggested as a possible mechanism of action (Busto *et al.,* 2022). Platinum (II) cyclooctadiene complexes were found to be active against several S. aureus strains, including MRSA, by Frei *et al*. Remarkably, no cytotoxicity against human cells was noted, even though their complexes shared structural similarities with cisplatin (Frei *et al.,* 2021).

Bernier *et al.* discovered a number of rhodium (III) and iridium (III) piano-stool compounds with strong anti-Mycobacterium smegmatis (M. smegmatis) properties. These complexes included alkylated cyclopentadienyl (Cp*) and NHC ligands. By making the Cp* and NHC ligands more hydrophobic, the activity of the overall neutrally charged complexes was increased (Bernier *et al.,* 2021). There are even fewer publications on metal compounds that have anti-gram-negative bacterial action. Thomas and colleagues' investigation of a dinuclear ruthenium (II) polypyridyl complex revealed that it was effective against Pseudomonas aeruginosa (P. aeruginosa) and Acinetobacter baumannii (A. baumannii) (MICs ranging from 0.5 to 9.6 μM). The complex's inherent emissive qualities make it suitable for application as a theranostic agent, enabling real-time infection monitoring (Smitten *et al.,* 2023).

2.1.5 Pyridazine derivatives as N, N’-bidentate ligands

N, N’-bidentate ligands are a class of compounds that coordinate to metal centers through two nitrogen atoms. These ligands are integral to the development of coordination chemistry due to their ability to stabilize various metal ions and influence the properties of metal complexes. Among these, pyridazines, a six-membered ring containing two adjacent nitrogen atoms, have garnered particular interest. N, N’-bidentate ligands can form stable chelates with metal ions, leading to enhanced catalytic activity and stability. They are widely utilized in the formation of coordination compounds, which are crucial in catalysis, materials science, and pharmaceuticals (Hadjikakou & Hadjiliadis, 2009). The electronic properties and spatial arrangement of these ligands enable fine-tuning of the metal center's characteristics, making them versatile in various applications.

Pyridazines are a subclass of N, N’-bidentate ligands characterized by a diazine ring, where two nitrogen atoms are positioned at the 1, 2-positions of the ring. This structural

arrangement facilitates strong coordination with metal centers, making pyridazines effective in stabilizing high oxidation states and enhancing catalytic properties (Schneider *et al.,* 2012). Pyridazines are particularly notable for their roles in the development of novel catalysts and therapeutic agents. Pyridazine-based ligands have shown significant potential in catalytic processes, including hydrogenation, hydro-amination, and cross-coupling reactions. Their ability to stabilize transition metal complexes and facilitate electron transfer makes them ideal for these applications. For example, palladium complexes with pyridazine ligands have demonstrated high efficiency in cross-coupling reactions (Zhou *et al.,* 2014).

In materials science, pyridazine ligands contribute to the development of metal-organic frameworks (MOFs) and coordination polymers. These materials exhibit unique properties such as high surface area, tunable porosity, and chemical stability, which are beneficial for gas storage, separation, and catalysis (Furukawa *et al.,* 2010). Pyridazine derivatives have also been explored for their biological activity. Their coordination with metal ions can lead to the formation of complexes with antimicrobial, anticancer, and anti-inflammatory properties. These biological applications highlight the versatility and importance of pyridazine ligands in medicinal chemistry (Mavrova *et al.,* 2010).

2.2 Synthesis and applications of Heterocyclic Ligands and Their Transition Metal Complexes

Heterocyclic ligands in particular N, N' donor bidentate ligands have a broad spectrum of applications. Transition metal (II) complexes of ligands like 3-chloro-6-(1H-pyrazol-1-yl) pyridazine, 3-chloro-6-(3,5-dimethyl-1H-pyrazol-1-yl) pyridazine,1,10- phenanthroline and 2,2-bipyridine among others can be used in pharmaceutical industry, catalysis and in fluorescence (Mambanda *et al.,* 2022). Their biological properties and methods of synthesis are discussed below.

2.2.1 Synthesis of 3-chloro-6-(1H-pyrazol-1-yl) pyridazine

3-chloro-6-(1H-pyrazol-1-yl) pyridazine is the compound formed when monomeric pyrazole (1H-pyrazole) is attached to 3-chloropyridazine at the *para* position. Between the aromatic rings, the dihedral angle is about 6.25 with the whole molecule assuming an

almost planar geometry. In the crystal, the molecule experiences $\pi - \pi$ interactions between the centroids of the rings (Ather *et al*., 2010a; Mambanda *et al.,* 2022). According to Selvanthan & Woi, (2021), the substitution of a halogenated pyridazine can be achieved by the reaction with 1H-pyrazole in the presence of a base like sodium hydride in an appropriate solvent like acetonitrile as illustrated in Figure 3.

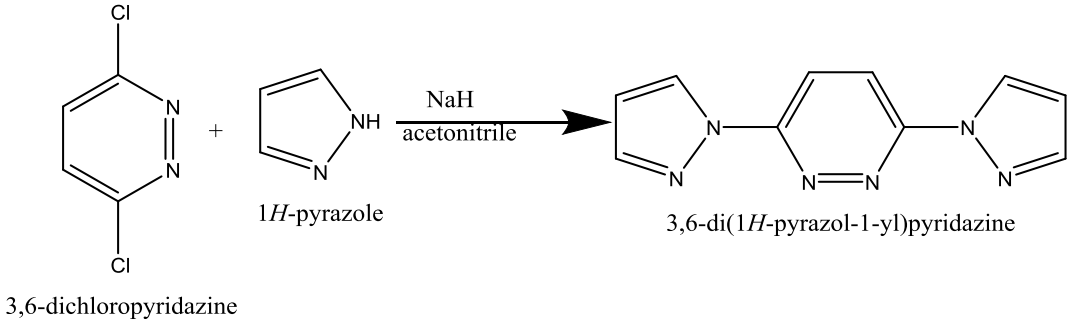

3,6-dichloropyridazine

1*H*-pyrazole

3,6-di(1*H*-pyrazol-1-yl)pyridazine

Figure 3: substitution of a halogenated pyridazine

High yields of 3-chloro-6-(1H-pyrazol-1-yl) pyridazine have been reported when 3-Chloro-6-hydrazinylpyridazine is dissolved in ethanol and acetylacetone in acetic acid added and heated for about a half an hour. The final product can be re-crystallized in ethanol to yield colourless prisms of 3-chloro-6-(1H-pyrazol-1-yl) pyridazine (Ather *et al.*, 2010). The general reaction is illustrated in Figure 4.

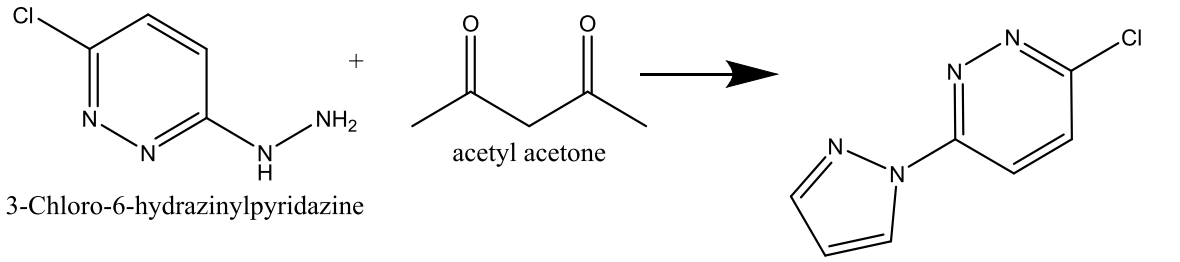

3-Chloro-6-hydrazinylpyridazine

acetyl acetone

3-chloro-6(1H-pyrazol-1-yl)pyridazine

Figure 4: Synthesis of 3-chloro-6-(1H-pyrazol-1-yl) pyridazine

2.2.2 Synthesis of 3-chloro-6-(3, 5-dimethyl-1H-pyrazol-1-yl) pyridazine

Synthesis of 3-chloro-6-(3, 5-dimethyl-1H-pyrazol-1-yl) pyridazine has been recorded by Ather and coworkers, as illustrated in Figure 5. They recorded a yield of 88% by reacting a mixture of equimolar amounts of 3, 6-dichloropyridazine, 3, 5-dimethyl pyrazole and a few drops of hexane-washed sodium hydride. The mixture was stirred in hexane at room

temperature for about one hour. The solvent hexane was removed under reduced pressure, poured on crushed ice. The precipitates formed were filtered, washed with water and purified with column chromatography on aluminium oxide, with benzene as an eluent (Ather *et al*., 2010).

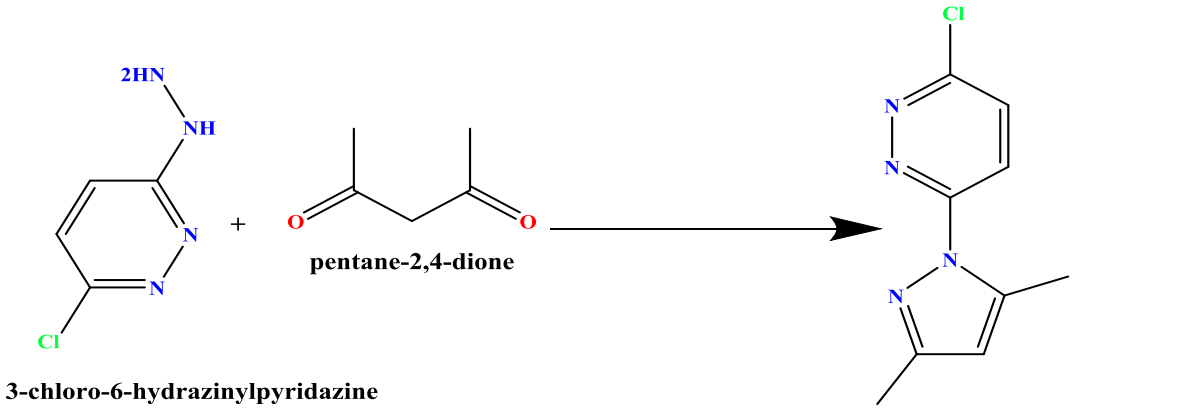

Figure 5: Synthesis of 3-chloro-6-(1H-pyrazol-1-yl) pyridazine

They also prepared the same compound by mixing equimolar amounts of 3-chloro-6-hydrazinylpyridazine, acetylacetone and a few drops of acetic acid. The mixture was stirred and heated at 80-90 ºC for 30 minutes, cooled and diluted with 25 mL of water; the precipitates formed were filtered, washed with water and recrystallized from ethanol.

2.2.3 Synthesis of 2, 2-bipyridine

2, 2'-bipyridine has a wide range of applications in various fields, such as materials science, organic synthesis, and coordination chemistry. It can be prepared by dehydrogenation followed by coupling of pyridine molecules in the presence of Raney nickel as shown in Figure 6 (Ismail *et al.*, 2023). It is grouped under neutral N, N' donor bidentate ligands useful in the study of electron and energy transfer, materials chemistry, antimicrobial activity, and catalysis.

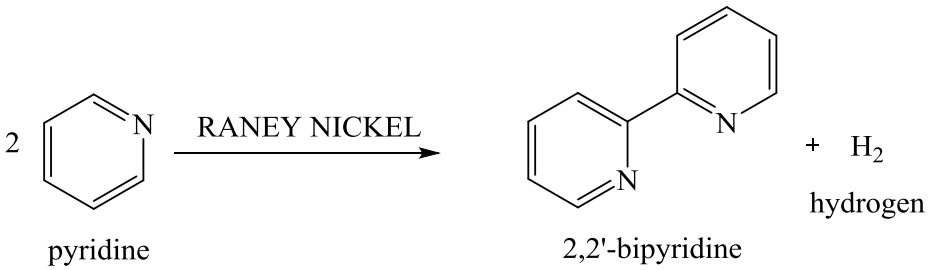

Figure 6: Synthesis of 2, 2-bipyridine

2.2.4 Applications and Biological Significance of Metals and their Organic Complexes

Metals and their organic complexes hold profound significance in biological systems, influencing a myriad of essential processes crucial for life. These elements, often incorporated into organic molecules, serve diverse functions ranging from enzymatic catalysis to structural support, impacting various physiological and biochemical pathways (Arif *et al.*, 2018). One of the most well-known examples is the role of iron in hemoglobin, a metalloprotein responsible for oxygen transport in blood. The coordination of iron within the heme group enables reversible binding of oxygen, facilitating its transport from the lungs to tissues throughout the body. This process is vital for cellular respiration and overall energy production (Bach *et al.*, 2017).

Similarly, zinc serves as a crucial cofactor in numerous enzymes involved in DNA replication, transcription, and repair. Zinc finger motifs, structural elements in proteins, coordinate zinc ions to facilitate interactions with DNA, regulating gene expression. This highlights the integral role of metals in maintaining genomic integrity and cellular function. Copper plays a pivotal role in electron transport chains, serving as a cofactor for various enzymes involved in energy production (Huang, 2016). Additionally, copper is essential for the formation of connective tissues and neurotransmitter synthesis. Its involvement in antioxidant defense mechanisms underscores its importance in maintaining cellular homeostasis (Frederickson, 2005).

Beyond individual metal ions, metalloproteins and metalloenzymes play central roles in biological systems. Examples include cytochrome c, a heme-containing protein crucial in

electron transport, and superoxide dismutase, an enzyme containing manganese or copper and zinc that protects cells from oxidative stress. The catalytic activities of these biomolecules highlight the intricate interplay between metals and biological processes. Understanding the applications and biological significance of metals extends beyond basic biochemistry. In medicine, metal-based drugs, such as platinum-containing anticancer agents, leverage the reactivity of metal complexes for therapeutic purposes (Frederickson, 2005). Additionally, research on metalloproteins contributes to drug development by targeting specific enzymatic pathways.

2.2.4.1 Applications and Biological Significance of Copper

Copper serves as a crucial metal essential for various biological functions in organisms, yet its high concentration can be toxic (Lemire *et al.,* 2013). Microbes contain copper-containing proteins where copper, transitioning between copper (II) and copper (I) ions, functions as an electron donor/acceptor (Kremer *et al.,* 2006). Researchers have explored the coordination of organic molecules with copper to enhance its antimicrobial activity, with mechanisms depending on complex geometry and ligand nature (Borthagaray *et al.,* 2016; Nandanwar & Kim 2019). While the precise antimicrobial mechanism of copper remains unknown, studies suggest that reactive oxygen species (ROS) generated through Fenton-type reactions, and the release of copper ions, can damage DNA and lead to enzyme inactivation, resulting in toxicity (Macomber & Imlay 2009). Evangelinou and colleagues synthesized a tetrahedral mixed-ligand copper (I) bromide complex, exhibiting significantly greater activity against Escherichia coli, Xanthomonas campestris, Bacillus subtilis, and Bacillus cereus compared to ampicillin. This complex disrupted bacterial membranes by generating ROS (Evangelinou *et al.,* 2014).

The antibacterial effectiveness of copper-based complexes often arises from the formation of phthalimide-based copper (II) complexes (Arif *et al.,* 2018). Phthalimide moieties and their derivatives, known for their anticancer, antimicrobial, anti-inflammatory, and antimalarial properties, disrupt DNA, contributing to their efficacy (Saravanan *et al.,* 2017; Pan *et al.,* 2016; Bach *et al.,* 2017; Housman *et al.,* 2003). Copper (II) complexes with sulfonamide ligands can interfere with the biosynthesis of tetrahydrofolic acid, crucial for bacterial metabolism (Kremer *et al.,* 2006; Pervaiz *et al.,*

2020). Notably, copper (II) complexes featuring five-membered heterocyclic ring substituents exhibit superior antimicrobial activity against both Gram-positive and Gram-negative bacteria compared to free sulfonamides (Kremer *et al.,* 2006). While the ionic form of free sulfonamides displays active antibacterial properties, the anionic form has low penetration efficiency across the lipoidal bacterial membrane due to its low lipophilicity. To enhance drug permeation, the complexation of these ligands with metal ions, as suggested by Claudel *et al*. (2020), could increase their lipophilicity.

Copper and its compounds exhibit potent antibacterial properties, known as the oligo-dynamic effect. Copper ions disrupt bacterial cell membranes, inhibit enzymatic activity, and induce oxidative stress, ultimately leading to bacterial cell death (Grass & Rensing, 2001; Cao *et al.,* 2021). Copper-based antimicrobial surfaces and coatings have been developed to prevent microbial colonization and reduce the risk of healthcare-associated infections (Gupta *et al*., 2019; Ramalingam *et al.,* 2020). Emerging evidence suggests that copper possesses antiviral activity against a range of viruses, including human coronaviruses. Copper ions interfere with viral attachment, replication, and maturation processes (Kruk & Duchnowicz, 2019; Li *et al*., 2021). Copper-based materials, such as masks, filters, and touch surfaces, have gained attention for their potential to mitigate viral transmission (Chellan *et al.,* 2018; Chen *et al*., 1993).

The field of copper-based pharmaceuticals is rapidly evolving, with ongoing research focused on exploring novel copper complexes, innovative drug delivery systems, and personalized medicine approaches (Brewer, 2019). Further studies are needed to elucidate the underlying mechanisms of copper's biological activities and optimize its therapeutic potential across various disease areas.

2.2.4.2 Applications and Biological Significance of Zinc

Zinc complexes have gained significant attention in the development of antimicrobial agents due to their potential to combat drug-resistant microorganisms (Huang, 2016). These complexes utilize the antimicrobial properties of zinc ions by incorporating them into various ligand systems. One area where zinc complexes are being explored is in the treatment of bacterial infections. Zinc complexes can enhance the delivery of zinc ions to

target sites, improving their antimicrobial efficacy (Haase & Maret, 2003). Antimicrobial zinc complexes inhibit bacterial enzymes involved in essential metabolic pathways, thereby impairing bacterial growth and survival. Furthermore, zinc complexes can stimulate the host immune system, enhancing the body's natural defense mechanisms against microbial pathogens (Pan, 2021).

Research is also being conducted on the use of zinc complexes in combating fungal infections. Zinc ions have been shown to inhibit the growth of various fungi, including Candida species (Frederickson, 2005). By incorporating zinc ions into complex structures, researchers aim to develop more potent antifungal agents that can overcome drug resistance and improve treatment outcomes. Zinc complexes hold promise in the development of novel antimicrobial agents. Their ability to target bacterial membranes, disrupt essential enzymes, stimulate the immune system, and inhibit microbial replication makes them attractive candidates for combating drug-resistant microorganisms (Milani, 2021). Ongoing research in this field aims to optimize the design and efficacy of zinc complexes for clinical applications in the fight against infectious diseases.

2.2.4.3 Applications and Biological Significance of Ruthenium

One significant application of ruthenium complexes is in cancer therapy. Several studies have demonstrated the cytotoxicity of ruthenium complexes towards cancer cells. For instance, Wang *et al.* (2020) investigated the anticancer activity of ruthenium (II) polypyridyl complexes against various cancer cell lines, including breast cancer and lung cancer. Their findings revealed potent anticancer effects, suggesting the potential of ruthenium complexes as chemotherapy agents (Wang *et al.,* 2020). Moreover, the unique properties of ruthenium complexes, such as their ability to undergo ligand exchange reactions and interact with biomolecules, contribute to their effectiveness in cancer treatment.

In addition to cancer therapy, ruthenium complexes have shown promise in photodynamic therapy (PDT). PDT is a non-invasive treatment approach that involves the administration of photosensitizing agents followed by exposure to light of specific wavelengths, leading to the generation of reactive oxygen species (ROS) and subsequent

cell death. Ruthenium complexes have been explored as photosensitizers in PDT due to their ability to efficiently generate ROS upon light activation. For example, Li and coworkers (2019) developed ruthenium (II) polypyridyl complexes as photosensitizers for PDT applications. Their study demonstrated the potential of ruthenium complexes to induce cytotoxicity in cancer cells upon light irradiation (Li *et al.*, 2019).

Moreover, ruthenium complexes exhibit promising antimicrobial properties, making them potential candidates for combating infectious diseases. Research has shown that certain ruthenium complexes possess antibacterial activity against both Gram-positive and Gram-negative bacteria. For instance, Navale and coworkers (2021) investigated the antimicrobial activity of ruthenium (II) complexes against various bacterial strains. Their findings indicated that ruthenium complexes exhibited significant antibacterial effects, suggesting their potential application as antimicrobial agents (Navale *et al.*, 2021).

Furthermore, ruthenium complexes have been studied for their potential role in bioimaging and diagnostic applications. Due to their unique photophysical properties, such as strong luminescence and long emission lifetimes, ruthenium complexes have been explored as imaging agents for fluorescence microscopy and bioimaging techniques. Additionally, the ability of ruthenium complexes to interact with biomolecules, such as DNA and proteins, makes them suitable candidates for biosensing and diagnostic applications (Wang *et al.*, 2020).

2.2.4.4 Applications and Biological Significance of Silver

One of the primary applications of silver complexes is in antimicrobial therapy. Silver has long been recognized for its antibacterial properties, and silver-containing compounds have been used for centuries as antimicrobial agents. Silver complexes exhibit broad-spectrum antimicrobial activity against both Gram-positive and Gram-negative bacteria, as well as fungi and viruses. For instance, Smith *et al.* (2020) investigated the antimicrobial activity of silver heterocyclic complexes against a range of pathogens, demonstrating their efficacy in inhibiting bacterial growth (Smith *et al.*, 2020). These complexes have the potential to combat drug-resistant bacteria and contribute to the development of novel antimicrobial agents.

Moreover, silver complexes have shown promise in wound healing and tissue regeneration. Silver ions have been found to promote wound healing by facilitating cell proliferation, migration, and angiogenesis, as well as reducing inflammation and preventing infection. Silver-containing dressings and scaffolds have been developed for the management of chronic wounds, burns, and other traumatic injuries. Research by Jones *et al.* (2019) investigated the use of silver-containing hydrogels for wound healing applications, demonstrating their ability to accelerate wound closure and reduce bacterial burden (Jones *et al.*, 2019). Silver complexes offer a potential solution for improving wound care and promoting tissue regeneration.

Furthermore, silver complexes have been explored for their potential use in diagnostic imaging and theranostic applications. Silver nanoparticles and nanocomposites have unique optical and photothermal properties that make them suitable for imaging and therapeutic purposes. These complexes can be functionalized with targeting ligands or imaging agents for specific molecular targeting and visualization. Research by Lee *et al*. (2021) demonstrated the use of silver nanocomposites for both diagnostic imaging and photothermal therapy of cancer (Lee *et al.*, 2021). Silver complexes hold promise as multifunctional agents for cancer diagnosis, treatment, and monitoring.

2.2.4.5 Applications and Biological Significance of Platinum

One of the most well-known applications of platinum complexes is in cancer chemotherapy. Platinum-based drugs, including cisplatin, carboplatin, and oxaliplatin, are widely used in the treatment of various cancers, such as ovarian, testicular, and lung cancers. These complexes exert their anticancer effects by forming DNA adducts, which interfere with DNA replication and transcription, ultimately leading to cell death. For instance, Frei and coworkers (2021) reported platinum complexes derived from cyclooctadiene with activity against gram-positive bacteria, highlighting their potential as therapeutic agents (Frei *et al.*, 2021).

Moreover, platinum complexes have shown promise in antimicrobial therapy. While primarily recognized for their anticancer properties, recent studies have demonstrated the antibacterial activity of platinum complexes against both Gram-positive and Gram-

negative bacteria. For example, Busto *et al*. (2022) investigated inert cationic iridium (III) complexes with phenanthroline-based ligands and their application in antimicrobial inactivation of multidrug-resistant bacterial strains (Busto *et al.,* 2022). These findings underscore the potential of platinum complexes as alternative antimicrobial agents.

Furthermore, platinum complexes have been explored for their potential role in antitubercular therapy. Navale *et al.* (2022) conducted studies on DNA binding, antitubercular, antibacterial, and anticancer activities of newly designed piano-stool ruthenium (II) complexes, revealing their potential as therapeutic agents against tuberculosis (Navale *et al.,* 2022). This highlights the versatility of platinum complexes in combating infectious diseases.

2.2.4.6 Antimicrobial properties of 2, 2-bipyridine and its transition metal complexes

2, 2'-bipyridine as a ligand exhibits significant antibacterial activity when tested against Gram-positive (*Micrococcus luteus, Staphylococcus aureus*, and *Bacillus subtilis*) and Gram-negative (*Escherichia coli, Klebsiella pneumoniae,* and *Proteus mirabilis*) bacteria (Ali *et al*., 2016). The presence of the azomethine group in the pyridine ring plays an important role by increasing both lipophilicity and metabolic stability of the compound, thus greater antimicrobial activity. It is reported that chelation of 2, 2-bipyridine with metals may or may not increase the antimicrobial activity. Ali and co-workers compared the zone of inhibition of the free ligand and that of the heteroleptic complex of ibuprofen and 2, 2-bipyridine. The free ligand was a better inhibitor than the complex. However, when it binds with other transition metals like copper, the complexes formed exhibit significant antibacterial activity as reported from the synthesis of copper complex with alanine salicylaldehyde and 2,2-bipyridine (Chandraleka *et al.,* 2011).

According to McCleverty and Meyer (2004), bipyridine forms complexes with many transition metals through both σ-donating nitrogen atoms and π-accepting property of pyridine ligands or by accepting electron density from metal d - orbitals into the π^* molecular orbitals of the pyridine ligands. The complex formation of bipyridine involves bidentate chelation with the two nitrogen atoms. Depending on the reaction conditions, it

forms complexes with both copper and zinc with a coordination number of either 4 or 6 (Nisbet *et al*., 2021). These complexes have been subjected to antimicrobial activity testing and exhibited significant activity through inhibition of the growth of different bacterial strains.

2.2.4.7 Antimicrobial activity of 3, 5-dimethyl-1H-pyrazol-1-yl moieties and its transition metal complexes

Fonseca *et al.,* (2018) reported the synthesis of transition metal complexes containing the dipyrazolylmethane moiety. The complexes were characterized using the physicochemical and spectroscopic methods and tested for their biological activity against the Chagas disease-causing parasite *Trypanosoma cruzi* strains. They compared the activity of Bis (3, 5-dimethyl-1H-pyrazol-1-yl) methane with that of Bis (3, 5-dimethyl-4-nitro-1H-pyrazolyl) methane and found that there was no significant difference indicating that the incorporation of the nitro group does not influence activity. The presence of the methyl groups attached to the pyrazole rings is said to enhance the activity of the compound by increasing the lipophilicity of the compound and the metabolic stability. Transition metals including among others Pt (II), Pd (II), Ru (II), Cu (II), Ni (II), Mn (II), and Co (II) show trypanocidal activity (Prayag, 2023). It was found that the biological activity of the complex was greater than that of the individual ligands. This observation is linked to the synergistic effects (combining the biological properties of both the metal and the ligand) that may lead to dual mechanisms of action (Bello-Vieda *et al.,* 2018; Castillo *et al*., 2016; Biot *et al.,* 2012 and Murcia *et al.,* 2018).

Bushuev *et al*., (2005) synthesized Bis (3, 5-dimethyl-1H-pyrazol-1-yl) methane complex with cobalt (II) iodide. The complex was a heteroleptic compound with one Bis (3, 5-dimethyl-1H-pyrazol-1-yl) methane chelating as a cyclic bidentate ligand and two iodide ions to form a tetrahedral geometry. The complex has $\pi - \pi$ stacking interactions between the pyrazole rings as characterized by electron spectroscopy and x-ray diffraction. However, the complex's antimicrobial activity against gram-positive and gram-negative bacterial strains and antifungals has not been explored exhaustively. Likewise, little work has been done in exploring the coordination chemistry of this ligand with other transition metals like copper and zinc as well as screening the antimicrobial

activity of such complexes despite both the metals and the ligand exhibiting significant activity independently.

2.2.4.8 Antimicrobial activity of 3-chloro-6-(1H-pyrazol-1-yl) pyridazine and its transition metal complexes

Ather *et al*., (2013) describe pyrazolylpyridazines as effective chelating agents. He further describes these compounds as potential antibacterials against gram-positive and gram-negative bacterial strains. From the screening using *staphylococcus aureus*, *Escherichia coli*, and *salmonella typhi*, 3-chloro-6-(1H-pyrazol-1-yl) pyridazine exhibited antibacterial activity about 50% when measured relative to Ciprofloxacin, the internal standard. Other pyrazolylpyridazines exhibited antibacterial and antioxidant properties close to 70% indicating that they have the potential, on further modification, to produce better active products as compared to the control. Such modifications can be achieved by chelation with transition metals like copper, zinc, and cobalt among others that have recorded antimicrobial complexes with N, N-bidentate ligands (Biot *et al.*, 2012). The presence of electron-withdrawing groups like Cl^- directly attached to the aromatic rings may be responsible for their high antibacterial activity as compared to the un-substituted compound. The electron-withdrawing substituents produce localized electron-deficient sites capable of promoting favorable conditions for interaction between the compounds and their target sites (Brown *et al.,* 2015).

Little coordination chemistry of 3-chloro-6-(1H-pyrazol-1-yl) pyridazine has been reported. In the complex formation reported in 2022 by Mambanda and co-workers, 3-chloro-6-(1H-pyrazol-1-yl) pyridazine chelate as a bidentate ligand through the second nitrogen of the pyrazole ring and the second nitrogen of the pyridazine ring to form a five-membered ring with the central metal as shown in Figure 7. The complex, [(η^6-*p*-cymene) (3-chloro-6-(1H-pyrazol-1-yl) pyridazine) Ru(X)] BF_4 formed has geometric distortions also called conformational arrangement of the octahedral η^6-arene-bearing complexes of Ru (II). It is formed by the reaction of 3-chloro-6-(1H-pyrazol-1-yl) pyridazine with (η^6-*p*-cymene) Ru(X) in the ratio 2:1. They liken the conformational arrangement to a 'piano stool' (Mambanda *et al*., 2022; Gichumbi *et al.,* 2018).

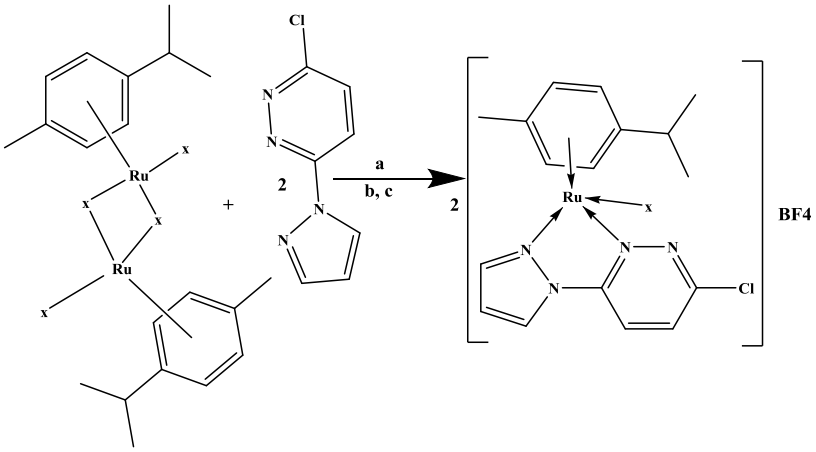

Figure 7: 3-chloro-6-(1H-pyrazol-1-yl) pyridazine complex formation

X- Cl, Br or I a- acetonitrile b- Ethanol c- NH_4BF_4

2.3 Common Methods of Characterization of Compounds

The most commonly used methods of characterizing compounds include the following among others. Melting point determination, measuring of molar conductivity, nuclear magnetic resonance, UV-VIS spectroscopy, atomic absorption spectroscopy, X-ray diffraction, Fourier Transform Infrared, and elemental analysis.

2.3.1 Melting Point Determination

The melting point of a substance is the temperature at which the solid phase exists in equilibrium with the liquid phase. It is at this point that the solid changes to a liquid. The melting point of a substance can be determined by using two common methods which are the Thiele tube method and the Meltemp apparatus (Willard *et al.,* 1988).

2.3.2 Molar Conductivity Measurement

Molar conductivity is a useful parameter for characterizing organic compounds, particularly those that can ionize or dissociate in solution. It provides valuable information about the extent of ionization, the degree of dissociation, and the conductivity of a compound in solution. Molar conductivity measurements can be used to understand the behavior of electrolytes, determine their ionic strengths, and investigate their structure and properties (Atkins & de Paula, 2006). One of the factors to consider is

the solvent used. In most cases, the criterion for solvent selection relies on its dielectric constant, viscosity, specific conductivity, donor capacity, and ease of purification. A solvent with a high dielectric constant and low viscosity is preferred. Therefore, acetonitrile, nitromethane, and methanol are preferred. DMSO and nitrobenzene suffer a big disadvantage from their high viscosity (Deswal *et al.,* 2022). Molar conductivity (Λ) is calculated by dividing the measured conductivity by the concentration of the compound in the solution. It represents the conductivity of a solution containing one mole of the compound.

Molar conductivity measurements allow for the determination of important parameters such as equivalent conductivity, limiting molar conductivity, and ion mobility. It allows for the assessment of the degree of ionization or dissociation, which can provide insights into the compound's acid-base properties, solubility, and reactivity. Molar conductivity can aid in the identification and differentiation of different species in solution. By comparing the measured molar conductivity values with reference data or theoretical calculations, it is possible to determine the composition and structure of complex mixtures or solutions. Molar conductivity measurements can be used to investigate the influence of various factors such as temperature, concentration, and solvent on the conductive behavior of organic compounds. This information can be critical in understanding the stability, behavior, and performance of electrolytes in various applications, including batteries, fuel cells, and electrochemical processes (Atkins & de Paula, 2006).

2.3.3 Fourier Transform Infrared Spectroscopy (FT-IR)

Fourier Transform Infrared Spectroscopy (FTIR) is a powerful analytical tool used in a wide range of scientific fields for characterizing materials by measuring their infrared absorption spectra. Its applications span across chemistry, physics, biology, and material science, enabling the identification of molecular structures, bonding environments, and chemical compositions. In recent years, significant advances have been made in improving both the technique's sensitivity and applicability, especially in diverse domains such as pharmaceuticals, nanomaterials, and environmental monitoring.

FTIR is based on the principle of molecular vibration. When infrared radiation is passed through a sample, specific wavelengths are absorbed by the molecules, leading to vibrational transitions. The absorbed frequencies correspond to the functional groups within the molecules. This interaction generates a unique spectral fingerprint for each compound. FTIR spectra are typically plotted as intensity versus wavelength, which helps in identifying molecular structures and detecting changes in material compositions (Smith, 2011).

Unlike traditional dispersive infrared spectroscopy, FTIR employs an interferometer, which generates an interference pattern from multiple beams of light. This pattern is then mathematically transformed into a spectrum using Fourier Transform algorithms, allowing for faster and more accurate measurements. This method also improves signal-to-noise ratios, making FTIR more sensitive to weak absorptions (Griffiths & de Haseth, 2018).

In recent years, FTIR has seen considerable advancements, especially in terms of instrumentation, sample preparation, and data analysis. Attenuated Total Reflectance (ATR) has emerged as one of the most significant innovations, allowing for easier sample handling and analysis without extensive preparation. ATR-FTIR enables the study of a wide range of sample types, including solids, liquids, and gases, while maintaining high sensitivity (Stuart, 2004). Another key development has been the miniaturization of FTIR instruments, making them more portable and suitable for in-field applications, particularly in environmental and industrial monitoring (Baker *et al.,* 2020).

FTIR has made a notable impact in the field of biological and medical research, particularly in the analysis of proteins, lipids, and nucleic acids. The technique’s ability to provide detailed information on the secondary structures of proteins has been critical in studying diseases related to protein misfolding, such as Alzheimer's and Parkinson's diseases (Jackson & Mantsch, 2010). Furthermore, FTIR microspectroscopy allows for the investigation of tissues and cells at the microscopic level, enabling researchers to detect biochemical changes that precede visible symptoms of diseases, including cancer (Baker *et al.,* 2020).

FTIR has also become an invaluable tool in environmental science. One of its most important applications is in air quality monitoring, where it can be used to detect gases like carbon dioxide, methane, and volatile organic compounds in real-time. The ability to perform rapid, non-destructive analysis makes FTIR an attractive option for tracking environmental pollutants. Portable FTIR spectrometers are increasingly used in situ for soil, water, and air analysis, allowing for immediate identification of contaminants (Huang *et al.*, 2021).

2.3.4 UV-VIS Spectroscopy

UV-visible spectroscopy is a widely used analytical technique that provides valuable information about the electronic transitions and absorbance properties of molecules in the ultraviolet (UV) and visible (VIS) regions of the electromagnetic spectrum. This spectroscopic method has found applications in various fields, including chemistry, biochemistry, pharmaceuticals, environmental analysis, and materials science (Williams & Fleming, 2018). UV-visible spectroscopy relies on the interaction between light and matter. When a sample is subjected to UV or visible light, it absorbs specific wavelengths of light corresponding to electronic transitions of its molecular or atomic components. The remaining transmitted or reflected light is detected and measured by a spectrophotometer, which generates a UV-visible absorption spectrum. UV-visible spectroscopy provides valuable information about the concentration of the sample components, the presence of impurities, and the chemical structure of the molecules. It is widely used for qualitative and quantitative analysis, kinetics studies, stability analysis, and identification of chromophores (Atkins & de Paula, 2006).

2.3.5 Nuclear Magnetic Resonance

NMR spectroscopy is based on the principle that certain atomic nuclei, when placed in a strong magnetic field, absorb and re-emit electromagnetic radiation at specific frequencies. Nuclei such as hydrogen (^{1}H), carbon (^{13}C), and phosphorus (^{31}P) possess a magnetic moment due to their nuclear spin. When subjected to a magnetic field, these nuclei resonate at characteristic frequencies depending on their chemical environment (Cavanagh *et al.*, 2010).

The resonance frequencies are influenced by the local electronic environment of the nuclei, allowing researchers to infer molecular structure and dynamics. By analyzing the chemical shifts, coupling constants, and relaxation times, it is possible to determine the atomic connectivity and spatial arrangement within a molecule (Claridge, 2016).

Over the past few decades, several advancements have transformed NMR spectroscopy, enhancing its sensitivity, resolution, and applicability. One of the key innovations is the development of multi-dimensional NMR techniques, such as two-dimensional (2D) NMR, which enables the detailed study of complex molecules by correlating the signals of different nuclei (Ernst, 2017). This has been particularly useful in analyzing larger biomolecules like proteins and nucleic acids, facilitating the determination of their three-dimensional structures.

Additionally, the advent of cryoprobes has significantly increased the sensitivity of NMR measurements, allowing for the detection of low-concentration samples (Kupče & Freeman, 2007). The use of high-field magnets has also improved resolution, enabling the observation of subtle interactions and providing clearer insights into molecular dynamics.

NMR has become a critical tool in biological research, particularly in structural biology. It is one of the few methods capable of providing detailed structural information about proteins and nucleic acids in solution, which closely resembles their natural biological environment. NMR can also offer insights into protein-ligand interactions, enzyme mechanisms, and conformational changes (Palmer, 2014).

One notable advancement is the development of solid-state NMR, which has expanded the technique's use beyond solutions to study membrane proteins, amyloid fibrils, and other insoluble biological materials. Solid-state NMR has been crucial in investigating the structures of proteins that are difficult to study using traditional methods like X-ray crystallography, particularly in their native lipid environments (Baldus & Günther, 2012).

In drug discovery, NMR plays an important role in screening for lead compounds and understanding drug-receptor interactions. Techniques like ligand-based NMR and structure-based NMR provide insights into the binding affinities and kinetics of small

molecules with target proteins, making NMR invaluable in the early stages of drug design (Shuker *et al.,* 2010). Additionally, NMR is widely used for the quality control of pharmaceuticals, enabling the identification of active ingredients, impurities, and degradation products.

NMR has also found applications in materials science, particularly in the study of polymers, nanomaterials, and catalysts. The technique allows for the characterization of molecular mobility, phase transitions, and the local structure of materials (Eckert, 2019). Magic angle spinning (MAS) NMR, in particular, has been used to study solid materials, providing high-resolution spectra and allowing for detailed structural analysis of heterogeneous systems.

2.3.6 Elemental Analysis

Elemental analysis refers to a group of techniques used to determine the quantities of individual elements within a sample. The two most common methods are qualitative and quantitative analysis. Qualitative analysis identifies the elements present in a sample, while quantitative analysis determines the concentration of each element. Methods such as combustion analysis for organic compounds, inductively coupled plasma (ICP) techniques, and X-ray fluorescence (XRF) are widely used for analyzing both organic and inorganic materials (Huffman, 2011).

Combustion analysis, also known as CHNS/O analysis, is used to determine the carbon, hydrogen, nitrogen, sulfur, and oxygen content in organic compounds. During this process, a sample is burned in an oxygen-rich environment, and the resulting combustion products (CO_2 , H_2 O, NO_2 and SO_2) are quantified to infer the sample's elemental composition. This technique has been invaluable in organic and pharmaceutical chemistry (Vogel *et al.,* 2010).

In contrast, ICP techniques, including ICP-Optical Emission Spectroscopy (ICP-OES) and ICP-Mass Spectrometry (ICP-MS), are widely employed for the detection and quantification of trace elements in complex samples. In these methods, a sample is ionized using an inductively coupled plasma source, and the emitted light (ICP-OES) or

the ions (ICP-MS) are analyzed to determine elemental concentrations with high sensitivity (Montaser, 2018).

Recent advancements in elemental analysis have focused on improving sensitivity, precision, and the ability to handle complex matrices. One of the significant developments is the use of high-resolution ICP-MS, which allows for the detection of ultra-trace levels of elements, making it ideal for environmental monitoring, food safety, and biomedicine (Beauchemin, 2020). The coupling of ICP techniques with laser ablation (LA-ICP-MS) has enabled spatially resolved elemental analysis, providing insights into the elemental distribution within heterogeneous samples such as biological tissues and geological materials (Evans & Guillong, 2021).

Elemental analysis has become a critical tool in environmental monitoring, particularly for tracking pollutants and studying geochemical processes. ICP-MS and ICP-OES are frequently employed to monitor the levels of toxic elements such as lead, mercury, and arsenic in water, soil, and air samples. These techniques provide high sensitivity, enabling the detection of trace elements even in complex environmental matrices (Ammann, 2016). Elemental analysis is crucial in studying the elemental cycling of nutrients such as carbon, nitrogen, and phosphorus in ecosystems. By determining the concentrations of these elements, researchers can gain insights into the health of ecosystems and the impact of anthropogenic activities such as agriculture and industrialization (Jickells & Moore, 2015).

In materials science, elemental analysis is used to characterize the composition of alloys, ceramics, polymers, and nanomaterials. Techniques like ICP-MS, XRF, and electron probe microanalysis (EPMA) are commonly used to determine the purity and composition of materials. For example, EPMA is widely employed to analyze metals and alloys at the micrometer scale, providing detailed information on elemental distribution within a sample (Goldstein *et al.,* 2017). This capability is particularly valuable for quality control in the production of advanced materials, where precise control over elemental composition is required.

2.3.7 Mass Spectrometry

Mass spectrometry (MS) is a powerful analytical technique used for identifying and quantifying molecules based on their mass-to-charge ratio (m/z). It has become indispensable in various scientific disciplines, including chemistry, biochemistry, pharmacology, environmental science, and forensic analysis. MS offers high sensitivity, specificity, and versatility, making it a valuable tool for a wide range of applications.

One of the fundamental components of MS is the ionization source, which converts analyte molecules into gas-phase ions. Common ionization techniques include electrospray ionization (ESI), matrix-assisted laser desorption/ionization (MALDI), and electron ionization (EI). Each ionization method has its advantages and limitations, depending on the sample type and analytical requirements.

After ionization, the ions are separated based on their mass-to-charge ratio using a mass analyzer. Different types of mass analyzers, such as quadrupole, time-of-flight (TOF), ion trap, and orbitrap, offer various capabilities in terms of mass resolution, accuracy, and scan speed. Mass analyzers can be used alone or in combination to achieve higher levels of performance and versatility in MS analysis.

Once separated, the ions are detected and measured to generate a mass spectrum, which provides information about the mass, abundance, and structure of the analyte molecules. Mass spectra can be interpreted to identify unknown compounds, elucidate molecular structures, and quantify analytes in complex mixtures. MS is often coupled with chromatographic techniques, such as gas chromatography (GC) or liquid chromatography (LC), to enhance separation capabilities and improve analytical sensitivity.

MS has numerous applications across various fields. In pharmaceutical analysis, MS is used for drug discovery, pharmacokinetic studies, and quality control of pharmaceutical products (Smith & Makarov, 2019). MS enables the rapid identification of drug metabolites, impurities, and degradation products, ensuring the safety and efficacy of pharmaceutical formulations. Additionally, MS imaging techniques allow for the spatial localization of drugs and metabolites within biological tissues, providing valuable insights into drug distribution and metabolism in vivo.

In proteomics, MS plays a crucial role in the identification and characterization of proteins and peptides (Liu & Zhang, 2017). MS-based proteomics techniques, such as shotgun proteomics and tandem mass spectrometry (MS/MS), enable large-scale protein profiling, post-translational modification analysis, and protein-protein interaction studies. MS is also used in metabolomics to study small molecule metabolites and their roles in biological systems (Liu & Zhang, 2017). Metabolomics approaches, such as liquid chromatography-mass spectrometry (LC-MS) and gas chromatography-mass spectrometry (GC-MS), facilitate the comprehensive analysis of metabolite profiles in biological samples, offering insights into metabolic pathways and disease mechanisms.

Environmental and food analysis are other important applications of MS (Pavlovich & Szymanski, 2021). MS is used to detect and quantify pollutants, pesticides, and contaminants in environmental samples, ensuring compliance with regulatory standards and monitoring environmental health. In food analysis, MS is employed for the detection of food adulterants, contaminants, and residues, as well as the characterization of food components and flavors. MS-based techniques, such as tandem mass spectrometry and high-resolution mass spectrometry, offer high sensitivity and specificity for trace-level analysis in complex matrices.

Forensic science relies heavily on MS for the identification of illicit drugs, explosives, toxins, and trace evidence in criminal investigations. MS enables the rapid and accurate detection of forensic analytes in diverse sample types, including biological fluids, tissues, and residues. MS-based forensic analysis provides critical evidence for crime scene investigation, forensic toxicology, and drug testing.

In conclusion, mass spectrometry is a versatile and powerful analytical technique with widespread applications in chemistry, biology, medicine, environmental science, and forensic analysis. MS offers unparalleled sensitivity, specificity, and versatility for the identification, quantification, and characterization of molecules in complex samples. Continued advancements in instrumentation, software, and methodology are driving innovation and expanding the capabilities of MS for diverse scientific and technological applications.

2.4 Antimicrobial Susceptibility Testing

The disc diffusion method, also known as the Kirby-Bauer method, is a widely used technique in microbiology for determining the susceptibility of bacteria to various antimicrobial agents. This method provides a relatively economical and simple way to assess the effectiveness of antibiotics and other antimicrobial compounds against different bacterial strains (Bauer *et al*., 1966). The principle of the disc diffusion method lies in the diffusion of antimicrobial agents from the discs into the surrounding agar medium. The agar acts as a solid support, allowing the diffusion of the compound through the concentration gradient. If the bacteria are susceptible to the antimicrobial agent, growth inhibition or a clear zone of inhibition will be observed around the disc. The size of the zone indicates the degree of susceptibility, with larger zones, indicating greater susceptibility (Forbes *et al*., 2007).

The procedure of the disc diffusion method involves several key steps. First, a standardized inoculum of the test organism is prepared and spread uniformly on the surface of a solid agar medium using a sterile swab. Next, paper discs impregnated with specific concentrations of antimicrobial agents are placed on the agar surface. The plates are then incubated at the optimal temperature for the bacterial strain being tested. After incubation, the diameter of the zones of inhibition is measured and compared to interpret the results.

The disc diffusion method is highly valuable in clinical microbiology for guiding appropriate antibiotic therapy (CLSI, 2018). It provides information on the susceptibility or resistance of bacteria to specific antimicrobial agents, aiding in the selection of the most effective treatment for bacterial infections (Jorgensen & Turnidge, 2015). Additionally, the method is used in research and development to evaluate the activity of new antimicrobial compounds and to monitor the emergence of antimicrobial resistance.

2.4.1 Preparation and Application of Mueller Hinton Agar Media

Mueller Hinton agar is a widely used medium in microbiology laboratories for antimicrobial susceptibility testing and bacterial culture. It provides a consistent and standardized environment for the growth and assessment of bacteria. The necessary

ingredients and equipment that should be gathered include Mueller Hinton agar powder, Distilled water, Heat-resistant glassware, a Stirring rod, an Autoclave, Sterilized Petri dishes, sterile swabs or inoculating loop, and an Incubator. The appropriate amount of Mueller Hinton agar powder is weighed according to the manufacturer's instructions. The recommended concentration is typically 38-40 grams per liter of distilled water (CLSI, 2020). The required volume of distilled water is poured into the heat-resistant glassware. The volume will depend on the amount of media you want to prepare, but it is usually 1 liter. The weighed Mueller Hinton agar powder is added to the distilled water while stirring gently with a stirring rod until all the powder is completely dissolved. Once the powder is dissolved, the mixture is heated to boiling while stirring occasionally to prevent sticking or burning. Boil the medium for about 1 minute to ensure complete sterilization (CLSI, 2020). After boiling, the glassware is removed from the heat source and allowed to cool down to approximately 50-55°C (122-131°F) to avoid damaging heat-sensitive components (Humphries & Hindler, 2015). While the medium is cooling, the Petri dishes are prepared by labeling them with appropriate identification, date, and any other necessary information (Humphries & Hindler, 2015). Once the medium has reached the desired temperature, it is poured into the sterile Petri dishes, filling them to a depth of approximately 4-5 mm. Pour enough medium to completely cover the bottom of the dish (CLSI, 2020). The medium is allowed to solidify by leaving the Petri dishes undisturbed at room temperature or by placing them horizontally in a laminar flow hood (Humphries & Hindler, 2015).

2.4.2 Application of Mueller Hinton Agar

Before using the Mueller Hinton agar plates, they are stored in a refrigerator to maintain their integrity and prevent contamination. Bring the plates to room temperature before using them (Humphries & Hindler, 2015). Bacterial inoculum is prepared by growing the bacteria overnight on a suitable nutrient agar medium (CLSI, 2020). To make the bacterial suspension as turbid as a 0.5 McFarland standard, its turbidity is modified (Gichumbi *et al.*, 2016e). This can be achieved by comparing the bacterial suspension to the standard using a spectrophotometer or by using a turbidity meter (CLSI, 2020).

Using a sterile swab or inoculating loop, the bacterial suspension is streaked evenly over the entire surface of the Mueller Hinton agar plate, making three or four quadrants or a lawn (Humphries & Hindler, 2015). The inoculum is allowed to dry on the agar surface for a few minutes (CLSI, 2020). Using sterile forceps or a calibrated dropper, antibiotic disks are applied to the surface of the agar, pressing them gently to ensure proper contact with the medium (Humphries & Hindler, 2015). The plates are incubated upside down in an appropriate incubator at the recommended temperature and duration for the bacteria being tested (CLSI, 2020). After incubation, the plates are observed for bacterial growth, and the zones of inhibition around each antibiotic disk are measured. These zones represent the susceptibility or resistance of the bacteria to antibiotics (Humphries & Hindler, 2015).

CHAPTER THREE: RESEARCH METHODOLOGY

3.1 Study Sites

Synthesis of ligands and their metal complexes was carried out at Chuka University laboratories. Analysis of the ligands and their complexes by proton NMR was done at the University of Nairobi chemistry laboratory. Analyses by *SHIMADZU AFFINITY IS* FT-IR spectrometer and *UV 1800 SHIMADZU* UV/VIS Spectrometer, molar conductivity and melting point determination were done at Chuka University chemistry laboratory. Biological assays were done at Kenya Medical Research Institute-Nairobi.

3.2 Materials and Reagents

The reagents were used without additional purification after being purchased from Sigma Aldrich. They included 2, 2-bipyridine ≥99%, 3,5-dimethyl-1H-pyrazole3,5-dimethylpyrazole 99%, 3-chloro-6-hydrazinylpyridazine 97%, acetonitrile, copper (II) chloride, dichloromethane 99.8%, dimethyl sulfoxide, ethanol 99%, acetic acid 99%, Mueller Hinton agar medium, pentane-2,4-dione (acetylacetone) ≥99% and zinc chloride ≥98%. The bacterial and fungal strains were bought from KEMRI.

3.3 Synthesis of Heterocyclic Ligands and their Transition Metal Complexes

The synthesis of the N, N' donor bidentate ligands was done by the acid-catalyzed addition of the hydrazinyl group to the diketone leading to cyclization to form the pyrazole ring (Aljamali *et al.,* 2019).

3.3.1 Synthesis of 3-chloro-6-(1H-pyrazol-1-yl) pyridazine

A mixture of 3-chloro-6-hydrazinylpyridazine (1 g, 6.917 mmol), ethanol 20 ml and acetic acid 5 ml was heated to a clear solution and an equimolar amount (0.4985 g, 6.9 mmol) of malonaldehyde which was already diluted with 10 ml ethanol was added drop-wise during reflux. After addition the reaction mixture was heated under reflux for 3 hours, cooled and diluted with 25 ml of water, precipitates formed were filtered and crystallized from ethanol (Ather *et al.,* 2010). The general equation of preparation is illustrated in Figure 8.

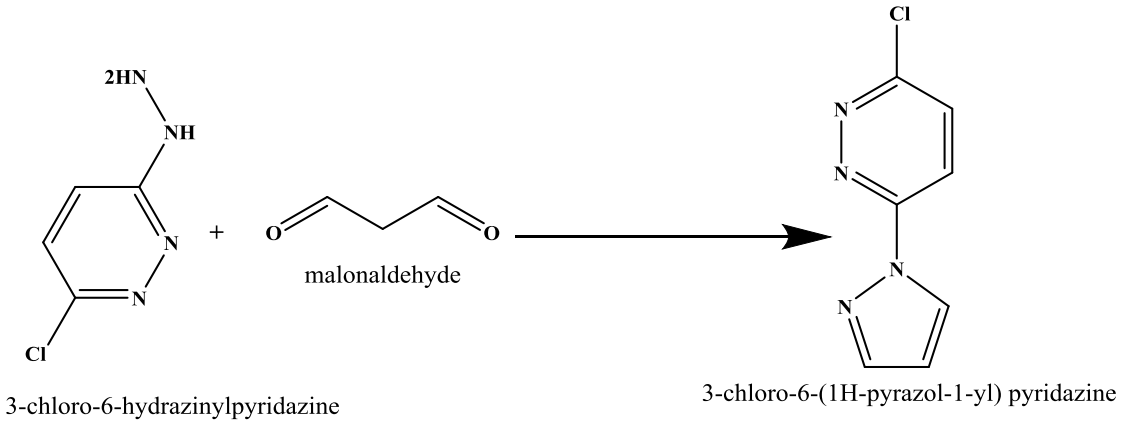

Figure 8: Synthesis of 3-chloro-6-(1H-pyrazol-1-yl) pyridazine using 3-chloro-6-hydrazinylpyridazine and malonaldehyde

3.3.2 Synthesis of 3-chloro-6-(3, 5-dimethyl-1H-pyrazol-1-yl) pyridazine

A mixture of equimolar amounts of 3-chloro-6-hydrazinylpyridazine (6.9 mmol, 1 g), acetylacetone (0.69 g, 6.917 mmol) and 2 ml acetic acid were stirred and heated at 80-90 ºC for 30 minutes and cooled. The unreacted acetic acid was removed under vacuum and the product was washed with 25 ml of distilled water and filtered. The final product was re-crystallized in ethanol to obtain colourless prisms of the compound (Ather *et al.*, 2010). The general equation of preparation is illustrated in Figure 9.

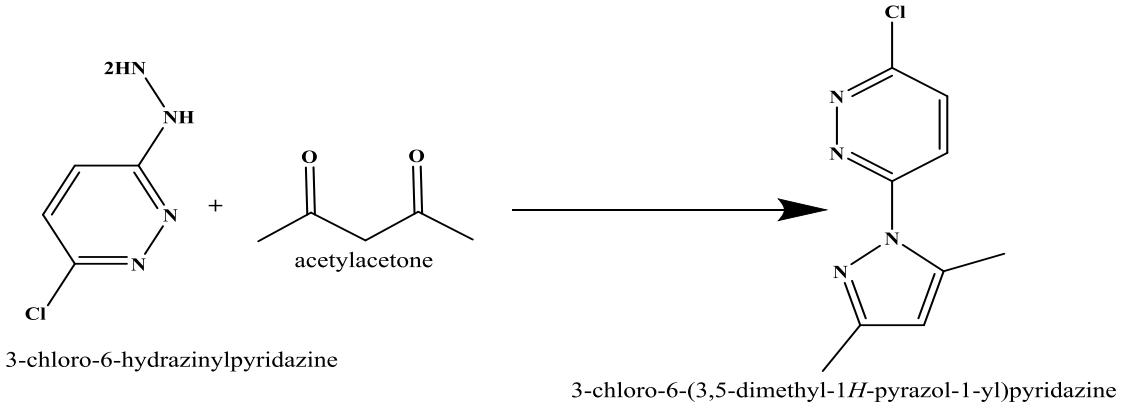

Figure 9: Synthesis of 3-chloro-6-(3, 5-dimethyl-1H-pyrazol-1-yl) pyridazine

3.3.3 Synthesis of Zinc Complex Derived from 2, 2-Bipyridine

Zinc chloride (0.044g, 0.32 mmol) was dissolved in 30ml ethanol and poured into a 150ml round-bottomed flask. 0.1g of 2, 2-bipyridine (0.64mmol) was added to this solution and refluxed at 80-90 ºC for 4 hours. The precipitate formed was obtained by

evaporating the excess solvent in the rotary evaporator, after which it was transferred into an oven at 80 ºC. The solid obtained was washed using diethyl ether and filtered at reduced pressure (Beletskaya & Cheprakov, 2000). The reaction is illustrated in Figure 10.

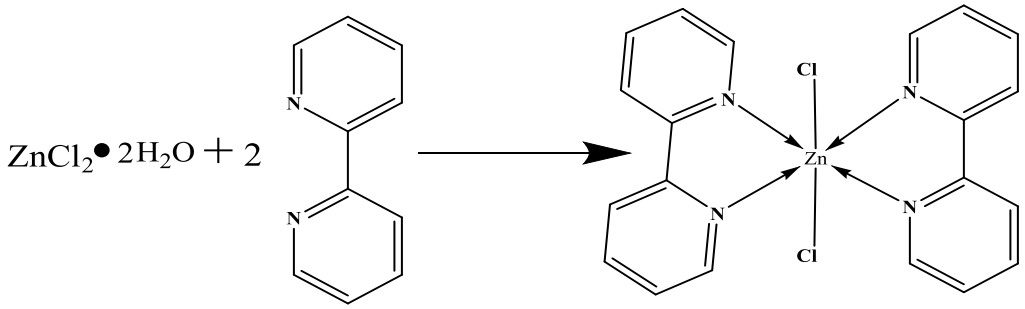

Figure 10: Predicted structure of zinc complex derived from 2,2-bipyridine

3.3.4 Synthesis of Copper Complex Derived from 2, 2-Bipyridine

Copper (II) chloride dihydrate (0.055g, 0.32mmol) and 0.1g of 2, 2-bipyridine (0.64mmol) were dissolved in 30ml ethanol and poured into a 150ml round-bottomed flask. For four hours, this mixture was refluxed at 80–90 ºC. The precipitate formed was obtained by evaporating the excess solvent in the rotary evaporator, after which it was transferred into an oven at 80 ºC. The solid obtained was washed using diethyl ether and filtered at reduced pressure (Beletskaya & Cheprakov, 2000; Eremina *et al.*, 2019). The predicted structure of the complex is shown in Figure 11.

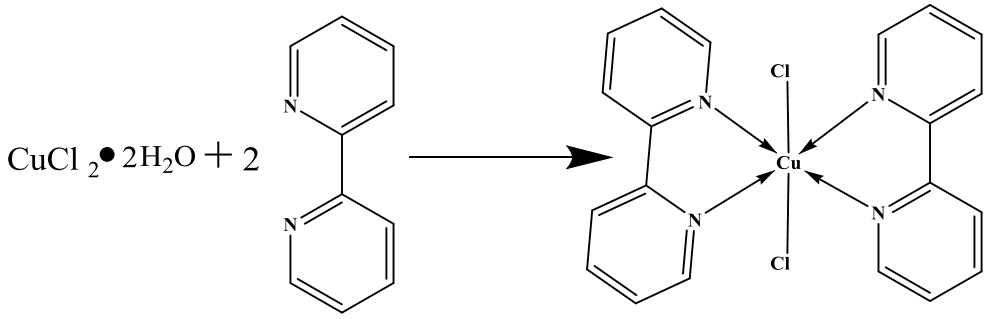

Figure 11: Predicted structure of copper complex derived from 2,2-bipyridine

3.3.5 Synthesis of Zinc Complex Derived from 3-chloro-6-(1H-pyrazol-1-yl) pyridazine

Zinc chloride (0.038g, 0.28 mmol) was dissolved in 30ml ethanol and poured into a 150ml round-bottomed flask. 0.1g of 3-chloro-6-(1H-pyrazol-1-yl) pyridazine (0.55mmol) was added to this solution and refluxed at 80-90 ºC for 4 hours. The precipitate formed was obtained by removing the excess solvent in the rotary evaporator, after which it was transferred into an oven at 80 ºC. The solid obtained was washed using diethyl ether and filtered at a reduced pressure. This reaction is illustrated in Figure 12.

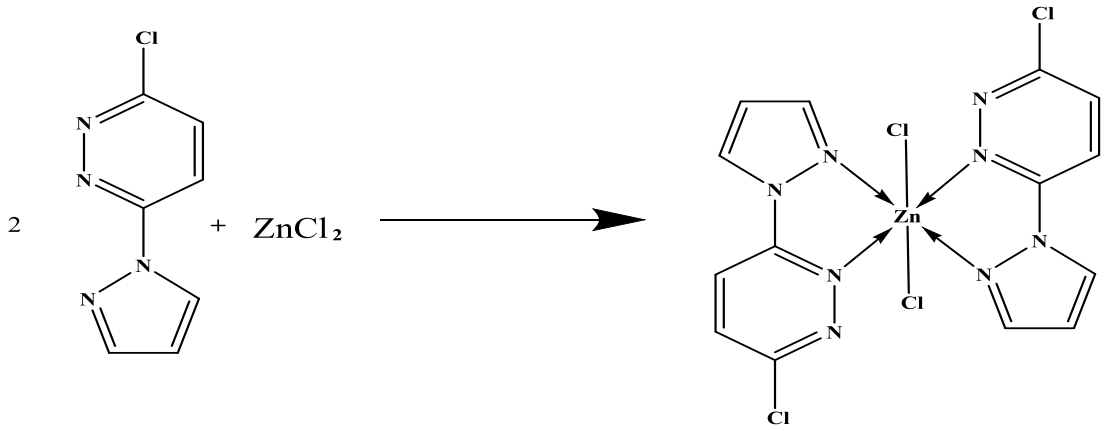

Figure 12: Structure of zinc complex derived from 3-chloro-6-(1H-pyrazol-1-yl) pyridazine

3.3.6 Synthesis of Copper Complex Derived from 3-chloro-6-(1H-pyrazol-1-yl) pyridazine

Copper (II) chloride dihydrate (0.047g, 0.28 mmol) was dissolved in 30ml ethanol and poured into a 150ml round-bottomed flask. 0.1g of 3-chloro-6-(1H-pyrazol-1-yl) pyridazine (0.55mmol) was added to this solution and refluxed at 80-90 ºC for 4 hours. The reaction is illustrated in Figure 13. The precipitate formed was obtained by removing the excess solvent in the rotary evaporator, after which it was transferred into an oven at 80 ºC. The solid obtained was washed using diethyl ether and filtered at a reduced pressure.

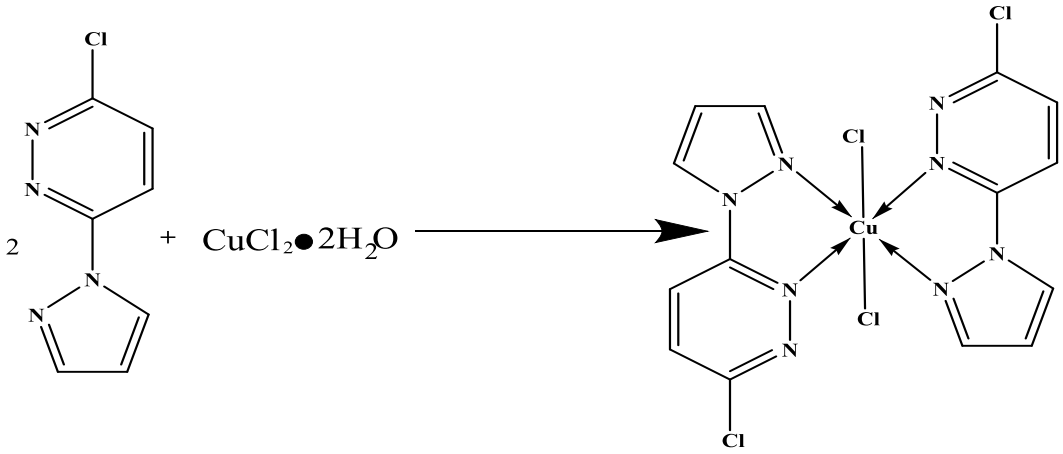

Figure 13: Structure of expected copper complex derived from 3-chloro-6-(1H-pyrazol-1-yl) pyridazine

3.3.7 Synthesis of Copper Complex Derived from 3-chloro-6-(3, 5-dimethyl-1H-pyrazol-1-yl) pyridazine

0.1 g of 3-chloro-6-(1H-pyrazol-1-yl) pyridazine synthesized (0.48mmol) was added to 0.032g of copper (II) chloride dihydrate in a 150ml round-bottomed flask with 30ml of ethanol. The mixture was refluxed at 80-90 ºC for 4 hours. The green precipitate formed was isolated from the solvent by use of the rotary evaporator followed by drying in the oven. The solid sample obtained was washed in diethyl ether, filtered under reduced pressure and dried under room temperature (Gichumbi *et al*., 2018). The reaction for complex formation is shown in Figure 14.

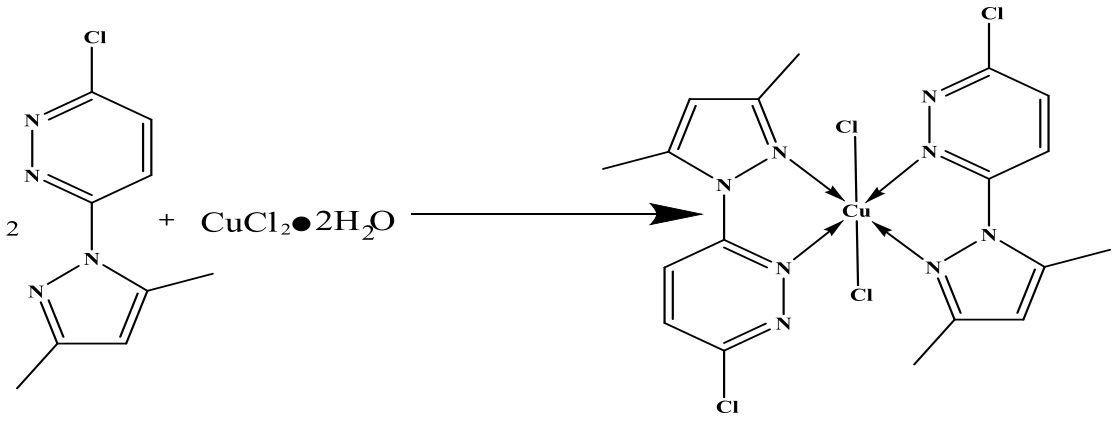

Figure 14: Predicted structure of copper complex derived from 3-Chloro-6-(3, 5-dimethyl-1H-pyrazol-1-yl) pyridazine

3.3.8 Synthesis of Zinc Complex Derived from 3-chloro-6-(3, 5-dimethyl-1H-pyrazol-1-yl) pyridazine

0.1 g of 3-chloro-6-(1H-pyrazol-1-yl) pyridazine (0.48mmol) was added to 0.033g of zinc (II) chloride (0.24mmol) in a 150ml round-bottomed flask with 30ml of ethanol. The mixture was refluxed at 80-90 ºC for 4 hours. The green precipitate formed was isolated from the solvent by use of the rotary evaporator followed by drying in the oven. The solid sample obtained was washed in diethyl ether, filtered under reduced pressure and dried under room temperature (Gichumbi *et al*., 2018). The structure of the predicted complex is shown in Figure 15.

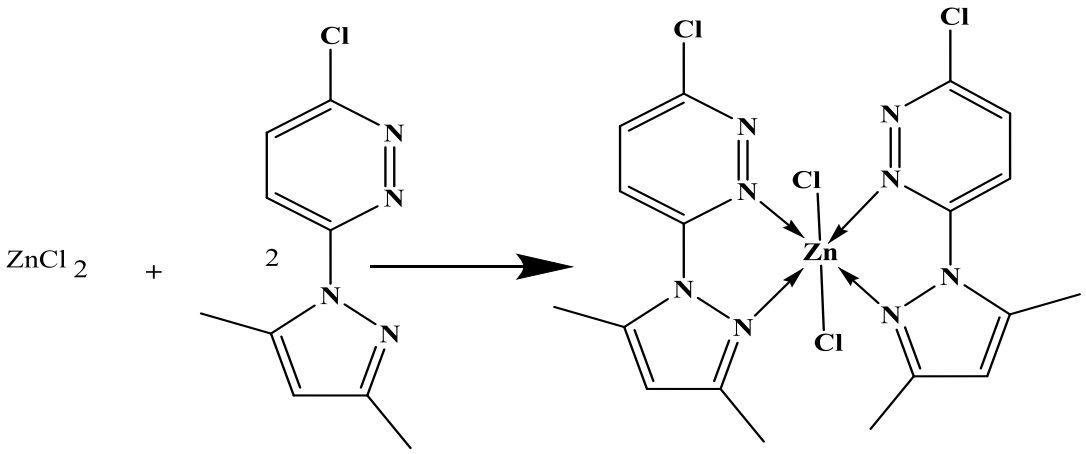

Figure 15: Predicted structure of zinc complex derived from 3-Chloro-6-(3, 5-dimethyl-1H-pyrazol-1-yl) pyridazine

3.4 Characterization of the Synthesized Compounds

3.4.1 Melting Point Determination

The melting point of the N, N'-bidentate ligands and their corresponding copper and zinc complexes was determined using the open capillary method. The dry solid substances whose melting points were to be determined were poured on a tile and crushed to form a fine powder, for easy entry into the capillary of diameter about 1 mm. The capillary tube with one end closed was held between the fingers. The open end of the capillary was dipped into the finely powdered solid sample. The solid was then gently tapped to fill a length of about 8-12 mm.

With the help of a heat-resistant rubber band, the capillary containing the sample was clamped on the thermometer such that the bulb of the thermometer was in line with the closed end of the capillary tube. The thermometer was then lowered into liquid paraffin and submerged to about 2cm. The thermometer was then held using a stand and clamp.

The sample was heated in a range of ambient temperature to 300℃. The liquid paraffin was heated using a non-luminous flame of the Bunsen burner (Basu & Date 1998). The temperature of the liquid was observed as it rose continuously and the temperature at which the substances started to melt was noted immediately as T_1. The temperature at which the solid had melted completely was recorded as T_2. The average of T_1 and T_2 was calculated to obtain the value of the melting point.

3.4.2 Molar Conductance Measurements

The electrolytic properties of the synthesized ligands and their transition metal complexes were determined at room temperature using the SIBATA Conductivity meter Model SC–17A using standard procedures according to Chen and coworkers (1993).

3.4.3 FT-IR Spectroscopy

The FT-IR spectra of the N, N-bidentate ligands and their metal complexes were recorded on a *SHIMADZU AFFINITY IS* FT-IR spectrometer in the range of 4000 and 380 cm^{-1}. This was achieved after grinding 2 mg of the sample using an agate mortar and mixing it with 0.1 g of KBr pellets. The hard press was used to press the mixture to form pellet disks that were mounted on the IR spectrometer and recorded directly (Koske, 2018).

3.4.4 UV-VIS Spectroscopy

The electronic spectra of the synthesized ligands and their respective transition metal (II) complexes were obtained in acetonitrile using the *UV 1800 SHIMADZU* UV/VIS Spectrometer. The spectrometer was set to scan the blank sample of acetonitrile (reference material) followed by the samples of the ligands and their complexes. The variations in absorbance were recorded according to Ommenya *et al*., (2019).

3.4.5 ^{1}H NMR Spectroscopy

The proton NMR of the synthesized ligands and their respective transition metal (II) complexes was done according to Matsinha and co-workers, in deuterated DMSO using a Bruker Avance III HD Nanobay 400 MHz NMR spectrometer (Matsinha *et al*., 2013). The determination of ^{1}H NMR spectra of the synthesized N, N'-donor bidentate ligands and their copper and zinc complexes was determined using standard procedures (Bhatt *et al.,* 2019). 6mg of each solid synthesized sample material was measured and deuterated DMSO used as a solvent. 0.7ml of deuterated solvent was added to the measured NMR sample and shaken to dissolve completely. The soluble NMR sample was then transferred into a clean NMR tube with a glass Pasteur pipette and then closed by a clean cab. TMS was used as an internal standard for chemical shift calibration. One drop of TMS was used for each NMR tube used. The NMR tube was then inserted in an NMR spectrometer and then scanned for ^{1}H resonance frequency.

3.6 Antimicrobial Screening

The synthesized ligands and their transition metal complexes were screened *in vitro* for their antibacterial and antifungal activities against gram-positive and negative bacterial strains cultivated on Mueller Hinton agar medium (Mapari *et al.,* 2011). The diameter of inhibition was measured relative to that of the ampicillin and fluconazole standards (Murray *et al.,* 1995; Zaidan *et al.,* 2006; Dickert *et al.,* 1981).

3.6.1 Preparation of Inoculums

The selected bacterial strains, *Escherichia coli* (gram-negative) and *Staphylococcus aureus* (gram-positive), and the fungal strain *candida albicans* were transferred from the stock cultures and streaked on Mueller Hinton agar (MHA) plates and incubated for about 24 hours at 37 ºC in an oven. Bacteria were transferred using a bacteriological loop to autoclaved MHA that was cooled at 45 ºC in a water bath with swirling of the flask. The medium was then poured into sterile Petri dishes, allowed to solidify, and used for bioassay. The medium containing spore suspension was then poured into sterile plates, allowed to solidify, and used for the paper disc diffusion bioassay.

3.6.2 Preparation of the Test Solution

The solutions of the ligands and the copper and zinc complexes were prepared by dissolving 10mg of the compound in 10 ml DMSO (stock solution 1000µg/ml). From this solution, further subsequent dilutions were made to obtain solutions of 800µg/ml, 600µg/ml, and 400µg/ml that were subjected to antimicrobial testing.

3.6.3 Procedure for Antimicrobial Screening

The paper discs made by puncturing Whatman number one filter paper were carefully transferred to the inoculated agar surface using sterile forceps, leaving sufficient space between the discs to avoid overlap. The plates were incubated at 37°C for 24 hours. The zones of inhibition were measured thereafter around the antimicrobial discs (Matar *et al.*, 2015). Ampicillin and fluconazole were used as the positive control and DMSO as the negative control.

3.6 Data Analysis

The raw data obtained from antimicrobial studies (the diameters of inhibition in relation to the concentrations of the test solutions dissolved in DMSO) was analyzed using one-way ANOVA Complete Randomised Design (CRD) with three replicates, using the SPSS software.

3.7 Ethical Consideration

Before commencing the research, the researcher obtained ethical clearance from the Chuka University Ethics Committee and NACOSTI (Appendix 26). The study was conducted with strict adherence to ethical standards, ensuring that methods, results, and data were reported with utmost honesty. Plagiarism, biases, and carelessness were diligently avoided. Information sourced from other works was properly acknowledged and cited. The research focused on publishing only new findings to contribute to knowledge and guide future research. Additionally, all relevant laws and regulations related to environmental pollution, toxic material handling, and disposal were strictly followed to mitigate health risks throughout the research process.

CHAPTER FOUR: RESULTS AND DISCUSSION

4.1 Melting Point Determination

The melting points, colour and yields of the synthesized ligands and their transition metal (II) complexes are summarized in Table 4.1.

Table 4.1: Melting Points of the Selected Ligands and Their Copper and Zinc Complexes

Ligand/complex	Molecular Weight	Colour	Melting Point (°C)	Yield (%)
2, 2- bipyridine (L1)	156.2	White	70 – 72	-
3-chloro-6-(1H-pyrazol-1-yl) pyridazine (L2)	180.6	White	138 – 144	89
3- chloro-6-(3,5-dimethyl-1H-pyrazol-1-yl) pyridazine (L3)	208.6	White	145 – 152	84
Copper complex of L1	446.8	Blue	248 – 254	79
Copper complex of L2	495.6	Green	258-262	86
Copper complex of L3	551.7	Green	260 – 268	80
Zinc complex of L1	448.7	Pale pink	248	77
Zinc complex of L2	497.5	Brown	232 – 238	69
Zinc complex of L3	553.6	Brown	242 – 250	73

L2 was obtained as a white solid with a melting point range of 138-144 °C and a yield of 89%. L3 was obtained as a white solid with a melting point of 145-152 °C and yielded 84%. The melting points of the complexes were higher than those of the ligands. CuL1 (blue crystalline solid with a melting point of 248-254 °C and yielded 79%), CuL2 (green solid with a melting point of 258-262 °C and yielded 86%), CuL3 (green solid with a melting point of 260-268 °C and yielded 80%), ZnL1 (pale pink solid with a melting point of 248 °C and yielded 77%), ZnL2 (brown solid with a melting point of 232-238 °C and yielded 69%) and ZnL3 (brown solid with a melting point of 242-250 °C and yielded 73%).

The melting point of the samples was found to increase with an increase in the branching of the carbon chain of the ligands. It was observed that the complexes decomposed in the range of 268-320 °C and that decomposition temperature was dependent on the increase in the molecular weights of the complexes. This might be because an increase in the

molecular weight makes a compound to be compact in the solid state thereby requiring more energy to weaken the intermolecular interactions (Dong & Hao 2010).

4.2 FTIR Spectroscopy Analysis

The synthesized ligands and their transition metal complexes exhibited a range of characteristic peaks (Appendix 10-18) that are summarized in Table 4.2. They show common characteristic features of a series of weak to moderate absorption bands above the 3000 cm^{-1} region, which can be assigned to aromatic C–H stretch in the complexes (Nandiyanto *et al.,* 2019).

Table 4.2: Selected FT-IR absorption bands (cm^{-1}) of the heterocyclic N, N' donor bidentate ligands and their copper and zinc complexes

Compound	υ(C=N) (cm^{-1})	υ(C-Cl) (cm^{-1})	υ(C=C) (cm^{-1})	υ(C-N) (cm^{-1})	υ(M-N) (cm^{-1})
L1	1653	-	1530	1247	-
L2	1660	764	1398	1140	-
L3	1624	785	1425	1265	-
Copper complex of L1	1645	-	1438	1319	644
Copper complex of L2	1645	777	1469	1167	592
Copper complex of L3	1579	790	1423	1161	528
Zinc complex of L1	1641	-	1436	1311	648
Zinc complex of L2	1625	767	1460	1155	601
Zinc complex of L3	1598	795	1419	1132	522

L1 (2, 2-bipyridine) has a medium peak at 1653 cm^{-1} that can be assigned to the –C=N- stretching vibration. A duet at 1400 cm^{-1} and 1450 cm^{-1} could be a result of the –C=C- stretching vibrations in the rings. A medium band at 1530 cm^{-1} is due to the –C=C- stretching vibrations. A medium peak at 754 cm^{-1} can be due to the C-H out-of-plane bending (Nandiyanto *et al.,* 2019). The –C=N- stretching vibration shifts to lower wavenumbers upon complexation (1645 cm^{-1} and 1641 cm^{-1} for copper and zinc complexes respectively), indicating that complexation took place via the azomethine nitrogen of the pyridine rings (Alias *et al.,* 2014).

3-chloro-6-(1H-pyrazol-1-yl) pyridazine (L2) showed medium peaks at 1660 cm^{-1} and 1575 cm^{-1} as shown in Figure 18, which might be due to the presence of the azomethine bond, indicating the successful cyclization of 3-chloro-6-hydrazinylpyridazine with malonaldehyde to form the pyrazole ring. The peak at 764 cm^{-1} confirms that the chloro is not substituted in the reaction. A duet at 1398 cm^{-1} and 1450 cm^{-1} that are unaffected by complexation (Figure 19), confirms the presence of -C=C- in the rings. Upon complexation, the peak due to the azomethine group shifts to lower wavenumbers (1645 cm^{-1} and 1625 cm^{-1} for copper and zinc complexes respectively) showing that complexation must have taken place through the –C=N- nitrogen.

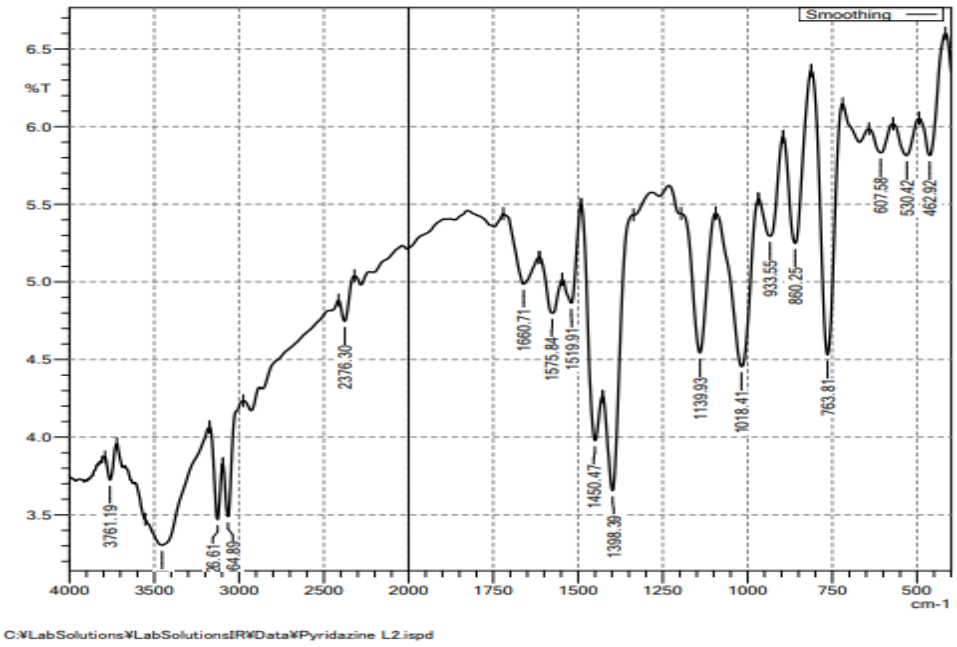

Figure 16: FTIR spectrum of L2

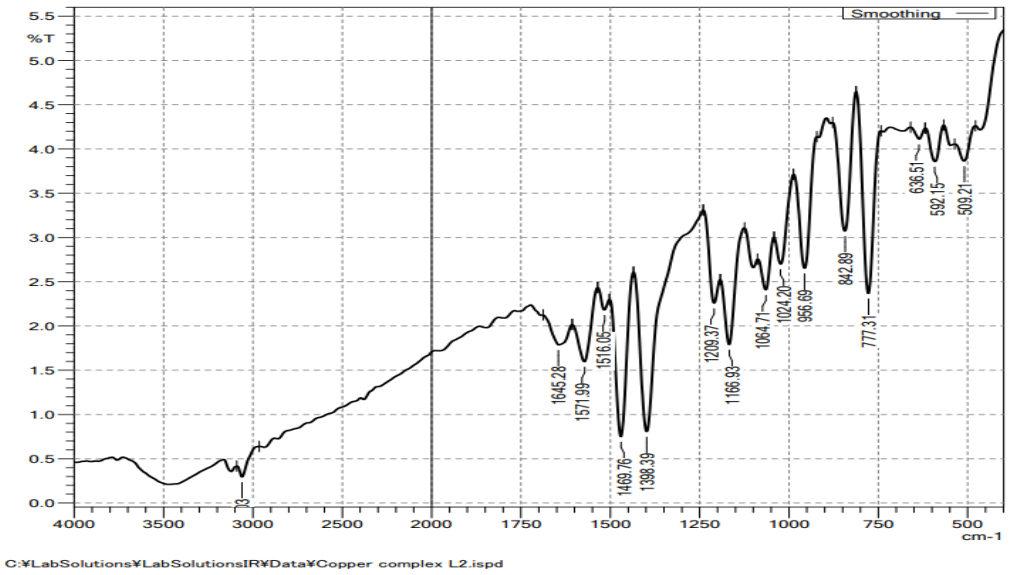

Figure 17: FTIR spectrum of CuL2

3-chloro-6-(3, 5-dimethyl-1H-pyrazol-1-yl) pyridazine (L3) has a strong peak at 1624 cm^{-1} that can be assigned to the –C=N- group stretching. This suggests that the cyclization of pentane 2, 4-dione and 3-chloro-6-hydrazinylpyridazine was successful. A weak band at 2990 cm^{-1} confirms the presence of aliphatic C-H stretching (Adeloye *et al.*, 2012) that arises from the methyl groups attached to the pyrazole rings. Like L2, a peak at 785 cm^{-1} is observed showing that the –Cl is not affected by the incoming diketone. The compound has also a peak at 1425 cm^{-1} which is due to the –C=C- stretching in the aromatic rings. The band due to the –C=N- stretching shifts to lower wavenumbers (1579 cm^{-1} and 1598 cm^{-1} for copper and zinc complexes respectively) upon complexation, confirming that the azomethine nitrogen is directly bonded to the metal centre.

Moreover, there are weak bands in the range 500-600 cm^{-1} in all the complexes (648 cm^{-1}, 644 cm^{-1}, 601 cm^{-1}, 592 cm^{-1}, 522 cm^{-1} and 528 cm^{-1} for ZnL1, CuL1, ZnL2, CuL2, ZnL3 and CuL3 respectively), further confirming that the azomethine nitrogen took part in complexation (Chruszcz-Lipska *et al.*, 2022; Nakamoto 2009).

4.3 UV/Vis spectroscopy analysis

The electronic spectra of the synthesized ligands and their corresponding transition metal (II) complexes showed a range of absorption bands mainly in the UV region, tailing to the visible region (Appendix 1-9). The absorption bands are summarized in Table 4.3.

Table 4.3: Assignment of the observed λ_{max} (nm) of the N, N' donor bidentate ligands and their transition metal (II) complexes

Compound	λ_{max} (nm)	Absorbance	Transition
L1	280.50	0.190	$\pi \rightarrow \pi^*$
	236.00	0.099	$\pi \rightarrow \pi^*$
L2	259.00	0.553	$\pi \rightarrow \pi^*$
L3	261.50	0.620	$\pi \rightarrow \pi^*$
CuL1	296.50	0.302	$\pi \rightarrow \pi^*$
	238.50	0.312	$\pi \rightarrow \pi^*$
CuL2	455.50	0.023	MLCT
	259.00	0.358	$\pi \rightarrow \pi^*$
CuL3	260.50	0.480	$\pi \rightarrow \pi^*$
ZnL1	307.50	0.509	$n \rightarrow \pi^*$
	296.00	0.553	$\pi \rightarrow \pi^*$
	244.00	0.365	$\pi \rightarrow \pi^*$
ZnL2	259.50	0.283	$\pi \rightarrow \pi^*$
ZnL3	261.00	0.879	$\pi \rightarrow \pi^*$

Ligands L1-L3 showed absorption bands in the wavelength range of 259- 281 nm (Figure 20). These bands can be assigned to the Intra- Ligand Transitions (ILT) $\pi \rightarrow \pi^*$, from the pi electrons of the conjugated rings. The copper and zinc complexes showed absorption bands in the wavelength range of 238 – 456 nm (Figure 21).

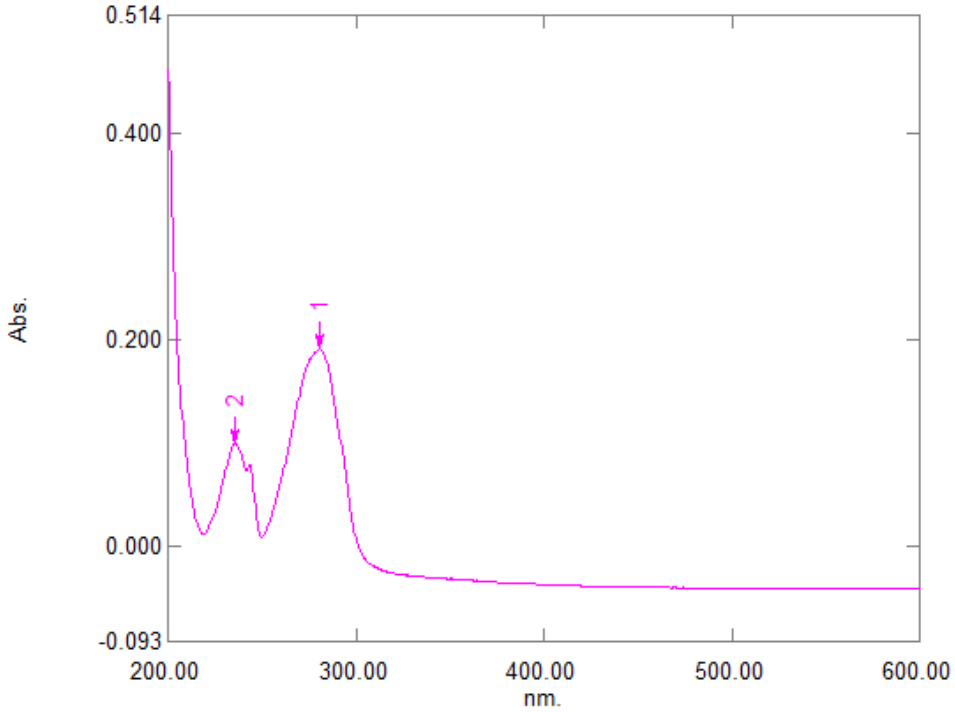

Figure 18: UV/VIS spectrum of L1

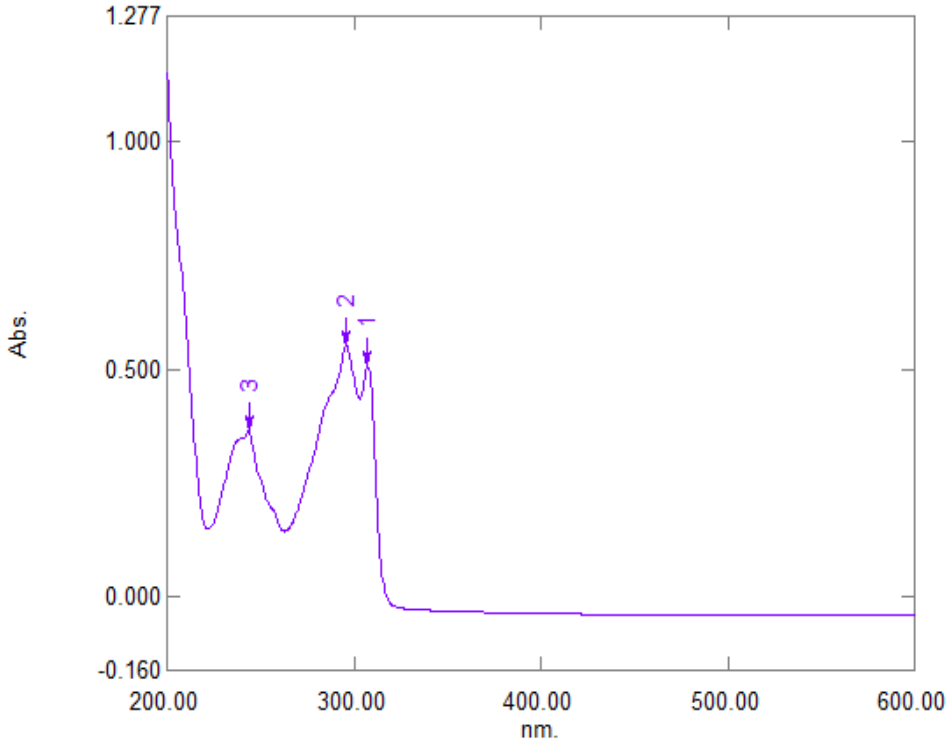

Figure 19: UV/VIS spectrum of ZnL1

These transitions can be assigned to the π→π*, n→π* and MLCT transitions. The bathochromic shifts observed in the complexes can be attributed to the back-bonding that takes place since both zinc and copper are electron-rich and can donate to the empty pi anti-bonding orbitals of the ligands (Mc Crudden 2008). According to Sun and coworkers, the presence of bands in the range of 220 – 280 nm is associated with compounds with aromatic structures (Sun *et al.*, 2016). The presence of such bands in the ligands and the complexes suggests that ligand formation was successful.

4.4 ^{1}H-NMR spectroscopy analysis

The proton NMR spectra of the synthesized ligands and complexes were recorded in deuterated DMSO. The spectra of the ligands L1, L2 and L3 typically show peaks at □ = 8.2, 8.1 and 7.8 ppm respectively, that correspond to the azomethine (-N=CH-) hydrogen (Mambanda *et al.*, 2022). They however show other peaks that can be assigned to the aryl proton and the methyl groups in L3 (□ =2.0-2.4 ppm corresponding to the 3-methyl group protons and □ =3.20 ppm corresponding to the 5-methyl group protons on the pyrazole ring). This is an indication that there is a successful cyclization of the selected hydrazinyl pyridazine to form the preferred pyrazolyl pyridazine. Upon complexation, all these bands are observed to shift to lower frequencies (Appendix 19-24). In the complexes derived from L1, the peaks corresponding to the azomethine hydrogen shift downfield (8.2 to 8.44 ppm with an integral value of 1.95 for the copper complex) as shown in Figure 20.

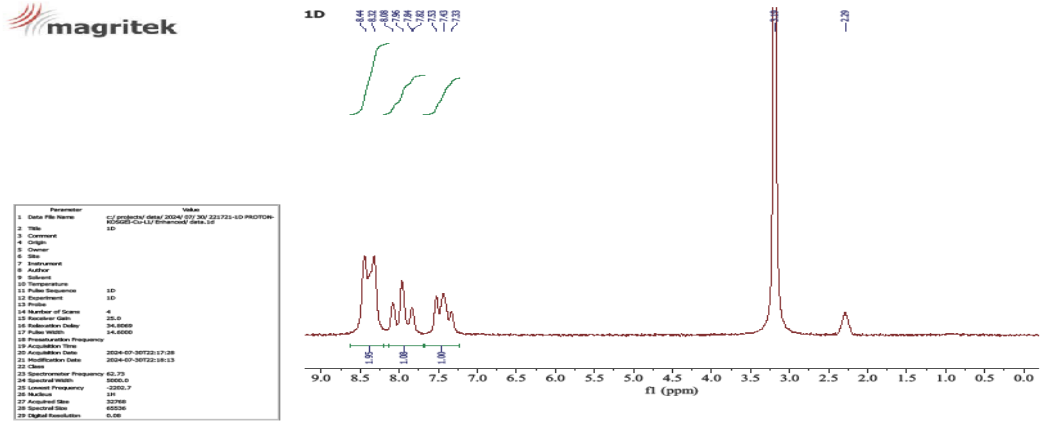

Figure 20: NMR spectrum of CuL1

This is an indication that coordination took place through the N, N'-donor atoms of the ligand, which is associated with deshielding as the lone pair of electrons in the N atoms are donated to occupy the empty orbitals of the metal. Similarly, in the complexes of L2 and L3 (Figure 21), the peaks corresponding to the azomethine proton shift to lower frequencies (= 8.10 ppm to 8.57 ppm with an integral value of 1.00 for zinc complex of L2 and = 7.8 ppm to 7.89 ppm for the zinc complex of L3). Other peaks like those of the aryl hydrogen and the methyl groups remain unchanged indicating that the reaction with transition metal (II) salts only affected the chemical environment of the azomethine proton. The chloro group exerts an electron-withdrawing effect, leading to deshielding and downfield shifts of nearby protons (Arul & Manjula 2013). Zinc complexation results in similar but slightly smaller downfield shifts (0.1-0.3 ppm), reflecting zinc's weaker ability to deshield protons compared to copper. The shifts depend on the metal-ligand interaction strength and the geometry of the complex (Elie 2007).

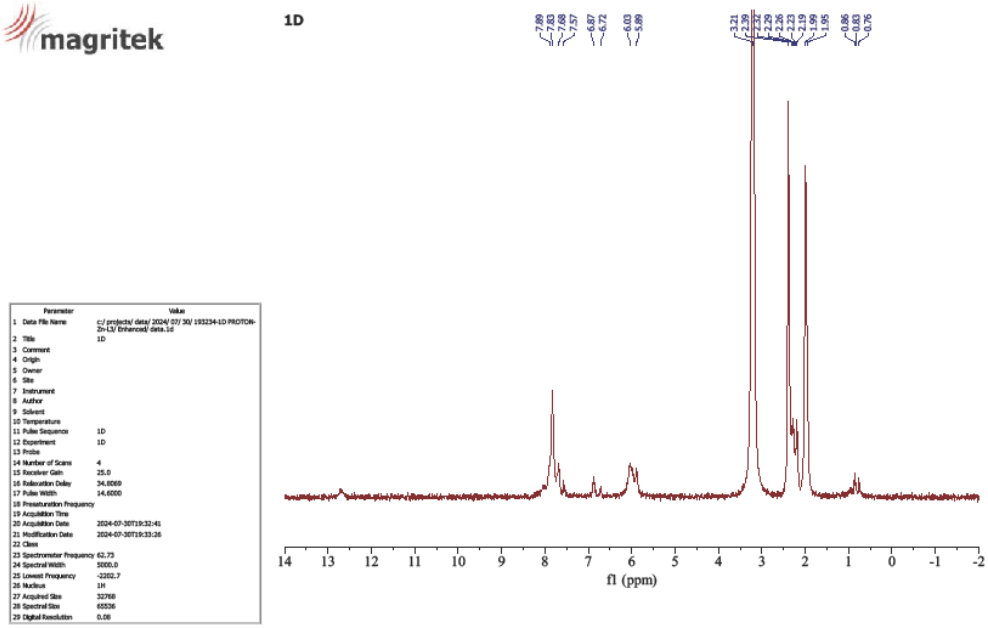

Figure 21: NMR spectrum of ZnL3

4.5 Molar conductivity measurements

The molar conductance values of the synthesized compounds were measured at room temperature. All the conductance values of the synthesized compounds were below 50 Ω^{-}

^{1} cm ^{2}mol^{-1} as shown in Table 4.4, indicating their non-electrolytic nature (Chen *et al.*, 1993). This suggested that there were no free ions present outside the coordination sphere of all the complexes i.e., the complexes formed were neutral.

Table 4.4: Molar conductivity measurements of the synthesized ligands (L1-L3) and their complexes

Compound	Conductance (Ω^{-1} cm^{2}mol^{-1})
L1	13
L2	9
L3	8
CuL1	16
CuL2	15
CuL3	15
ZnL1	19
ZnL2	17
ZnL3	20

4.6 Antimicrobial Activity of Different Synthetic Compounds and their Copper and Zinc Complexes against *C. albicans, E. coli,* and *S. aureus*

The effect of the N, N'-donor ligands and their copper and zinc complexes on *in vitro* biological screening against fungi and bacteria was investigated. The petri dishes containing microbial strains were incubated at 37°C, and the inhibitory zone was measured after 24 hours of incubation. The synthesized compounds' antibacterial and antifungal properties were ascertained by observing the inhibitory zone that these complexes formed against the strain of test bacteria and fungi. Appendix 25 presents the antimicrobial activity results of the investigated compounds against three pathogens using the reference antibiotic, ampicillin and the antifungal reference, fluconazole. In all the infections, the commercial antibiotic ampicillin demonstrated a high level of action, with an inhibition zone measuring between 23 and 28mm.

4.7.1 Antimicrobial Activity of Compound L1 and its Copper and Zinc Complexes

The antimicrobial activity of compound L1 was evaluated against three microbial strains - *Candida albicans, Escherichia coli,* and *Staphylococcus aureus* - at different concentrations (1000 μg/ml, 800 μg/ml, 600 μg/ml, and 400 μg/ml). Table 4.5 presents

the mean inhibition zones for each strain and concentration, with statistical analysis indicating the significance of the results.

4.7.1.1 Antimicrobial Activity of Compound L1

Table 4.5 gives a summary of the antimicrobial activity of L1 against the three microbial strains. It shows the mean zones of inhibition from the different test solutions as measured relative to the antimicrobial standards.

Table 4.5: Antimicrobial Activity of Compound L1 against *Candida albicans*, *Escherichia coli*, and *Staphylococcus aureus*.

Conc	Organism	N	Zone of inhibition (mm)	Mean (mm)	Lsd (α=.05)	Cv (%)	P value
1000 µg/ml	*C. albicans*	3	13.27[b]	13.64	0.383	1.40	0.0136
	E. coli	3	13.73[a]				
	S. aureus	3	13.93[a]				
800 µg/ml	*C. albicans*	3	12.20[b]	12.20	0.46	1.87	0.0072
	E. coli	3	11.733[c]				
	S. aureus	3	12.67[a]				
600 µg/ml	*C. albicans*	3	11.57	11.68	0.73	3.13	0.667
	E. coli	3	11.63				
	S. aureus	3	11.83				
400 µg/ml	*C. albicans*	3	11.67	11.43	0.606	2.34	0.099
	E. coli	3	11.20				
	S. aureus	3	11.83				
Mean (mm)			12.31				
Lsd (α=.05)			0.28				
P value			<.0001				

At 1000 µg/ml, *S. aureus* was the most highly inhibited (13.93 mm), while *C. albicans* was the least inhibited (13.27 mm). The differences among these inhibition zones were significant ($p < 0.05$). At 800 µg/ml, *S. aureus* was the most highly inhibited (12.67 mm), whereas E. coli was the least inhibited (11.73 mm). The difference between *S. aureus* and E. coli was significant ($p < 0.05$). At 600 µg/ml, S. aureus showed the highest inhibition

(11.83 mm), followed closely by *C. albicans* (11.67 mm) and E. coli (11.63 mm). No significant differences were observed among these inhibition zones ($p > 0.05$). At 400 µg/ml, both *S. aureus* and *C. albicans* were the most highly inhibited (11.83 mm), while E. coli was the least inhibited (11.20 mm). The difference in inhibition zones was not significant ($p > 0.05$).

4.7.1.2 Antimicrobial Activity of Compound CuL1

The results of the antimicrobial activity of compound CuL1 are summarized in table 4.6.

Table 4.6: Antimicrobial Activity of Compound CuL1 against *Candida albicans, Escherichia coli,* and *Staphylococcus aureus.*

Conc	Organism	N	Zone of inhibition (mm)	Mean (mm)	Lsd (α=.05)	Cv (%)	P value
1000 µg/ml	*C. albicans*	3	19.03[a]	17.40	0.51	1.47	<.0001
	E. coli	3	14.50[b]				
	S. aureus	3	18.67[a]				
800 µg/ml	*C. albicans*	3	18.57[a]	16.59	0.84	2.53	<.0001
	E. coli	3	14.37[c]				
	S. aureus	3	16.83[b]				
600 µg/ml	*C. albicans*	3	17.17[a]	15.71	0.85	2.70	0.0001
	E. coli	3	13.63[b]				
	S. aureus	3	16.33[a]				
400 µg/ml	*C. albicans*		17.03[a]	15.27	0.56	1.83	<.0001
	E. coli		12.80[c]				
	S. aureus		15.97[b]				
Mean (mm)			16.24				
Lsd (α=.05)			0.29				
Cv (%)			2.17				
P value			<.0001				

[a] Means followed with same letters are not statistically significant an α=0.05

At 1000 µg/ml, *S. aureus* was the most highly inhibited (18.67 mm), while *E. coli* was the least inhibited (14.50 mm). The differences among these inhibition zones were significant ($p < 0.05$). At 800 µg/ml, *C. albicans* was the most highly inhibited (18.57 mm), whereas *E. coli* was the least inhibited (14.37 mm). The differences among these inhibition zones were significant ($p < 0.05$). At 600 µg/ml, *C. albicans* was the most highly inhibited (17.17 mm), while *E. coli* showed the lowest inhibition (13.63 mm). The differences among these inhibition zones were significant ($p < 0.05$). At 400 µg/ml, *C. albicans* was the most highly inhibited (17.03 mm), whereas *E. coli* was the least inhibited (12.80 mm). The differences among these inhibition zones were significant ($p < 0.05$).

4.7.1.3 Antimicrobial Activity of Compound ZnL1

At 1000 µg/ml, *E. coli* was the most highly inhibited (16.07 mm), while *C. albicans* showed the lowest inhibition (15.57 mm). The differences among these inhibition zones were not significant ($p > 0.05$). At 800 µg/ml, *C. albicans* was the most highly inhibited (15.43 mm), while *S. aureus* showed the lowest inhibition (14.43 mm). The differences among these inhibition zones were significant ($p < 0.05$). At 600 µg/ml, *S. aureus* was the most highly inhibited (13.93 mm), while *E. coli* showed the lowest inhibition (13.70 mm). The differences among these inhibition zones were significant ($p < 0.05$). At 400 µg/ml, *S. aureus* was the most highly inhibited (14.93 mm), while *E. coli* showed the lowest inhibition (12.87 mm). The differences among these inhibition zones were significant [($p < 0.05$) Table 4.7].

Table 4.7: Antimicrobial Activity of Compound ZnL1 against *Candida albicans*, *Escherichia coli*, and *Staphylococcus aureus*

Conc	Organism	N	Zone of inhibition (mm)	Mean (mm)	Lsd (α=.05)	Cv (%)	P value
1000 µg/ml	*C. albicans*	3	15.57	17.33	0.82	2.07	0.349
	E. coli	3	16.07				
	S. aureus	3	15.97				
800 µg/ml	*C. albicans*	3	15.43[a]	14.84	0.48	1.60	0.005
	E. coli	3	14.67[b]				
	S. aureus	3	14.43[b]				
600 µg/ml	*C. albicans*	3	14.43[b]	14.11	0.717	2.54	0.022
	E. coli	3	13.70[b]				
	S. aureus	3	13.93[a]				
400 µg/ml	*C. albicans*	3	13.63[a]	13.47	0.541	2.01	0.007
	E. coli	3	12.87[c]				
	S. aureus	3	14.93[b]				
Mean (mm)			14.58				
Lsd (α=.05)			0.378				
Cv (%)			2.24				
P value			<.0001				

[a] Means followed with same letters are not statistically significant an α=0.05

The data demonstrate that Compound L1 exhibits measurable bioactivity against *C. albicans*, *E. coli*, and *S. aureus*, with varying degrees of inhibition depending on the concentration. At 1000 µg/ml, *S. aureus* was the most inhibited, while *C. albicans* were the least inhibited. As the concentration decreased, *S. aureus* consistently showed the highest inhibition among the pathogens tested. This trend continued at lower concentrations, indicating that while Compound L1 is effective, its antimicrobial potency varies among different microorganisms. Compared to the findings of Ismail *et al.* (2023) for 2, 2′-bipyridine (2, 2′-Bipy), the inhibition zones observed for Compound L1 were slightly lower. For instance, the maximum inhibition of *S. aureus* by L1 was 13.93 mm at 1000 µg/ml, whereas Ismail *et al.* (2023) reported 17 mm for 2, 2′-Bipy. Similarly, *E. coli* exhibited a maximum inhibition of 13.73 mm with L1, compared to 12 mm for 2, 2′-

Bipy. For *C. albicans*, L1 showed 13.27 mm, while 2, 2′-Bipy achieved 18 mm. These differences may be due to experimental conditions, medium composition, and specific microbial strains used.

The data reveal that Compound CuL1 exhibits notably higher bioactivity compared to Compound L1 across various concentrations and pathogens. Specifically, CuL1 shows enhanced antifungal activity against *C. albicans*, with consistently larger inhibition zones compared to L1. For instance, at 1000 µg/ml, CuL1 achieves a maximum inhibition zone of 19.03 mm, significantly greater than the 13.27 mm observed with L1. This trend continues at lower concentrations, indicating that the copper complex substantially improves the antifungal efficacy of the bipyridine derivative.

Similarly, in terms of antibacterial activity, Compound CuL1 outperforms Compound L1, particularly against *S. aureus*. Although both compounds exhibit effective inhibition, CuL1 generally shows greater activity. For example, at 1000 µg/ml, CuL1 inhibits *S. aureus* by 18.67 mm, compared to the 13.93 mm achieved by L1. This suggests that the copper complex enhances antibacterial performance as well. When compared to the findings of Rajee *et al.* (2020) for [Cu(MET)$(bpy)_2$], CuL1 shows significant antimicrobial activity but with slightly lower inhibition zones. For instance, CuL1 achieves a maximum inhibition of 18.67 mm against *S. aureus* at 1000 µg/ml, whereas [Cu(MET)$(bpy)_2$] shows 21 mm. For *E. coli*, CuL1 reaches 14.50 mm, while [Cu(MET)$(bpy)_2$] exhibits 24 mm. Despite the lower inhibition zones, CuL1 demonstrates notable antimicrobial potential, indicating that the copper complex enhances bioactivity. The improved bioactivity of Compound CuL1 can be attributed to the role of copper in the complex. Copper ions likely enhance antimicrobial activity through several mechanisms, including increased permeability of microbial cell membranes, interference with essential enzyme systems and cellular processes, and generation of reactive oxygen species (ROS) that damage microbial cells.

The bioactivity results for Compound ZnL1 also indicate significant antimicrobial activity against *C. albicans*, *E. coli*, and *S. aureus*. At 1000 µg/ml, *E. coli* was the most inhibited (16.07 mm), while *C. albicans* showed the lowest inhibition (15.57 mm). At lower concentrations, *S. aureus* and *C. albicans* often showed the highest inhibition

zones. Comparing these results to Rajee *et al.* (2020) for [Zn(MET)(bpy)$_2$], ZnL1 exhibited lower inhibition zones. [Zn(MET)(bpy)$_2$] achieved inhibition zones of 24 mm for both *S. aureus* and *E. coli*, and 28 mm for *C. albicans*. In contrast, ZnL1 showed maximum inhibition zones of 15.97 mm for *S. aureus*, 16.07 mm for *E. coli*, and 15.57 mm for *C. albicans*. The reduced effectiveness of ZnL1 suggests it is less potent compared to [Zn(MET)(bpy)$_2$]. This variation likely stems from the ligand differences, with the methionine ligand in [Zn(MET)(bpy)$_2$] enhancing the zinc center's stability and reactivity, thereby improving its antimicrobial activity. The superior performance of [Zn(MET)(bpy)$_2$] highlights the critical role of ligand choice in optimizing the antimicrobial efficacy of metal complexes.

The results indicate that while Compound L1 and its metal complexes (CuL1 and ZnL1) exhibit notable antimicrobial activity, their effectiveness is generally lower than that of the previously studied [Cu(MET)(bpy)$_2$] and [Zn(MET)(bpy)$_2$] complexes. The enhanced bioactivity of the copper complex CuL1 over L1 suggests that copper's higher redox potential and greater reactivity offer a substantial antimicrobial advantage. Similarly, the zinc complex ZnL1 demonstrates significant activity but still falls short of the performance observed with [Zn(MET)(bpy)$_2$]. These differences underscore the importance of the ligand environment in enhancing the bioactivity of metal complexes and suggest potential areas for optimization in future research.

4.7.2 Antimicrobial Activity of Compound L2 and its Copper and Zinc Complexes

The antimicrobial activities of Compounds L2, ZnL2, and CuL2 were evaluated against three microbial strains—*Candida albicans, Escherichia coli,* and *Staphylococcus aureus*—at different concentrations. The data reveals the inhibitory effectiveness of each compound, with a focus on their mean inhibition zones and statistical significance, as indicated by LSD and p-values. Compound CuL2 demonstrated the highest bioactivity, particularly against *C. albicans* and *E. coli*, compared to Compounds L2 and ZnL2, suggesting the enhanced efficacy of copper.

4.7.2.1 Antimicrobial Activity of Compound L2

At 1000 μg/ml, *C. albicans* was the most highly inhibited (14.87 mm), while *E. coli* was the least inhibited (14.17 mm) as shown in Table 4.8.

Table 4.8: Antimicrobial Activity of L2 against *Candida albicans*, *Escherichia coli*, and *Staphylococcus aureus*

Conc	Organism	N	Zone of inhibition (mm)	Mean (mm)	Lsd (α=.05)	Cv (%)	P value
1000 µg/ml	*C. albicans*	3	14.87[a]	14.53	0.447	1.538	0.024
	E. coli	3	14.17[ab]				
	S. aureus	3	14.57[b]				
800 µg/ml	*C. albicans*	3	14.56[a]	13.24	0.99	3.77	0.0037
	E. coli	3	13.24[b]				
	S. aureus	3	12.80[b]				
600 µg/ml	*C. albicans*	3	13.17[a]	12.38	0.85	3.43	0.013
	E. coli	3	11.63[b]				
	S. aureus	3	12.33[ab]				
Mean (mm)			13.22				
Lsd (α=.05)			0.393				
Cv (%)			2.87				
P value			<.0001				

[a] Means followed with same letters are not statistically significant an α=0.05

The differences among these inhibition zones were significant ($p < 0.05$). At 800 µg/ml, *C. albicans* was the most highly inhibited (14.56 mm), whereas *S. aureus* was the least inhibited (12.80 mm). The differences among these inhibition zones were significant ($p < 0.05$). At 600 µg/ml, *C. albicans* was the most highly inhibited (13.17 mm), while *E. coli* showed the lowest inhibition (11.63 mm). The differences among these inhibition zones were significant ($p < 0.05$).

4.7.2.2 Antimicrobial Activity of Compound ZnL2

At 1000 µg/ml, *C. albicans* was the most highly inhibited (19.20 mm), while *E. coli* showed the lowest inhibition (14.33 mm) as shown in Table 4.9.

Table 4.9: Bioactivity of Compound ZnL2 against *C. albican, E. coli* and *S. aureus*

Conc	Organism	N	Zone of inhibition (mm)	Mean (mm)	Lsd (α=.05)	Cv (%)	P value
1000 µg/ml	*C. albicans*	3	19.20[a]	17.33	0.72	2.07	<.0001
	E. coli	3	14.33[c]				
	S. aureus	3	18.47[b]				
800 µg/ml	*C. albicans*	3	18.33[a]	16.52	0.92	2.79	0001
	E. coli	3	14.40				
	S. aureus	3	16.83[b]				
600 µg/ml	*C. albicans*	3	17.20 [a]	15.86	0.89	2.83	0.0002
	E. coli	3	13.80[b]				
	S. aureus	3	16.57[a]				
400 µg/ml	*C. albicans*	3	17.13[a]	15.44	0.50	1.62	<.0001
	E. coli	3	13.03[c]				
	S. aureus	3	16.17[b]				
Mean (mm)			16.28				
Lsd (α=.05)			0.378				
Cv (%)			2.38				
P value			<.0001				

[a] Means followed with same letters are not statistically significant an α=0.05

The differences among these inhibition zones were significant ($p < 0.05$). At 800 µg/ml, *C. albicans* was the most highly inhibited (18.33 mm), while *E. coli* showed the lowest inhibition (14.40 mm). The differences among these inhibition zones were significant ($p < 0.05$). At 600 µg/ml, *C. albicans* was the most highly inhibited (17.13 mm), while *E. coli* showed the lowest inhibition (13.80 mm). The differences among these inhibition zones were significant ($p < 0.05$). At 400 µg/ml, *C. albicans* was the most highly inhibited (17.13 mm), while *E. coli* showed the lowest inhibition (13.03 mm). The differences among these inhibition zones were significant ($p < 0.05$).

4.7.2.3 Antimicrobial Activity of Compound CuL2

At 1000 µg/ml, *C. albicans* was the most highly inhibited (19.03 mm), while *E. coli* was the least inhibited (14.50 mm). The differences among these inhibition zones were

significant ($p < 0.05$). At 800 µg/ml, *C. albicans* exhibited the highest inhibition (18.57 mm), while *E. coli* was the least inhibited (14.37 mm). The differences among these inhibition zones were significant ($p < 0.05$). At 600 µg/ml, *C. albicans* had the highest inhibition (17.17 mm) and *E. coli* showed the lowest inhibition (13.63 mm). The differences among these inhibition zones were significant ($p = 0.05$). At 400 µg/ml, *C. albicans* showed the highest inhibition (17.03 mm) and *E. coli* was the least inhibited (12.80 mm). The differences among these inhibition zones were significant [($p < 0.05$) Table 4.10].

Table 4.10: Bioactivity of Compound CuL2 against *C. albican, E. coli* and *S. aureus*

Conc	Organism	N	Zone of inhibition (mm)	Mean (mm)	Lsd (α=.05)	Cv (%)	P value
1000 µg/ml	*C. albicans*	3	19.03[a]	17.40	0.51	1.47	<.0001
	E. coli	3	14.50[b]				
	S. aureus	3	18.67[a]				
800 µg/ml	*C. albicans*	3	18.57[a]	16.59	0.84	2.53	<.0001
	E. coli	3	14.37[b]				
	S. aureus	3	16.83[c]				
600 µg/ml	*C. albicans*	3	17.17[a]	15.71	0.85	3.13	0.0001
	E. coli	3	13.63[b]				
	S. aureus	3	16.33[a]				
400 µg/ml	*C. albicans*	3	17.03[a]	15.17	0.56	1.83	<.0001
	E. coli	3	12.80[c]				
	S. aureus	3	15.97[b]				
Mean (mm)			16.24				
Lsd (α=.05)			0.29				
Cv (%)			2.18				
P value			<.0001				

[a] Means followed with same letters are not statistically significant an α=0.05

The data demonstrate that Compound CuL2 exhibits notably higher bioactivity compared to Compound L2 across various concentrations and pathogens. Specifically, CuL2 shows enhanced antifungal activity against *Candida albicans*, with consistently larger inhibition

zones compared to L2. For instance, at 1000 μg/ml, CuL2 achieves a maximum inhibition zone of 19.03 mm, significantly greater than the 14.87 mm observed with L2. This trend continues at lower concentrations, indicating that the copper complex substantially improves the antifungal efficacy of the pyrazole derivative. Similarly, in terms of antibacterial activity, Compound CuL2 outperforms Compound L2, particularly against *Escherichia coli*. Although both compounds exhibit effective inhibition, CuL2 generally shows slightly greater activity. For example, at 1000 μg/ml, CuL2 inhibits *E. coli* by 14.50 mm, compared to the 14.17 mm achieved by L2. This suggests that the copper complex enhances antibacterial performance as well. When compared to Compound ZnL2, both CuL2 and ZnL2 exhibit strong bioactivity, but CuL2 performs slightly better. For instance, CuL2 achieves slightly higher inhibition zones against *Candida albicans* and *E. coli* compared to ZnL2. At 1000 μg/ml, CuL2 inhibits *C. albicans* by 19.03 mm and *E. coli* by 14.50 mm, while ZnL2 shows 19.20 mm and 14.33 mm, respectively. This comparison indicates that while zinc complexes also exhibit significant antimicrobial properties, copper complexes may offer superior efficacy.

The improved bioactivity of Compound CuL2 can be attributed to the role of copper in the complex. Copper ions likely enhance antimicrobial activity through several mechanisms. First, copper may increase the permeability of microbial cell membranes, allowing for better penetration and disruption. Additionally, copper ions can interfere with essential enzyme systems and cellular processes such as DNA replication and repair. Furthermore, copper complexes can generate reactive oxygen species (ROS), like hydroxyl radicals and hydrogen peroxide, which are highly reactive and can damage microbial cells, contributing to the higher antimicrobial activity of CuL2.

In contrast, while zinc also contributes to antimicrobial effects, the slightly less pronounced activity compared to copper complexes suggests that copper's higher redox potential and greater reactivity offer a more substantial antimicrobial advantage. This observation supports the broader trend noted in the literature, where metal complexes, particularly those containing copper, often demonstrate superior antimicrobial properties compared to their non-metallic or zinc-based counterparts. As Kumar (2022) noted, metal complexes frequently exhibit enhanced antimicrobial activity, reinforcing the superior

effectiveness of copper-based complexes observed in this study. Supporting the relevance of pyrazole derivatives, studies by Kendre *et al.* (2015) and B'Bhatt and Sharma (2017) show that pyrazole-based compounds exhibit significant antibacterial and antifungal activities. Kendre *et al.* (2015) reported good antibacterial activity for certain pyrazole derivatives, while B'Bhatt and Sharma (2017) highlighted potent activity against both *E. coli* and *Candida albicans*. These findings align with the observed performance of Compound CuL2, emphasizing the potential of pyrazole derivatives as effective antimicrobial agents.

4.7.3 Antimicrobial Activity of Compound L3 and its Copper and Zinc Complexes against *C. albicans, E. coli* and *S. aureus*

The antimicrobial activity of Compound L3 (3-chloro-6-(3,5-dimethyl-1H-pyrazol-1-yl)pyridazine) and its metal complexes, ZnL3 and CuL3, was evaluated against *Candida albicans, Escherichia coli,* and *Staphylococcus aureus*. Compound L3 exhibited strong antifungal effects, particularly against *C. albicans*, but showed weaker antibacterial activity against *E. coli*.

4.7.3.1 Antimicrobial Activity of Compound L3

At 1000 μg/ml, *C. albicans* was the most highly inhibited (17.13 mm), while *E. coli* was the least inhibited (15.33 mm). The differences among these inhibition zones were significant ($p < 0.05$). At 800 μg/ml, *C. albicans* was the most highly inhibited (16.80 mm), while *E. coli* showed the lowest inhibition (14.67 mm). The differences among these inhibition zones were significant ($p < 0.05$). At 600 μg/ml, *C. albicans* was the most highly inhibited (15.70 mm), while *E. coli* showed the lowest inhibition (13.73 mm). The differences among these inhibition zones were significant ($p < 0.05$). At 400 μg/ml, *C. albicans* was the most highly inhibited (14.93 mm), while *E. coli* showed the lowest inhibition (13.53 mm). The differences among these inhibition zones were significant [($p < 0.05$) Table 4.11].

Table 4.11: Antimicrobial activity of Compound L3 against *C. albican, E. coli* and *S. aureus*

Conc	Organism	N	Zone of inhibition (mm)	Mean (mm)	Lsd (α=.05)	Cv (%)	P value
1000 µg/ml	*C. albicans*	3	17.13[a]	16.26	0.52	1.61	0.0005
	E. coli	3	15.33[c]				
	S. aureus	3	16.30[b]				
800 µg/ml	*C. albicans*	3	16.80	15.59	0.723	2.32	0.0007
	E. coli	3	14.67				
	S. aureus	3	15.50				
600 µg/ml	*C. albicans*	3	15.70[a]	14.63	0.85	2.92	0.0038
	E. coli	3	13.73[b]				
	S. aureus	3	14.47[b]				
400 µg/ml	*C. albicans*	3	14.93[a]	14.19	0.67	2.36	0.0063
	E. coli	3	13.53[b]				
	S. aureus	3	14.00[b]				
Mean (mm)			15.16				
Lsd (α=.05)			0.753				
Cv (%)			5.98				
P value			<.0001				

[a] Means followed with same letters are not statistically significant an α=0.05

4.7.3.2 Antimicrobial Activity of Compound ZnL3

At 1000 µg/ml, *S. aureus* was the most highly inhibited (21.60 mm), while *E. coli* showed the lowest inhibition (19.70 mm). The differences among these inhibition zones were significant ($p < 0.05$). At 800 µg/ml, *S. aureus* was the most highly inhibited (21.03 mm), while *C. albicans* showed the lowest inhibition (20.20 mm). The differences among these inhibition zones were significant ($p < 0.05$). At 600 µg/ml, *S. aureus* was the most highly inhibited (19.97 mm), while *E. coli* showed the lowest inhibition (18.37 mm). The differences among these inhibition zones were significant ($p < 0.05$). At 400 µg/ml, *S. aureus* was the most highly inhibited (18.50 mm), while *E. coli* showed the lowest

inhibition (16.93 mm). The differences among these inhibition zones were significant [($p < 0.05$) Table 4.12].

Table 4.12: Antimicrobial activity of Compound ZnL3 against *C. albican, E. coli and S. aureus*

Conc	Organism	N	Zone of inhibition (mm)	Mean (mm)	Lsd (α=.05)	Cv (%)	P value
1000 µg/ml	*C. albicans*	3	21.57[a]	20.95	0.603	1.44	0.0004
	E. coli	3	19.70[b]				
	S. aureus	3	21.60[a]				
800 µg/ml	*C. albicans*	3	21.27[a]	20.31	0.642	1.58	<.0001
	E. coli	3	18.63[b]				
	S. aureus	3	21.03[a]				
600 µg/ml	*C. albicans*	3	20.20[c]	19.51	0.821	2.11	0.003
	E. coli	3	18.37[b]				
	S. aureus	3	19.97[a]				
400 µg/ml	*C. albicans*	3	19.33[a]	18.26	0.669	1.83	0.0003
	E. coli	3	16.93[c]				
	S. aureus	3	18.50[b]				
Mean (mm)			19.75				
Lsd (α=.05)			0.335				
Cv (%)			1.74				
P value			<.0001				

[a] Means followed with same letters are not statistically significant an α=0.05

4.7.3.3 Antimicrobial Activity of Compound CuL3

At 1000 µg/ml, *S. aureus* was the most highly inhibited (21.30 mm), while *E. coli* was the least inhibited (19.37 mm) as shown in Table 4.13. The differences among these inhibition zones were significant ($p = 0.05$). At 800 µg/ml, *C. albicans* was the most highly inhibited (20.90 mm), whereas *E. coli* was the least inhibited (18.20 mm). The differences among these inhibition zones were significant ($p = 0.05$). At 600 µg/ml, *C. albicans* was the most highly inhibited (19.70 mm), while *E. coli* showed the lowest inhibition (17.87 mm). The differences among these inhibition zones were significant (p

= 0.05). At 400 µg/ml, *C. albicans* was the most highly inhibited (19.93 mm), whereas *E. coli* was the least inhibited (17.53 mm). The differences among these inhibition zones were significant (p = 0.05).

Table 4.13: Antimicrobial activity of Compound CuL3 against *C. albican, E. coli and S. aureus*

Conc	Organism	N	Zone of inhibition (mm)	Mean (mm)	Lsd (α=.05)	Cv (%)	P value
1000 µg/ml	*C. albicans*	3	21.27[a]	20.64	0.51	1.52	0.0004
	E. coli	3	19.37[b]				
	S. aureus	3	21.30[a]				
800 µg/ml	*C. albicans*	3	20.90[a]	19.87	0.72	1.81	0.0002
	E. coli	3	18.20[b]				
	S. aureus	3	20.50[a]				
600 µg/ml	*C. albicans*	3	19.70[a]	19.01	0.82	2.16	0.003
	E. coli	3	17.87[b]				
	S. aureus	3	19.47[a]				
400 µg/ml	*C. albicans*	3	19.93[a]	18.86	0.67	1.78	0.0003
	E. coli	3	17.53[c]				
	S. aureus	3	19.10[b]				
Mean (mm)			16.24				
Lsd (α=.05)			0.29				
Cv (%)			2.18				
P value			<.0001				

[a] Means followed with same letters are not statistically significant an α=0.05

The bioactivity of Compound L3 (3-chloro-6-(3, 5-dimethyl-1H-pyrazol-1-yl) pyridazine) and its copper (Cu) and zinc (Zn) complexes was evaluated against *Candida albicans*, *Escherichia coli*, and *Staphylococcus aureus*. Compound L3 demonstrated strong antifungal activity, especially against *C. albicans*, with consistently high inhibition zones across all tested concentrations. This suggests that L3 is particularly effective as an antifungal agent. However, its antibacterial activity was less effective against *E. coli*, which showed the least inhibition, indicating weaker activity against Gram-negative

bacteria. The copper complex CuL3 exhibited a notable enhancement in antimicrobial activity compared to L3 alone. Compound CuL3 produced significantly larger inhibition zones, particularly against *S. aureus* and *C. albicans*. At 1000 μg/ml, CuL3 effectively inhibited both *S. aureus* and *C. albicans*, while its effect on *E. coli* was comparatively lower. This enhanced activity at various concentrations highlights the superior antimicrobial potential of CuL3.

Similarly, the zinc complex ZnL3 also showed improved bioactivity over L3. ZnL3 was effective against *S. aureus* at 1000 μg/ml and also showed activity against *C. albicans*, though *E. coli* was still the least inhibited. This trend was consistent across lower concentrations, further demonstrating the effectiveness of ZnL3. The superior antimicrobial activity of CuL3 and ZnL3 can be attributed to several factors. The metal ions in these complexes likely enhance microbial cell membrane permeability, disrupt essential enzymatic systems, and generate reactive oxygen species (ROS) that damage microbial cells (Barua *et al.,* 2024). Specifically, the higher redox potential and reactivity of copper contribute significantly to its enhanced performance over zinc. Copper ions can engage in redox reactions that produce ROS, which are highly harmful to microbial cells (Chohan *et al.*, 2004).

4.7.4 Comparison of Compound Complexes

The antimicrobial activity of various compounds against *S. aureus, E. coli*, and *C. albicans* revealed significant differences in their effectiveness. Among the tested compounds, ZnL3 consistently demonstrated strong inhibition, particularly against S. *aureus* and *C. albicans*, highlighting its superior antimicrobial potential. Ampicillin and fluconazole served as reference standards, showing the highest inhibition against *S. aureus* and *C. albicans*, respectively, while ZnL3 followed closely behind. On the other hand, CuL3 also exhibited notable bioactivity, though it was less effective than ZnL3. The results suggest that metal ion complexes, particularly those involving zinc and copper, enhance antimicrobial efficacy by increasing cell membrane permeability and generating reactive oxygen species (ROS), thereby damaging microbial cells.

4.7.4.1 Antimicrobial activity of different compounds against *S. aureus*

The zone of inhibition of different compounds ranged from 15.93 mm to 27.73 mm. Analysis of variance revealed that there were significantly different inhibition zones among these compounds [$F(6, 14) = 500.10$, $p < 0.0001$]. Post hoc comparisons using the LSD test indicated that the inhibition zone for ampicillin was significantly higher (27.73 mm) and was followed by compound ZnL3 (21.60 mm), while that of compound CuL1 was significantly lower [(15.93 mm) Figure 22].

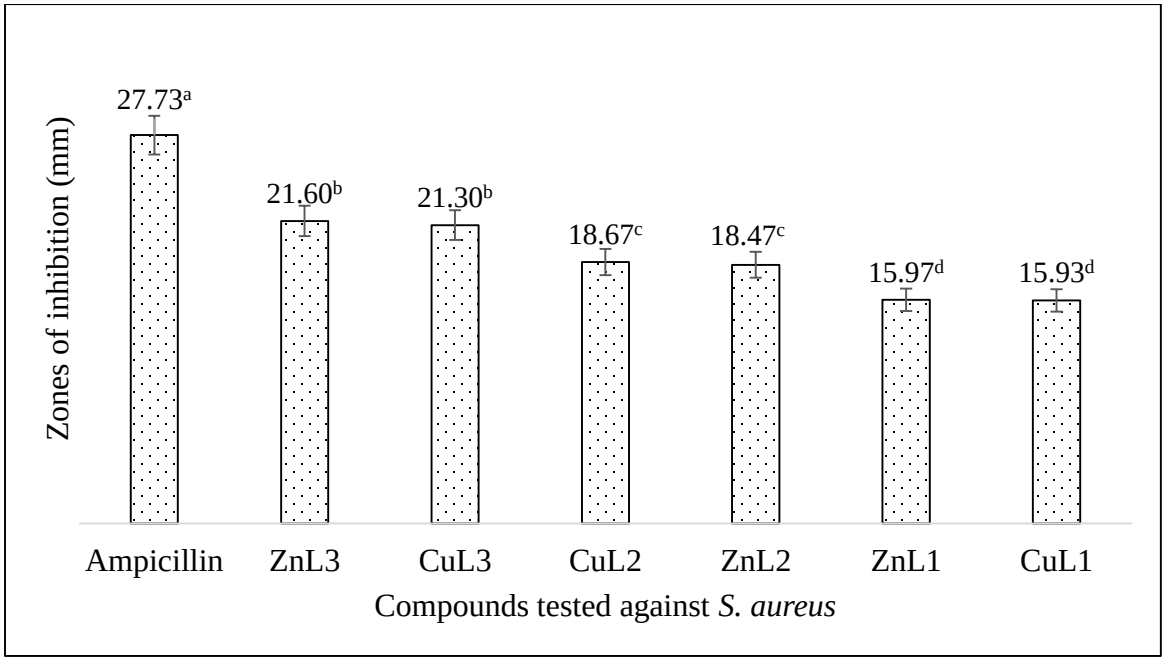

Figure 22: Bioactivity of different complexes compounds against S. aureus

4.7.4.2 Antimicrobial activity of different compounds against *E. coli*

The zone of inhibition of different compounds ranged from 14.33 mm to 25.47 mm. Analysis of variance revealed that there were significantly different inhibition zones among these compounds [$F(6, 14) = 492.24$, $p < 0.0001$]. Post hoc comparisons using the LSD test indicated that the inhibition zone for ampicillin was significantly higher (25.47 mm) and was followed by compound ZnL3 (19.70 mm), while that of compound ZnL2 was significantly lower [14.33 mm (Figure 23)].

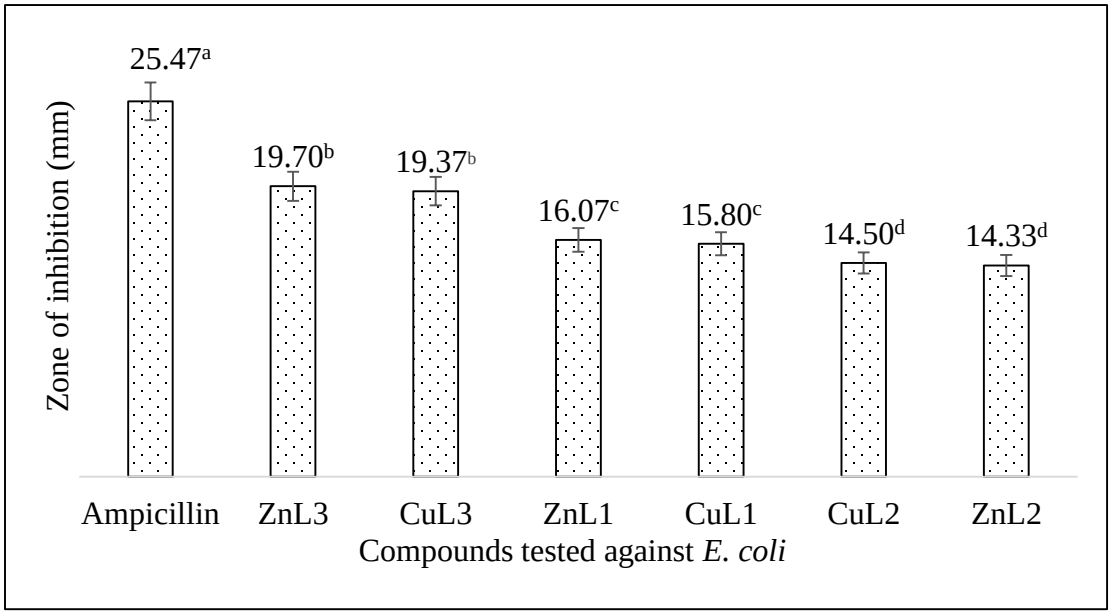

Figure 23: Bioactivity of different compounds against *E. coli*

4.7.4.3 Antimicrobial activity of different compounds against *C. albicans*

The zone of inhibition of different compounds ranged from 15.27 mm to 25.00 mm. Analysis of variance revealed that there were significantly different inhibition zones among these compounds [$F(6, 14) = 334.31$, $p < 0.0001$]. Post hoc comparisons using the LSD test indicated that the inhibition zone for fluconazole was significantly higher (25.00 mm) and was followed by compound ZnL3 (21.57 mm), while that of compound CuL1 was significantly lower [(15.27 mm) Figure 24].

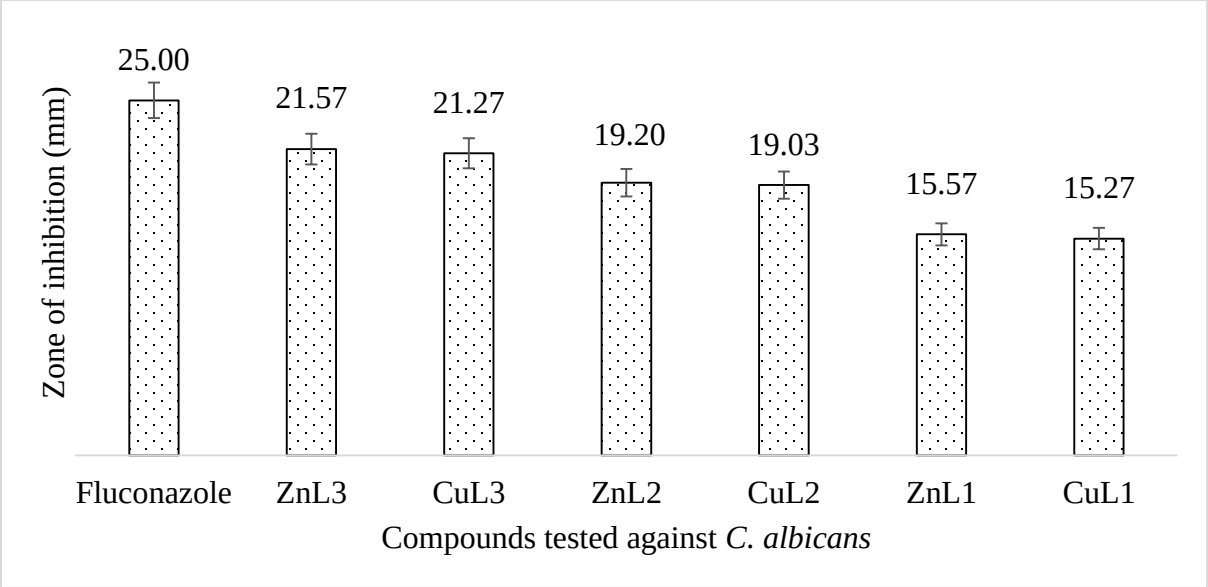

Figure 24: Inhibition of different compounds against microorganisms at 1000 µg/ml of Compound ZnL3

The zinc complex ZnL3 emerged as the most outstanding in terms of antimicrobial activity. ZnL3 demonstrated significant inhibition across all tested microorganisms, with the highest efficacy observed against *S. aureus* at 1000 µg/ml, and also effective against *C. albicans*. While *E. coli* was still the least inhibited, ZnL3 showed consistent and notable activity at lower concentrations, underscoring its superior antimicrobial potential. In contrast, the copper complex CuL3 also showed improved bioactivity compared to L3 alone, but it was less effective than ZnL3. CuL3 exhibited larger inhibition zones, particularly against *S. aureus* and *C. albicans*. At 1000 µg/ml, CuL3 was effective against both *S. aureus* and *C. albicans*, though its effect on *E. coli* was less pronounced. This enhanced activity highlights CuL3's antimicrobial potential, though it did not surpass ZnL3 in overall effectiveness.

The superior antimicrobial activity of ZnL3 and CuL3 can be attributed to several key factors. The metal ions in these complexes likely enhance microbial cell membrane permeability, disrupt essential enzymatic systems, and generate reactive oxygen species (ROS) that damage microbial cells (Barua *et al.*, 2024). Specifically, the ability of zinc to disrupt microbial cells and the higher redox potential of copper contribute to its

performance. Copper ions engage in redox reactions that produce ROS, which are highly harmful to microbial cells (Chohan *et al.*, 2004).

A search of the literature on the antimicrobial activity of 3-chloro-6-(3,5-dimethyl-1H-pyrazol-1-yl)pyridazine found no comparable studies, underscoring the originality of our findings. This lack of prior research highlights the novelty of our results for this specific compound and its metal complexes. Moreover, the enhanced antimicrobial activity of ZnL3 and the general effectiveness of metal complexes align with documented research. For instance, the copper complex $[Cu(bpy)(phen)(H_2O)_2]Cl_2.{}_2H_2O$ has been reported to exhibit exceptionally high antimicrobial activity, reinforcing the notion that copper complexes often outperform other metal complexes in efficacy (Agwara *et al.*, 2010).

4.7.5 Inhibition of Microorganisms at 1000 µg/ml of Compound ZnL3

At 1000 µg/ml of Compound ZnL3, *S. aureus* was the most highly inhibited with a mean inhibition zone of 21.60 mm, while *E. coli* showed the lowest inhibition with a mean inhibition zone of 19.70 mm. The inhibition zones for *S. aureus* and *C. albicans* were significantly higher than those for *E. coli* ($p < 0.05$). The overall mean inhibition zone across all organisms was 20.96 mm, with a coefficient of variation of 1.44%. The least significant difference (LSD) was 0.603, indicating that differences between the inhibition zones greater than this value are statistically significant (Figure 25).

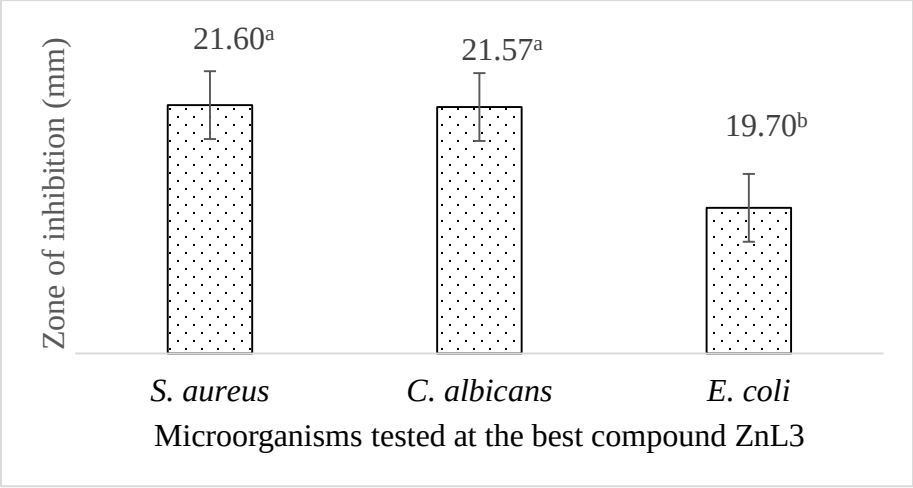

Figure 25: Inhibition of different compounds against microorganisms at 1000 µg/ml of Compound ZnL3

The antimicrobial activity of Compound ZnL3 at a concentration of 1000 µg/ml demonstrates promising results, particularly in its effectiveness against *Staphylococcus aureus* and *Candida albicans*. The inhibition of *S. aureus* at this concentration, which yielded the highest inhibition zone, displays the potent activity of ZnL3 against this Gram-positive bacterium. This result is noteworthy given the clinical significance of *S. aureus* as a pathogen, often associated with serious infections and known for its ability to develop resistance to various antibiotics (Nikolic and Mudgil, 2023; Tuon *et al*., 2023). In contrast, *Escherichia coli* exhibited the lowest inhibition zone in response to ZnL3, indicating a lower efficacy of the compound against this Gram-negative bacterium. This differential activity is consistent with the general observation that Gram-negative bacteria, such as *E. coli*, possess more impermeable cell membranes and additional efflux mechanisms that can reduce the efficacy of antimicrobial agents (Zhou *et al*., 2023). The effectiveness of ZnL3 against *C. albicans* highlights its potential as an antifungal agent. The significant inhibition observed against *C. albicans* aligns with its application in antifungal therapy, suggesting that ZnL3 could be beneficial in treating fungal infections.

CHAPTER FIVE: CONCLUSIONS AND RECOMMENDATIONS

5.1 Summary

The N, N' bidentate ligands were successfully synthesized from the reactions of equimolar amounts of 3-chloro-6-hydrazinylpyridazine with malonaldeyde and acetylacetone in an appropriate solvent. The transition metal (II) complexes were synthesized by the reaction of the ligands and the metal salts in the ratio 2:1. They were isolated and characterized using spectroscopic and analytical techniques.

The ligands L1-L3 as well as their complexes were investigated for their antimicrobial activity against selected Gram-positive and a Gram-negative bacteria. The observed activities indicate that a good number of the synthesized complexes are active. Of significance are the copper and zinc complexes of L3 which are significantly active against both *C. albicans*, *S. aureus* and *E. coli*. Complexes of L1 are the least active towards either of the microbial strains.

5.2 Conclusion

The heterocyclic N, N' bidentate ligands and their copper and zinc complexes were successfully synthesized and characterized. The ligand exclusively coupled to the metal (II) ion via the azo-methine nitrogen, according to the results of the UV-VIS, FT-IR, and ^{1}H-NMR spectral analyses. For the metal (II) complexes, an octahedral structure has been suggested. The synthesized compounds are not electrolytes, according to conductance measurements where they all have conductivities below 50 $\Omega^{-1}cm^{2}mol^{-1}$. The complexes showed improved antimicrobial properties in comparison to the parent ligands. *E. coli* was the most resistant bacterial strain, while the most efficient compound against all the microorganisms was the ZnL3 complex. As concentration grew, so did the N, N'-bidentate ligands' and its metal (II) complexes' capacity to inhibit these bacterial strains.

5.2 Recommendations of the study

i. These compounds in particular the complexes should be considered as lead candidates in the development of more effective antibacterial agents targeting common pathogens such as *E. coli, S. aureus,* and *C. albicans.*

ii. Given the stability of the synthesized complexes and their activity against certain bacteria, additional research with different ligands complexed with the metals is recommended to elucidate their mechanisms of action.

iii. The study focused solely on the bacterial and fungal activity of the synthesized compounds. Further investigation is needed to explore other antimicrobial properties, such as antiviral and anti-parasitic activities.

iv. It is advisable to conduct toxicity tests and determine the Minimum Inhibitory Concentration (MIC) of these compounds.

v. The synthesized complexes should also be evaluated for their catalytic properties to assess their potential catalytic activity.

REFERENCES

Adeloye, A. O., Olomola, T. O., Adebayo, A. I. & Ajibade, P. A. (2012). A high molar extinction coefficient bisterpyridyl homoleptic Ru (II) complex with trans-2-methyl-2-butenoic acid functionality: Potential dye for dye-sensitized solar cells. *International Journal of Molecular Sciences,* 13, 3511-3526.

Agwara, M. O., Ndifon, P. T., Ndosiri, N. B., Paboudam, A. G., Yufanyi, D. M., & Mohamadou, A. (2010). Synthesis, characterisation and antimicrobial activities of cobalt (II), copper (II) and zinc (II) mixed-ligand complexes containing 1, 10-phenanthroline and 2, 2'-bipyridine. *Bulletin of the Chemical Society of Ethiopia*, 24, 313-317.

Ali, H.A., Omar, S.N., Darawsheh, M.D. & Fares, H. (2016). Synthesis, characterization, and antimicrobial activity of zinc (II) ibuprofen complexes with nitrogen-based ligands. *Journal of Coordination Chemistry. 69*(6), 1110-1122.

Alias, M., Kassum, H., & Shakir, C. (2014). Synthesis, physical characterization and biological evaluation of Schiff base M(II) complexes. *Journal of the Association of Arab Universities for Basic and Applied Sciences,* 15(1), 954-966.

Aljamali, N. M., Hadi, M. A., Mohamad, M. S., & Salih, A. M. (2019). Review on imine derivatives and their applications. *International Journal of Photochemistry, 5*(1), 1-10.

Ammann, A. A. (2016). Inductively coupled plasma mass spectrometry (ICP-MS): A versatile tool. *Journal of Mass Spectrometry, 51(*1), 49-54.

Amudat, L. (2020). Preparation, characterization and antibacterial activity of Mn (II), Cu (II) and Zn (II) complexes of methionine and 2, 2-bipyridine co-ligands. *Journal of the Kenya Chemical Society*, 13-1, 16-21.

Ang, W. H., Casini, A., Sava, G., & Dyson, P. J. (2011). Organometallic ruthenium-based antitumor compounds with novel modes of action. *Journal of Organometallic Chemistry*, *696*(5), 989-998.

Arias, C. A., & Murray, B. E. (2012). The rise of the Enterococcus: beyond vancomycin resistance. *Nature Reviews Microbiology*, *10*(4), 266–278.

Arif, R., Nayab, P. S., Ansari, I. A., Shahid, M., Irfan, M., Alam, S., & Abid, M. (2018). Synthesis, molecular docking and DNA binding studies of phthalimide-based copper (II) complex: *In vitro* antibacterial, hemolytic and antioxidant assessment. *Journal of Molecular Structure*, *1160*, 142-153.

Arul S., & Manjula, B. (2013). Preparation, characterization, antimicrobial activities and DNA cleavage studies of Schiff base complexes derived from 4-amino antipyrine. *Asian Journal of Biochemical and Pharmaceutical Research,* 3(1), 168-178.

Ather, A. Q., Tahir, M. N., Khan, M. A., Athar, M. M., & Bueno, E. A. S. (2010). 3-Chloro-6-(3, 5-dimethyl-1H-pyrazol-1-yl) pyridazine. *Acta Crystallographica Section E: Structure Reports Online*, *66*(10), o2493-o2493.

Ather, A.Q., Chaudhry, F., Muhammad, N., Eliana, A. S., Misbahul, A. K., Aslam, N., Khalid, M. K., Athar, M. M., Munawar, A. M., Muhammad, A. & Syeda, A. (2013). Synthesis, antibacterial and antioxidant properties of pyrazolylpyridazines. *Asian Journal of Chemistry; 25*(14), 7743-7748.

Atkins, P., & de Paula, J. (2006). *Physical Chemistry (8th Ed.).* Oxford University Press.

B'Bhatt, H., & Sharma, S. (2017). Synthesis and antimicrobial activity of pyrazole nucleus containing 2-thioxothiazolidin-4-one derivatives. *Arabian Journal of Chemistry.*, 10, S1590–S1596.

Bach, D. H., Liu, J. Y., Kim, W. K., Hong, J. Y., Park, S. H., Kim, D., ... & Lee, S. K. (2017). Synthesis and biological activity of new phthalimides as potential anti-inflammatory agents. *Bioorganic & medicinal chemistry*, *25*(13), 3396-3405.

Baker, M. J., Byrne, H. J., & Sockalingum, G. D. (2020). Recent advances in FTIR spectroscopy and imaging: Disease diagnosis and beyond. *Trends in Analytical Chemistry, 132,* 116029.

Baldus, M., & Günther, G. (2012). Solid-state NMR spectroscopy: An emerging technique in structural biology. *Nature Reviews Molecular Cell Biology*, *13*(3), 168-178.

Barua, M., Bandyopadhyay, S., Wasai, A. G., Roy, I. G., & Mandal, S. (2024). A trinuclear Zn (II) schiff base dicyanamide complex attenuates bacterial biofilm formation by ROS generation and membrane damage and exhibits anticancer activity. *Microbial Pathogenesis*, 188, 106548.

Basu, B., & Date, A. W. (1998). Numerical modelling of melting and solidification problems—A review. *Sadhana*, 13(3), 169-213

Batley, G. E., Kirby, J. K., & McLaughlin, M. J. (2013). Fate and risks of nanomaterials in aquatic and terrestrial environments. *Accounts of Chemical Research*, *46(*3), 854-862.

Bauer, A. W., Kirby, W. M., Sherris, J. C., & Turck, M. (1966). Antibiotic susceptibility testing by a standardized single disk method. *American Journal of Clinical Pathology, 45(4), 493-496.*

Bax, R., Mullan, N., Verhoef, J. (2000). The millennium bugs — the need for and development of new antibacterials. *International Journal of Antimicrobial Agents 16* (1) 51– 59

Beauchemin, D. (2020). Inductively coupled plasma mass spectrometry. *Spectrochimica Acta Part B: Atomic Spectroscopy, 169,* 105861.

Beletskaya, I. P. & Cheprakov, A. V. (2000). The synthesis of bipyridines and their complexes. *Chemical Reviews*. *100* (8): 3009–3066.

Bello-Vieda, N.J., Pastrana, H.F. & Garavito, M.F. (2018). Antibacterial activities of azole complexes combined with silver nanoparticles. *Molecules 23*(1):1–17

Bernier, C. M., Duchane, C. M., Martinez, J. S., Falkinham, J. O., & Merola, J. S. (2021). Synthesis, characterization, and antimicrobial activity of RhIII and IrIII N-heterocyclic carbene piano-stool complexes. *Organometallics, 40*(10), 1670–1681.

Bhatt, J. J., Suresh, K. D., & Mrugesh, H. T. (2019). Synthesis, characterization and anti-microbial activity of pyrazole capped 2-azitidinone derivatives. *RJLBPCS*, 5(1), 647-662.

Biot, C., Castro, W., Botté, C. Y., & Navarro, M. (2012). The therapeutic potential of metal-based antimalarial agents: implications for the mechanism of action. *Dalton Transactions, 41*(21), 6335-6349.

Blair, J. M. A., Webber, M. A., Baylay, A. J., Ogbolu, D. O., & Piddock, L. J. V. (2015). Molecular mechanisms of antibiotic resistance. *Nature Reviews Microbiology, 13*(1), 42–51.

Blake, A. J., Champness, N. R., & Schroder, M. (Eds.). (2017). *X-ray crystallography*. Royal Society of Chemistry.

Boni, A., Pampaloni, G., Peloso, R., Belletti, D., Graiff, C., & Tiripicchio, A. (2006). Synthesis of copper (I) bis(3,5-dimethyl pyrazolyl)methane olefin complexes and their reactivity towards carbon monoxide. *Journal of Organometallic Chemistry, 691*(26), 5602–5609.

Boros, E., Dyson, P. J., & Gasser, G. (2020). Classification of metal-based drugs according to their mechanisms of action. *Chem, 6*(1), 41–60.

Borthagaray, G., Mondelli, M., & Torre, M. H. (2016). Essential transition metal ion complexation as a strategy to improve the antimicrobial activity of organic drugs. *Journal of Infectious Diseases and Epidemiol*ogy, *2*(2).

Brewer, G. J. (2019). Copper toxicity in the general population. *Clinical Neurophysiology Practice, 4,* 183-191.

Brown, D. G., Gagnon, M. M. & Bostrom, J. (2015). Understanding our love affair with 4 p-chlorophenyl: present-day implications from historical biases of reagent 5 selection. *Journal of Medicinal Chemistry* 58, 2390–2405.

Bush, K., Courvalin, P., Dantas, G., Davies, J., Eisenstein, B., Huovinen, P., Jacoby, G.A., Kishony, R., Kreiswirth, B.N. & Kutter, E. (2011). Tackling antibiotic resistance. *Native Review of Microbiology*, 9, 894–896.

Bushuev, M. B., Virovets, A. V., Peresypkina, E. V., Naumov, D. Y., Potapov, A. S., Khlebnikov, A. I., Vasilevsky, S. F., & Lavrenova L. G. (2005). Synthesis and structure of (Bis(3,5-Dimethyl-1H-Pyrazol-1-yl)Methane)diiodocobalt(II). *Journal of Structural Chemistry, 46*(6), 1099-1103.

Büssing, R., Karge, B., Lippmann, P., Jones, P. G., Brönstrup, M., & Ott, I. (2021). Gold (I) and Gold (III) N- Heterocyclic Carbene Complexes as Antibacterial Agents and Inhibitors of Bacterial Thioredoxin Reductase. *ChemMedChem*, *16*(22), 3402-3409.

Busto, N., Vigueras, G., Cutillas, N., García, B., & Ruiz, J. (2022). Inert cationic iridium(III) complexes with phenanthroline-based ligands: application in antimicrobial inactivation of multidrug-resistant bacterial strains. *Dalton Transactions, 51*(29), 9653–9663.

Cao, Z., Zhang, L., Jiang, S., & Lai, Y. (2021). Copper complexes with anticancer activity. *European Journal of Medicinal Chemistry, 220, 113534.*

Castillo, K. F., Bello-Vieda, N. J., Nuñez-Dallos, N. G., Pastrana, H. F., Celis, A. M., Restrepo, S., ... & Ávila, A. G. (2016). Metal complex derivatives of azole: A study on their synthesis, characterization, and antibacterial and antifungal activities. *Journal of the Brazilian Chemical Society*, *27*(12), 2334-2347.

Catalano, A., Iacopetta, D., Ceramella, J., Scumaci, D., Giuzio, F., Saturnino, C., Aquaro, S., Rosano, C., & Sinicropi, M. S. (2022). Multidrug resistance (MDR): a widespread phenomenon in pharmacological therapies. *Molecules*, *27*(3), 616.

Caubet, M.S., Laplante, A., Caillé, J. & Brazier, J.L. (2002). "[^{13}C]aminopyrine and [^{13}C]caffeine breath test: influence of gender, cigarette smoking, and oral contraceptives intake". *Isotopes in Environmental and Health Studies. 38* (2): 71–7.

Cavanagh, J., Fairbrother, W. J., Palmer, A. G., & Skelton, N. J. (2010). *Protein NMR spectroscopy: Principles and practice*. Academic Press.

Chandraleka, S. Ramya, K., Chandramohan, G., Dhanasekaran, D., Priyadharshini, A. & Panneerselvam, A. (2011). Antimicrobial mechanism of copper (II) 1,10-phenanthroline and 2,20 - bipyridyl complex on bacterial and fungal pathogens. *Journal of Saudi Chemical Society*. *280,* 41129–41136.

Chellan, P., Landino, L. M., & Fridovich, I. (2018). Copper, an important player in human disease. *Cellular and Molecular Life Sciences, 75(18),* 3371-3384.

Chen L., Thompson K., Bridson N., & Chenvol L. (1993). Dinuclear copper (II) and copper (I) complexes of tetra dentate (N4) thio-diazine ligands; synthetic, structural, magnetic and electrochemical studies: in situ oxidation of copper(I) complexes to produce dinuclear hydroxo-bridged copper(II) complexes. *Inorganica Chimica Acta, 214*, 67–76.

Cheng, M.-L., Li, H.-X., Zang, Y., & Lang, J.-P. (2006). Dichloro[(3,5-dimethyl-1H-pyrazol-1-yl)methane]zinc(II) and di-μ-chloro-bis{chloro[(3,5-dimethyl-1H-pyrazol-1-yl)methane]cadmium(II)}. *Acta Crystallographica Section C Crystal Structure Communications, 62*(2), 74–77.

Chohan, Z. H., Supuran, C. T., & Scozzafava, A. (2004). Metalloantibiotics: synthesis and antibacterial activity of cobalt (II), copper (II), nickel (II) and zinc (II) complexes of kefzol. *Journal of Enzyme Inhibition and Medicinal Chemistry*, 19(1), 79-84.

Chruszcz-Lipska, K., Zelek-Pogudz, S., Solecka, U., Solecki, M. L., Szostak, E., Zborowski, K. K., & Zając, M. (2022). Use of the far infrared spectroscopy for NaCl and KCl minerals characterization—A case study of halides from Kłodawa in Poland. *Minerals, 12*(12), 1561.

ChunYan, Z., RuJian, Y., LiQiang, W., HaiYan, H., JinTao, W., XiangWen, L., XueMin, D., & YanShi, X. (2022). Design, synthesis, and evaluation of arylthioether ruthenium polypyridine complexes: a multi-target antimicrobial agents against gram-positive bacteria. *European Journal of Medicinal Chemistry, 240,* 114562.

Claridge, T. D. W. (2016). *High-resolution NMR techniques in organic chemistry*. Elsevier.

Claudel, M., Schwarte, J. V., & Fromm, K. M. (2020). New antimicrobial strategies based on metal complexes. *Chemistry*, *2*(4), 849-899.

Clinical and Laboratory Standards Institute (CLSI). (2018). Performance Standards for Antimicrobial Susceptibility Testing. *28th edition.* CLSI supplement M100. Wayne, PA: *Clinical and Laboratory Standards Institute.*

Clinical and Laboratory Standards Institute (CLSI). (2020). Performance Standards for Antimicrobial Susceptibility Testing. *30th Edition*. *CLSI Supplement M100. Wayne, PA, USA.*

Cooper, S. M., Siakalli, C., White, A. J. P., Frei, A., Miller, P. W., & Long, N. J. (2022). Synthesis and anti-microbial activity of a new series of bis (diphosphine) rhenium(V) dioxo complexes. *Dalton Transactions, 51*(40), 12791–12795.

Davies, J., & Davies, D. (2010). Origins and evolution of antibiotic resistance. *Microbiology and Molecular Biology Reviews, 74*(3), 417–433.

Denning, D. W., & Bromley, M. J. (2015). Infectious disease. How to bolster the antifungal pipeline. *Science, 347*(6229), 1414–1416.

Deswal, Y., Asija, S., Dubey, A., Deswal, L., Kumar, D., Jindal, D. K., & Devi, J. (2022). Cobalt (II), nickel (II), copper (II) and zinc (II) complexes of thiadiazole based Schiff base ligands: Synthesis, structural characterization, DFT, antidiabetic and molecular docking studies. *Journal of Molecular Structure*, *1253*, 132266.

Dickert, H., Machka, K., & Braveny, I. (1981). The uses and limitations of disc diffusion in the antibiotic sensitivity testing of bacteria. *Infection*, *9*(1), 18-24.

Dickey, S. W., Cheung, G. Y. C. & Otto, M. (2017). Different drugs for bad bugs: antivirulence strategies in the age of antibiotic resistance. *Nature Reviews Drug Discovery, 16*(7), 457–471.

Dong, R., & Hao, J. (2010). Complex fluids of poly (oxyethylene) monoalkyl ether nonionic surfactants. *Chemical reviews*, *110*(9), 4978-5022.

DuChane, C. M., Karpin, G. W., Ehrich, M., Falkinham, J. O., & Merola, J. S. (2019). Iridium piano stool complexes with activity against *S. aureus* and MRSA: it is past time to truly think outside of the box. *MedChemComm, 10*(7), 1391–1398.

Eckert, H. (2019). Applications of solid-state NMR in materials chemistry. *Journal of Solid State Chemistry, 272*, 82-97.

Eicher, T., Hauptmann, S., & Speicher, A. (2013). *The chemistry of heterocycles: structures, reactions, synthesis, and applications*. John Wiley & Sons.

Elie, M., (2007). NMR and computational studies of substituted 2,2'-bipyridines in solution. *The Journal of Physical Chemistry A*, 111(47), 11842-11848. DOI: 10.1021/jp075436r

Eremina, J. A., Lider, E. V., Samsonenko, D. G., Sheludyakova, L. A., Berezin, A. S., Klyushova, L. S., ... & Trifonov, R. E. (2019). Mixed-ligand copper (II) complexes with tetrazole derivatives and 2, 2′-bipyridine, 1, 10-phenanthroline: Synthesis, structure and cytotoxic activity. *Inorganica Chimica Acta*, *487*, 138-144.

Ernst, R. R. (2017). Nuclear magnetic resonance Fourier transform spectroscopy (Nobel lecture). *Angewandte Chemie International Edition in English*, *56*(12), 1452-1462.

Evangelinou, O., Hatzidimitriou, A. G., Velali, E., Pantazaki, A. A., Voulgarakis, N., & Aslanidis, P. (2014). Mixed-ligand copper (I) halide complexes bearing 4, 5-bis (diphenylphosphano)-9, 9-dimethyl-xanthene and N-methylbenzothiazole-2-thione: Synthesis, structures, luminescence and antibacterial activity mediated by DNA and membrane damage. *Polyhedron*, *72*, 122-129.

Evans, J. S. O., & Prince, E. (2012). *Crystallography and crystal defects*. Cambridge University Press.

Evans, R. D., & Guillong, M. (2021). Advances in laser ablation ICP-MS for in situ analysis. *Elements, 17*(1), 27-32.

Fernandez, L., & Hancock, R. E. W. (2012). Adaptive and mutational resistance: role of porins and efflux pumps in drug resistance. *Clinical Microbiology Reviews, 25*(4), 661–681.

Fonseca, D., Páez, C., Ibarra, L., García-Huertas, P., Macías, M. A., Triana-Chávez, O., & Hurtado, J. J. (2019). Metal complex derivatives of bis (pyrazol-1-yl) methane ligands: Synthesis, characterization and anti-Trypanosoma cruzi activity. *Transition Metal Chemistry*, *44*, 135-144.

Forbes, B. A., Sahm, D. F., & Weissfeld, A. S. (2007). *Diagnostic microbiology*. St Louis: Mosby.

Frederickson, C. J. (2005). Zinc and the brain: Progress in understanding the role of zinc in neurodegenerative disorders. *Annual Review of Nutrition, 25*, 257-281.

Frei, A., Ramu, S., Lowe, G. J., Dinh, H., Semenec, L., Elliott, A. G., Zuegg, J., Deckers, A., Jung, N., & Bräse, S. (2021). Platinum cyclooctadiene complexes with activity against gram-positive bacteria. *ChemMedChem*, *16*(20), 3165–3171.

Frei, A., Ramu, S., Lowe, G. J., Dinh, H., Semenec, L., Elliott, A. G., Zuegg, J., Deckers, A., Jung, N., & Bräse, S. (2021). Platinum cyclooctadiene complexes with activity against gram-positive bacteria. *ChemMedChem*, *16*(20), 3165–3171.

Frost, L. S., Leplae, R., Summers, A. O., & Toussaint, A. (2005). Mobile genetic elements: the agents of open source evolution. *Nature Reviews Microbiology*, *3*(9), 722–732.

Furukawa, H., Cordova, K. E., O'Keeffe, M., & Yaghi, O. M. (2010). The chemistry and applications of metal-organic frameworks. *Science*, 329(5993), 424-428.

Giacovazzo, C., & Monaco, H. L. (Eds.). (2012). *Fundamentals of crystallography*. Oxford University Press

Giancardo, G.L. & Bonati, F. (1989). Bis(pyrazolyl)methanetetracarbonyl-chromium(0), -molybdenum(0) and -tungsten(0). *Journal of Organometallic Chemistry*. *366*,(1 – 2), 121 – 127.

Gichumbi, J. M., Friedrich, H. B., Omondi, B., Singh, M., Naicker, K., & Chenia, H. Y. (2016). Synthesis, characterization, and cytotoxic and antimicrobial activities of ruthenium (II) arene complexes with N, N-bidentate ligands. *Journal of Coordination Chemistry*, *69*(23), 3531-3544.

Gichumbi, J.M. & Friedrich, H.B. (2018**)**. Half-sandwich complexes of platinum group metals (Ir, Rh, Ru, and Os) and some recent biological and catalytic applications. *Journal of Organometallic Chemistry 866*, 123–143.

Gichumbi, J.M.; Friedrich, H.B.; Omondi, B.; Lazarus, G.G.; Singh, M.; Chenia, H.Y. (2018). Synthesis, characterization, anticancer and antimicrobial study of arene ruthenium(II) complexes with 1,2,4-triazole ligands containing an α-diimine moiety. *Z. Naturforsch. B 73*, 167–178.

Goldstein, J. I., Newbury, D. E., Michael, J. R., & Ritchie, N. W. (2017). *Scanning electron microscopy and X-ray microanalysis.* Springer.

Grass, G., & Rensing, C. (2001). CueO is a multi-copper oxidase that confers copper tolerance in *Escherichia coli. Biochemical and Biophysical Research Communications, 286*(5), 902-908.

Griffiths, P. R., & de Haseth, J. A. (2018). *Fourier transform infrared spectrometry*. John Wiley & Sons.

Gupta, A., Das, S., & Mitra, S. (2019). Copper complexes: Promising therapeutic agents in pursuit of cancer therapy. *European Journal of Medicinal Chemistry*, *176*, 69-103.

Haase, H., & Maret, W. (2003). Intracellular zinc fluctuations modulate protein tyrosine phosphatase activity in insulin/insulin-like growth factor-1 signaling. *Experimental Cell Research, 291(2), 289-298.*

Hadjikakou, S. K., & Hadjiliadis, N. (2009). Antiproliferative and anti-tumor activity of organometallic compounds: DNA interactions. *Coordination Chemistry Reviews*, 253(17-18), 2350-2362.

Hall-Stoodley, L., Costerton, J. W., & Stoodley, P. (2004). Bacterial biofilms: from the natural environment to infectious diseases. *Nature Reviews Microbiology*, *2*(2), 95–108.

Hayden, F. G., & Shindo, N. (2019). Influenza virus polymerase inhibitors in clinical development. *Current Opinion in Infectious Diseases*, *32*(2), 176–186.

Helliwell, J. R., & Tanaka, I. (Eds.). (2017). *High-resolution X-ray diffraction and imaging*. CRC Press.

Hernández-Molina, M., González-Platas, J., Ruiz-Pérez, C., Lloret, F., & Julve, M. (1999). Crystal structure and magnetic properties of the single-μ-chloro copper (II) chain [Cu (bipy) Cl2](bipy= 2, 2′-bipyridine). *Inorganica chimica acta*, *284*(2), 258-265.

Hookey, J. V., Richardson, J. F., & Cookson, B. D. (1998). Molecular typing of Staphylococcus aureus based on PCR restriction fragment length polymorphism and DNA sequence analysis of the coagulase gene. *Journal of clinical microbiology*, *36*(4), 1083-1089.

Housman, T. S., Jorizzo, J. L., McCarty, M. A., Grummer, S. E., Fleischer, A. B., & Sutej, P. G. (2003). Low-dose thalidomide Therapy for Refractory Cutaneous Lesions of *LupusErythematosus*. *Archives of dermatology*, *139*(1), 50-54.

Hu, Q., Yu, Y., Gu, D., Xie, L.I., Chen, X., Xu, N., Ruan, J.J., Dowson, C., Ruan, B.H. (2019). Detection of ‘‘Hidden” antimicrobial drug resistance, *ACS Infectious Diseases* 5 (7) 1252–1263,

Huang, Y., Zhang, Y., & Chen, X. (2021). Portable FTIR spectroscopy for in situ environmental monitoring. *Environmental Science & Technology, 55*(2), 1123-1131.

Huang, Z. (2016). The multifunctional roles of zinc in the nervous system of insects. *Metallomics*, *8*(2), 245-255.

Huffman, G. P. (2011). Methods for elemental analysis of coal and coal ash. *Energy & Fuels*, *25*(4), 1812-1826.

Humphries, R. M., & Hindler, J. A. (2015). Susceptibility test methods: fastidious bacteria. *Manual of clinical microbiology*, 1314-1341.

Ioachim, E., & Hanan, G.S. (2005). Spectroscopy and electrochemistry of new 6,6′-disubstituted-4,4′-bi-pyrimidine molybdenum(0) and tungsten(0) tetracarbonyl complexes. *Canadian Journal of Chemistry. 83, 1114-1119.*

Ismail, B. A., Abd El-Wahab, Z. H., Ali, O. A., & Nassar, D. A. (2023). Synthesis, structural characterization, and antimicrobial evaluation of new mononuclear mixed ligand complexes based on furfural-type imine ligand, and 2, 2′-bipyridine. *Scientific Reports*, 13(1), 9196.

Jackson, M., & Mantsch, H. H. (2010). The use and misuse of FTIR spectroscopy in the determination of protein structure. *Critical Reviews in Biochemistry and Molecular Biology*, *45*(2), 141-151.

Jarvis, L.M. (2019). The new drugs of 2019. *Chemical & Engineering News.* [online]. Available at: cen.acs.org/pharmaceuticals/drug-development/new-drugs-2019/98/i3.

Jickells, T. D., & Moore, C. M. (2015). The importance of atmospheric deposition for ocean productivity. *Annual Review of Ecology, Evolution, and Systematics*, *46*, 481-501.

Jones, K., Brown, S., & Miller, D. (2019). Silver-containing hydrogels for wound healing applications. *Journal of Wound Care*, *28*(6), 332–341.

Jorgensen, J. H., & Ferraro, M. J. (2009). Antimicrobial susceptibility testing: a review of general principles and contemporary practices. *Clinical Infectious Diseases*, *49*(11), 1749–1755. https://doi.org/10.1086/64795

Jorgensen, J. H., & Turnidge, J. D. (2015). Susceptibility test methods: dilution and disk diffusion methods. *Manual of clinical microbiology*, 1253-1273.

Keiser, J., & Utzinger, J. (2010). The drugs we have and the drugs we need against major helminth infections. *Advances in parasitology*, *73*, 197-230.

Kendre, B. V., Landge, M. G., & Bhusare, S. R. (2019). Synthesis and biological evaluation of some novel pyrazole, isoxazole, benzoxazepine, benzothiazepine and benzodiazepine derivatives bearing an aryl sulfonate moiety as antimicrobial and anti-inflammatory agents. *Arabian Journal of Chemistry*, *12*(8), 2091-2097.

Khalid, S. E. H. E. R., Sumrra, S. H., & Chohan, Z. H. (2020). Isatin endowed metal chelates as antibacterial and antifungal agents. *Sains Malays*, *49*(8), 1891-1904.

Koske, M. C. (2018). *Synthesis, characterization, electrochemical properties of half-sandwich n, n'-bidentate ruthenium (ii) complexes and their antimicrobial activity* (Doctoral dissertation, Egerton University).

Kremer, E., Facchin, G., Estévez, E., Alborés, P., Baran, E. J., Ellena, J., & Torre, M. H. (2006). Copper complexes with heterocyclic sulfonamides: Synthesis, spectroscopic characterization, microbiological and SOD-like activities: Crystal structure of [Cu (sulfisoxazole) 2 (H2O) 4]· 2H2O. *Journal of Inorganic Biochemistry*, *100*(7), 1167-1175.

Kruk, J., & Duchnowicz, P. (2019). Copper chelation in neurodegenerative diseases. *Advances in Experimental Medicine and Biology, 1178, 85-108.*

Kumar, M. &. (2022). Pyrazole and its derivatives: An excellent n-hetrocycle with wide range of biological applications. *Oriental Journal of Chemistry*, 38(3), 568.

Kupče, Ē., & Freeman, R. (2007). Cryoprobes: Sensitivity and cryogenics. *Progress in Nuclear Magnetic Resonance Spectroscopy*, *51*(1), 1-26.

Lee, C., Kim, D., & Park, S. (2021). Silver nanocomposites for diagnostic imaging and photothermal therapy of cancer. *Nano Research*, *14*(2), 425–439.

Lemire, J. A., Harrison, J. J., & Turner, R. J. (2013). Antimicrobial activity of metals: mechanisms, molecular targets and applications. *Nature Reviews Microbiology*, *11*(6), 371-384.

Li, S., Chen, H., Yang, M., Ning, X., Zheng, Y., Ye, R., & Zhao, Q. (2019). Ruthenium(II) polypyridyl complexes as photosensitizers for photodynamic therapy: Advances and perspectives. *European Journal of Medicinal Chemistry*, 183, 111702. https://doi.org/10.1016/j.ejmech.2019.111702

Li, Z., Wang, C., Wang, Z., & Xu, J. (2021). Antibacterial mechanisms and applications of copper nanoparticles. *Frontiers in Microbiology, 12, 706336.*

Liu, H., & Zhang, X. (2017). Recent advances in mass spectrometry-based proteomics for protein profiling and characterization. *Scientia Sinica Chimica*, *47*(11), 1597–1610.

Livermore, D. M., Warner, M., & Mushtaq, S. (2021). Activity of temocillin against Enterobacterales with extended-spectrum β-lactamases: maintaining the threat of a largely forgotten antimicrobial agent. *The Journal of Antimicrobial Chemotherapy, 76*(1), 26–30.

Logan, L. K., & Weinstein, R. A. (2017). The epidemiology of carbapenem-resistant Enterobacteriaceae: the impact and evolution of a global menace. *The Journal of Infectious Diseases, 215*(Suppl_1), S28–S36.

Maares, M., & Haase, H. (2016). Zinc and immunity: An essential interrelation. *Archives of Biochemistry and Biophysics, 611, 58-65.*

Macomber, L., & Imlay, J. A. (2009). The iron-sulfur clusters of dehydratases are primary intracellular targets of copper toxicity. *Proceedings of the National Academy of Sciences, 106*(20), 8344-8349.

Makvana, S. & Krilov, L. R. (2015). *Escherichia coli* Infections. *Pediatrics in Review* 67(36), 167-176

Malladi, S., Isloor, A. M., Peethambar, S. K., & Fun, H. K. (2012). Synthesis of new 3-aryl-4-(3-aryl-4,5-dihydro-1H-pyrazol-5-yl)-1-phenyl-1H-pyrazole derivatives as potential antimicrobial agents. *Medicinal Chemistry Research, 22(6), 2654–2664.*

Mambanda, A., Ongoma, P., Gichumbi, J., Omondi, R. O., Hunter, L. A., & Kanyora, A. K. (2022). Crystal structures of half-sandwich Ru (II) complexes,[(η6-p-Cymene)(3-chloro-6-(1 H-pyrazol-1-yl) pyridazine) Ru (X)] BF4,(X= Cl, Br, I). *Molbank*, *2022*(4), M1477.

Mapari, A. K., & Mangaonkar, K. V. (2011). Synthesis, characterization and antimicrobial activity of mixed Schiff base ligand complexes of transition metal (II) ions. *International Journal of ChemTech Research*, *3*(1), 477-482.

Maret, W. (2019). Zinc biochemistry: From a single zinc enzyme to a key element of life. *Advances in Nutrition, 10(1), 112-139.*

Matar, S. A., Talib, W. H., Mustafa, M. S., Mubarak, M. S., & AlDamen, M. A. (2015). Synthesis, characterization, and antimicrobial activity of Schiff bases derived from benzaldehydes and 3,3′-diaminodipropylamine. *Arabian Journal of Chemistry*, *8*(6), 850-857.

Matsinha, L. C., Malatji, P., Hutton, A. T., Venter, G. A., Mapolie, S. F., & Smith, G. S. (2013). Water- Soluble Half- Sandwich RuII–Arene Complexes: Synthesis, Structure, Electrochemistry, DFT Studies, and Aqueous Phase Hydroformylation of 1- Octene. *European journal of inorganic chemistry*, *2013*(24), 4318-4328.

Mavrova, A. T., Yancheva, D. Y., & Kondratenko, R. M. (2010). Antimicrobial activity of some new 1,2,4-triazole and pyridazine derivatives. *European Journal of Medicinal Chemistry*, 45(5), 1906-1911.

Mc Crudden, D. (2008). Synthesis and characterisation of some osmium and ruthenium complexes and the application of Os (bpy) 2-(pyridine-4-COOH)-CI in an electrochemical DNA biosensor.

McCleverty, J.A & Meyer, T. J. (2004). Comprehensive coordination chemistry II*: Elsevier Ltd.*

Milani, M. (2021). Zinc supplementation for the prevention of acute respiratory tract infection in adults: A systematic review and meta-analysis of randomized controlled trials. *Journal of Infection, 83(1), 1-9.*

Mohan, C., Kumar, V., Kumari, N., Kumari, S., Yadav, J., Gandass, T., Yadav S. (2020). Synthesis, characterization, and antibacterial activity of semicarbazide-based Schiff bases and their Pb(II), Zr(IV), and U(VI) complexes. *Advanced Journal of Chemistry-Section B.; 2:187*–196.

Montaser, A. (2018). *Inductively coupled plasma mass spectrometry*. Wiley.

Monteiro, D.R., Arias, L.S., Fernandes, R.A., Deszo da Silva, L.F., de Castilho, M.O.V.F., da Rosa, T.O., Vieira, A.P.M., Straioto, F.G., Barbosa, D.B. & Delbem, A.C.B (2010). Antifungal activity of tyrosol and farnesol used in combination against Candida species in the planktonic state or forming biofilms. *Journal of Applied Microbiology 19*(4), 3201-3209

Mulani, F. A., Leekha, A., & Sood, S. (2019). Copper-based antimicrobial strategies and medical applications. *Applied Microbiology and Biotechnology*, 103(11), 4275-4289.

Müller, R. H., Mäder, K., & Gohla, S. (2000). Solid lipid nanoparticles (SLN) for controlled drug delivery–a review of the state of the art. *European journal of pharmaceutics and biopharmaceutics*, *50*(1), 161-177.

Muñoz, S., Josefina, P., García-Antón, J., Xavier, S., Font-Bardia, M. & Josep, R. (2009). Cleavage of NpzCH2 -OP and unexpected formation of bis(3,5dimethyl-1H-pyrazol-1-yl)methane (dmbpm): X-ray crystal structure of [$PdCl_2$(dmbpm)], *Journal of Coordination Chemistry,* 62:24, 3940-3950.

Murcia, R. A., Leal, S. M., Roa, M. V., Nagles, E., Muñoz-Castro, A., & Hurtado, J. J. (2018). Development of antibacterial and antifungal triazole chromium (III) and cobalt (II) complexes: synthesis and biological activity evaluations. *Molecules*, *23*(8), 2013.

Murray, C. J., Ikuta, K. S., Sharara, F., Swetschinski, L., Robles Aguilar, G., & Gray, A. (2022). Global burden of bacterial antimicrobial resistance in 2019: a systematic analysis. *The Lancet, 399*(10334), 629–655.

Murray, P. R., Baron, E. J., Pfaller, M.A. Tenover, F. C. & Yolke, R. H. (1995). Antimicrobial screening of suspected compounds using the disc-diffusion method. *Manual of Clinical Microbiology 43*(7), 3497-3499

Nakamoto K. (2009). *Infrared and Raman spectra of inorganic and coordination compounds, part B: applications in coordination, organometallic, and bioinorganic chemistry*.John Wiley & Sons.

Nandanwar, S. K., & Kim, H. J. (2019). Anticancer and antibacterial activity of transition metal complexes. *Chemistry Select*, *4*(5), 1706-1721.

Nandiyanto, D., A., B., Oktiani, R. & Ragadhita, R. (2019). How to read and interpret FTIR spectroscope of organic material. *Indonesian Journal of Science & Technology*. 4(1) 97-118.

Navale, A. S., Kawle, A. P., Park, J., Shin, H. S., & Lokhande, A. B. (2021). Ruthenium(II) complexes bearing a pyridine Schiff base Ligand: Synthesis, characterization, antimicrobial and cytotoxic activity. *Journal of Cluster Science,* 32(6), 1429–1442.

Navale, G., Singh, S., Agrawal, S., Ghosh, C., Roy Choudhury, A., Roy, P., Sarkar, D., & Ghosh, K. (2022). DNA binding, antitubercular, antibacterial and anticancer studies of newly designed piano-stool ruthenium(II) complexes. *Dalton Transactions, 51*(44), 16371–16382.

Nieuwenhuijse, B., & Reedijk, J. (1973). Jahn-teller distortions in copper(II) complexes as determined from ESR powder spectra. *Chemical Physics Letters*, *22*(1), 201-203.

Nikolic, P., & Mudgil, P. (2023). The cell wall, cell membrane and virulence factors of Staphylococcus aureus and their role in antibiotic resistance. *Microorganisms,* 11(2), 259.

Nisbet, M. L., Hiralal, E., & Poeppelmeier, K. R. (2021). Crystal structures of three copper (II)–2, 2′-bipyridine (bpy) compounds,$[Cu(bpy)_2(H_2O)][SiF_6]\cdot 4H_2O$,$[Cu(bpy)_2(TaF_6)_2]$ and $[Cu(bpy)_3][TaF_6]_2$ and a related coordination polymer,$[Cu(bpy)(H_2O)2SnF_6]$ n. *Acta Crystallographica Section E: Crystallographic Communications*, *77*(2), 158-164.

Ommenya, F. K., Nyawade, E. A., Andala, D. M., & Kinyua, J. (2021). Synthesis, Characterization and Antibacterial Activity of Schiff Base, 4- Chloro- 2- {(E)-[(4- Fluorophenyl) imino] methyl} phenol Metal (II) Complexes. *Journal of Chemistry*, *2020*(1), 1745236.

Ouyang, G., Cai, X.-J., Chen, Z., Song, B.-A., Bhadury, P. S., Yang, S., … Zeng, S. (2008). Synthesis and antiviral activities of Pyrazole Derivatives Containing an Oxime Moiety. *Journal of Agricultural and Food Chemistry, 56(21), 10160–10167.*

Paira, M. K., Dinda, J., Lu, T.-H., Paital, A. R., & Sinha, C. (2007). Zn(II), Cd(II) and Hg(II) complexes of 8-aminoquinoline. *Polyhedron, 26(15), 4131–4140.*

Palmer, A. G. (2014). NMR characterization of the dynamics of biomacromolecules. *Chemical Reviews, 114*(9), 4537-4568.

Pan (2021). Zinc-based coordination compounds: Design strategies and therapeutic applications. *Coordination Chemistry Reviews, 439, 213827.*

Pan, L., Li, X., Gong, C., Jin, H., & Qin, B. (2016). Synthesis of N-substituted phthalimides and their antifungal activity against *Alternaria solani* and *Botrytis cinerea*. *Microbial pathogenesis*, *95*, 186-192.

Park, S., Kwon, O. H., Kim, S., Park, S., Choi, M. G., Cha, M., ... & Jang, D. J. (2005). Imidazole-based excited-state intramolecular proton-transfer materials: synthesis

and amplified spontaneous emission from a large single crystal. *Journal of the American Chemical Society, 127*(28), 10070-10074.

Pavlovich, M. J., & Szymanski, C. M. (2021). Applications of mass spectrometry for food science research and beyond, *Analytical Chemistry, 93*(16), 6219–6236.

Pervaiz, M., Riaz, A., Munir, A., Saeed, Z., Hussain, S., Rashid, A. & Adnan, A. (2020). Synthesis and characterization of sulfonamide metal complexes as antimicrobial agents. *Journal of Molecular Structure, 1202,* 127284.

Pervaiz, M., Sadiq, S., Sadiq, A., Younas, U., Ashraf, A., Saeed, Z. & Adnan, A. (2021). Azo-Schiff base derivatives of transition metal complexes as antimicrobial agents. *Coordination Chemistry Reviews, 447,* 214128.

Prayag, K. S. (2023). *Development and Evaluation of Quinapyramine Sulphate Loaded Lipid-Based Nanocarriers for the Treatment of Trypanosomiasis* (Doctoral dissertation, BITS Pilani, Pilani campus).

Rahimizadeh, M., Pordel, M., Bakavoli, M., Rezaeian, S., & Sadeghian. (2010). A. Synthesis and antibacterial activity of some new derivatives of pyrazole. *World Journal of Microbiology and Biotechnology*, 26, 317–321.

Rajee, A. O., Aliyu, A. A., Babamale, H. F., Lawal, A., Ayinla, S. O., Osunniran, W. A., & Obaleye, J. A. (2020). Preparation, characterization and antibacterial activity of Mn (II), Cu (II) and Zn (II) complexes of methionine and 2, 2-bipyridine co-ligand. *Journal of the Kenya Chemical Society*, 13, 16-21.

Ramalingam, V., Varunkumar, K., Ravikumar, V., & Rajaram, R. (2020). Copper nanomaterials for cancer therapy. *Journal of Drug Delivery Science and Technology*, 55, 101469.

Safaa, E.E., Abd, M., Dina, E.A., Eldin, H. & Elham, A.A. (2013). Synthesis, spectroscopic, cytotoxic aspects, and computational study of N-(pyridine-2ylmethylene) benzo [d] thiazol-2-amine Schiff base and some of its transition metal complexes. *Journal of Molecular Structure, 1048(1)487-499.*

Sallusto, F., Lanzavecchia, A., Araki, K., & Ahmed, R. (2019). From vaccines to memory and back. *Immunity, 50*(1), 45–63

Sanguinetti, M., Posteraro, B., Fiori, B., Ranno, S., Torelli, R., & Fadda, G. (2005). Mechanisms of azole resistance in clinical isolates of Candida glabrata collected during a hospital survey of antifungal resistance. *Antimicrobial agents and chemotherapy*, *49*(2), 668-679.

Saravanan, K., Elancheran, R., Divakar, S., Anand, S. A. A., Ramanathan, M., Kotoky, J. & Kabilan, S. (2017). Design, synthesis and biological evaluation of 2-(4-phenylthiazol-2-yl) isoindoline-1, 3-dione derivatives as anti-prostate cancer agents. *Bioorganic & Medicinal Chemistry Letters, 27*(5), 1199-1204.

Schneider, C., Bannwarth, W., & Schmittel, M. (2012). Coordination and functional properties of pyridazine derivatives. *Coordination Chemistry Reviews,* 256(15-16), 2075-2090.

Selvanthan, S. & Woi, P.M. (2021). Synthesis, characterization, and electrochemical studies of transition metal complexes containing 3,6-bis(3,5dimethylpyrazolyl) pyridazine ligand. *Malaysian Journal of Analytical Sciences, 25*(1) 138 – 152.

Shankar, P. R. (2016). Book review: Tackling drug-resistant infections globally. *Archives of Pharmacy Practice, 7*(3), 110-111.

Sharma, P., Kumar, S., Kumar, P., Kaushik, P., Kaushik, D., & Dhingra, Y. (2010). Synthesis and biological evaluation of some pyrazolylpyrazolines as anti-inflammatory–antimicrobial agents, *European Journal of Medical Chemistry*, 45, 2650–2655.

Shugar, A. N., & Mass, J. L. (2012). *Handheld XRF for art and archaeology*. Leuven University Press.

Shuker, S. B., Hajduk, P. J., Meadows, R. P., & Fesik, S. W. (2010). Discovering high-affinity ligands for proteins: SAR by NMR. *Science, 274*(5292), 1531-1534.

Smith, B. C. (2011). *Fundamentals of Fourier transform infrared spectroscopy*. CRC press.

Smith, G. S., & Snyder, R. L. (2015). Introduction to X-ray powder diffraction. *Journal of Chemical Education, 92*(2), 232–242.

Smith, J., Johnson, A., & Martinez, P. (2020). Antimicrobial activity of silver heterocyclic complexes. *Journal of Inorganic Biochemistry, 236,* 111954.

Smith, R. D., & Makarov, A. (2019). Orbitrap mass spectrometry: Instrumentation, ion motion and applications. *Mass Spectrometry Reviews, 38*(4-5), 289–306.

Smitten, K., Southam, H. M., Fairbanks, S., Graf, A., Chauvet, A., & Thomas, J. A. (2023). Clearing an ESKAPE pathogen in a model organism; a polypyridyl ruthenium(II) complex theranostic that treats a resistant Acinetobacter baumannii infection in Galleria mellonella. *Chemistry - A European Journal, 29*(14), e202203555.

Sovari, S. N., Vojnovic, S., Bogojevic, S. S., Crochet, A., Pavic, A., & Nikodinovic-Runic, J. (2020). Design, synthesis and in vivo evaluation of 3-arylcoumarin derivatives of rhenium(I) tricarbonyl complexes as potent antibacterial agents against methicillin-resistant Staphylococcus aureus (MRSA). *European Journal of Medicinal Chemistry, 205,* 112533.

Spellberg, B., Bartlett, J. G., & Gilbert, D. N. (2013). The future of antibiotics and resistance, *The New England Journal of Medicine, 368*(4), 299–302.

Stuart, B. H. (2004). *Infrared spectroscopy: Fundamentals and applications*. John Wiley & Sons.

Sun, Y., Dai, Y., Wang, X., Cheng, J., & Jia, W. (2016). Preparation, crystal structures and properties of half-sandwich ruthenium complexes containing salicylbenzoxazole ligands. *Journal of Coordination Chemistry,* 69 (1) 48- 56.

Sylvia, E., Kurth, Y., & Wolfgang, K. (1986). Correlation between solvatochromism and back-bonding in four isomeric (α-diimine) M(CO)4 complexes, M = Cr, Mo, W. *Journal of Organometallic Chemistry, 302(2), 211 – 215.*

Szewczuk, Z., Sowa-Kasprzak, K., & Lankoff, A. (2017). Zinc complexes offer a new strategy for influenza antiviral therapy. *ACS Infectious Diseases,* 3(4), 227-233.

Tacconelli, E., Cataldo, M. A., Dancer, S. J., De Angelis, G., Falcone, M., Frank, U., Kahlmeter, G., Pan, A., Petrosillo, N., Rodríguez-Baño, J., Singh, N., Venditti, M., Yokoe, D. S., & Cookson, B. (2018). ESCMID guidelines for the management of the infection control measures to reduce transmission of multidrug-resistant Gram-negative bacteria in hospitalized patients. *Clinical Microbiology and Infection, 20*(1), 1–55.

Takfaoui, A., Lakehal, I., Bouabdallah, I., Halaimia, F., Nacer, H., Hammouti, B., Touzani, R., (2014). Synthesis of bis(3,5-dimethyl-1H-pyrazol-1-yl) methane derivatives. *Journal of Materials and Environmental Science, 6* (8) 2129-2136.

Tardito, S., Bassanetti, I., Bignardi, C., Elviri, L., Tegoni, M., Mucchino, C., & Bruno, S. (2018). Copper-binding agents acting as copper ionophores lead to caspase inhibition and paraptotic cell death in human cancer cells. *Journal of the American Chemical Society, 140*(1), 342-351.

Tonglairoum, P., Ngawhirunpat, T., Rojanarata, T., Kaomongkolgit, R., & Opanasopit, P. (2014). Fast-acting clotrimazole composited PVP/HPβCD nanofibers for oral candidiasis application. *Pharmaceutical research, 31*, 1893-1906.

Trivedi, V., Chand, P., Srivastava, K., Puri, S. K., Maulik, P. R., & Bandyopadhyay, U. (2005). Clotrimazole inhibits hemoperoxidase of Plasmodium falciparum and induces oxidative stress: proposed antimalarial mechanism of clotrimazole. *Journal of Biological Chemistry*, *280*(50), 41129-41136.

Tuon, F. F., Suss, P. H., Telles, J. P., Dantas, L. R., Borges, N. H., & Ribeiro, V. S. (2023). Antimicrobial treatment of Staphylococcus aureus biofilms, *Antibiotics*, 12(1), 87.

Ude, Z., Kavanagh, K., Twamley, B., Pour, M., Gathergood, N., & Kellett, A. M. (2019). A new class of prophylactic metallo-antibiotic possessing potent anti-cancer and anti-microbial properties, D*alton Transactions, 48*(24), 8578–8593.

Valerio, C., Perillo, T., Brescia, L. & Russo, F. (2013). Antifungal agents in current pediatric practice, *Current Infectious Disease Reports 15 (1),* 278–287.

Vanić, Ž. & Škalko-Basnet, N. (2013). Nanopharmaceuticals for improved topical vaginal therapy, *European Journal of Pharmaceutical Sciences 50(1)* 29–41.

Vicente, D., Basterretxea M., de la Caba, I., Sancho, R., López-Olaizola, M., Cilla, G. (2019).Low antimicrobial resistance rates of Mycobacterium tuberculosis complex between 2000 and 2015 in Gipuzkoa, northern Spain, *Enfermedades Infecciosas y Microbiología Clínica*, 37 (9) 574–579

Vijesh, A. M., Isloor, A. M., Shetty, P., Sundershan, S., & Fun, H. K. (2013). New pyrazole derivatives containing 1,2,4-triazoles and benzoxazoles as potent antimicrobial and analgesic agents, *European Journal of Medicinal Chemistry, 62(1) 410–415.*

Vogel, A. I., Furniss, B. S., Hannaford, A. J., & Tatchell, A. R. (2010). *Vogel's textbook of practical organic chemistry*. Pearson Education.

Wang, L., Li, J., Wang, C., & Yu, Y. (2020). Recent advances in the development of ruthenium complexes as anticancer agents, *Future Medicinal Chemistry*, 12(6), 519–539.

Wang, R., Wei, M., Wang, X., Chen, Y., Xiong, Y., Cheng, J., Tan, Y., Liao, X., & Wang, J. (2022). Synthesis of ruthenium polypyridine complexes with benzyloxyl groups and their antibacterial activities against Staphylococcus aureus, *Journal of Inorganic Biochemistry, 236,* 111954.

Weig, M. & Brown, A.J. (2007). Genomics and the development of new diagnostics and anti-Candida drugs, *Trends in Microbiology 15,* 310–31.

White, N. J. (2018). Tafenoquine—A radical improvement? *The New England Journal of Medicine, 379*(14), 1381–1383.

Willard, H. H., Merritt, J. L., Dean, J. A., & Settle, Jr, F A. (1988). *Instrumental methods of analysis, 7th edition*. United States.

Zaidan, M.R.S. Noor Rain, A., Badrul, A.R., Adlin, A., Norazah, A. & Zakiah, I. (2006). In vitro screening of five local medicinal plants for antibacterial activity using disc diffusion method, *Tropical Biomedicine, 22(2), 165–170.*

Zhou, G., Wang, Q., Wang, Y., Wen, X., Peng, H., Peng, R., & Li, L. (2023). Outer membrane porins contribute to antimicrobial resistance in gram-negative bacteria, *Microorganisms*, 11(7), 1690.

Zhou, J., Hartwig, J. F., & Wolfe, J. P. (2014). Highly active palladium catalysts for cross-coupling reactions, *Journal of the American Chemical Society*, 136(44), 15469-15473.

APPENDICES

APPENDIX 1: UV/VIS spectrum of L1

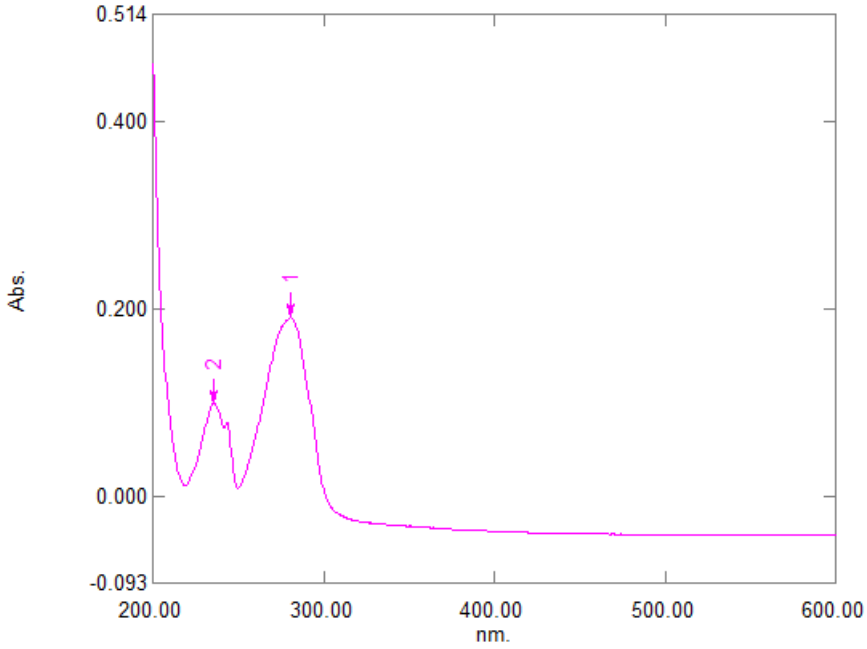

APPENDIX 2: UV/VIS spectrum of L2

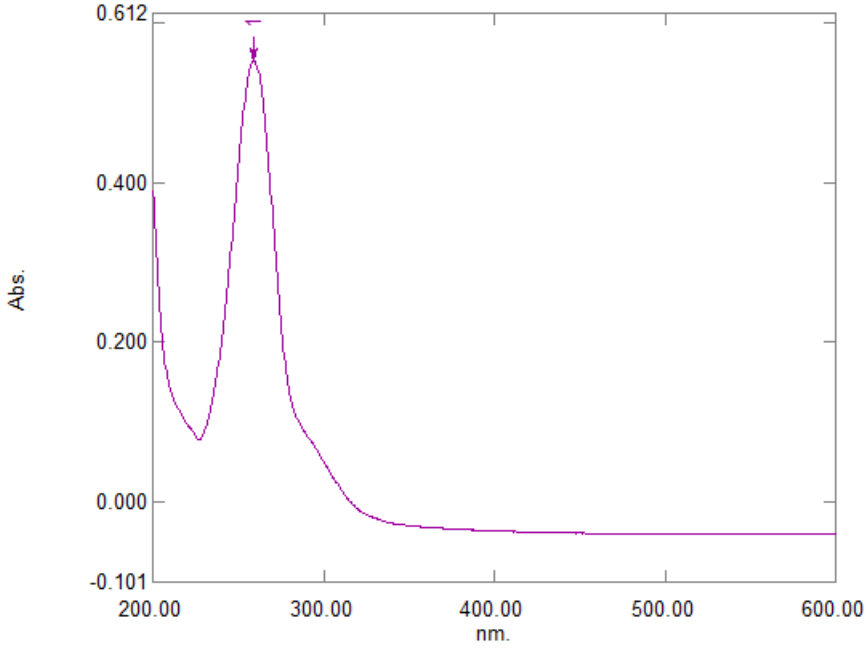

APPENDIX 3: UV/VIS spectrum of L3

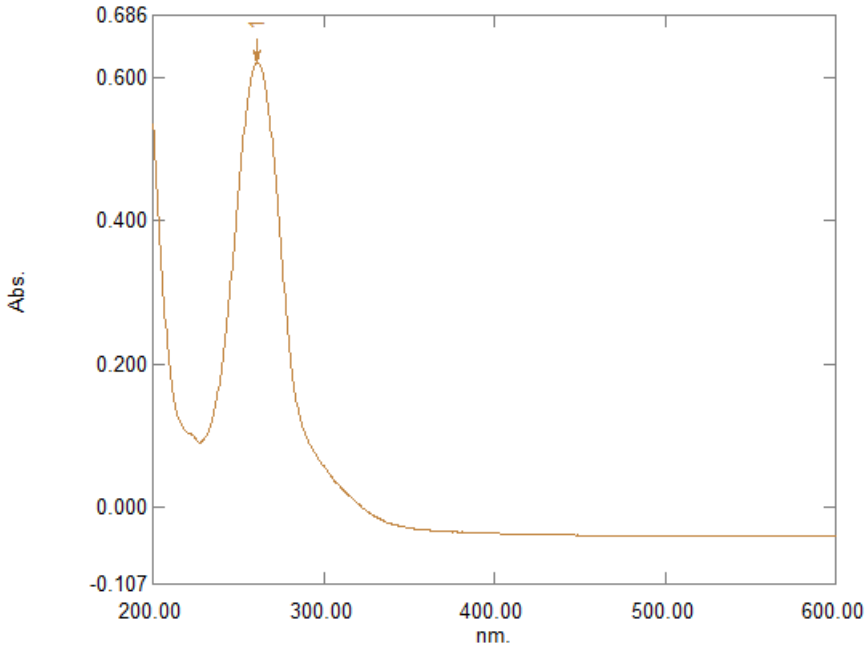

APPENDIX 4: UV/VIS spectrum of ZnL1

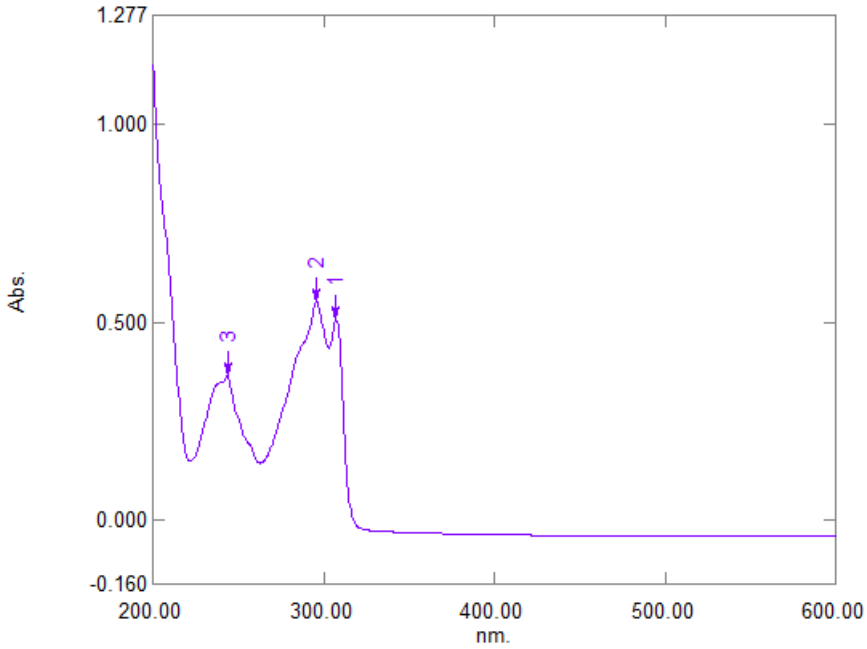

APPENDIX 5: UV/VIS spectrum of ZnL2

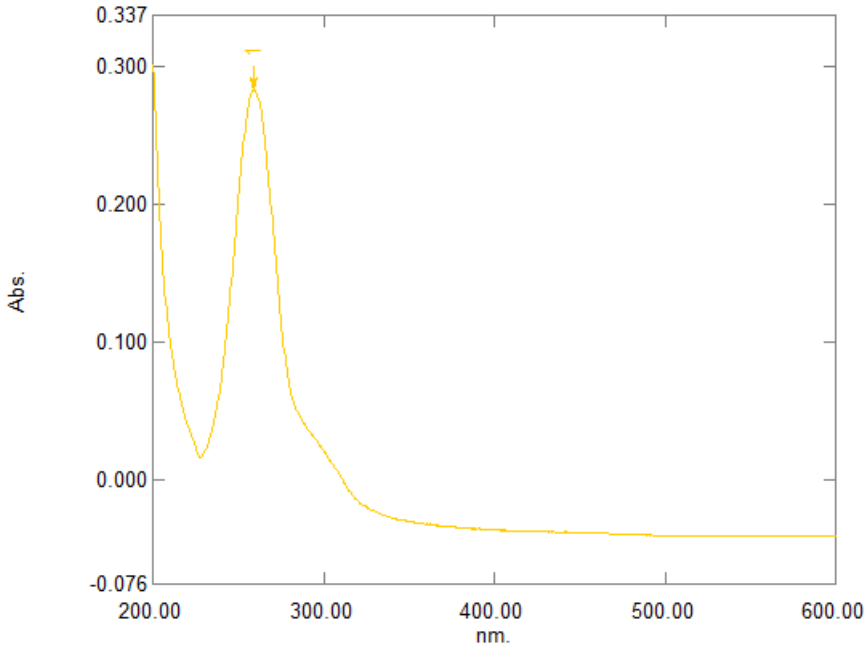

APPENDIX 6: UV/VIS spectrum of ZnL3

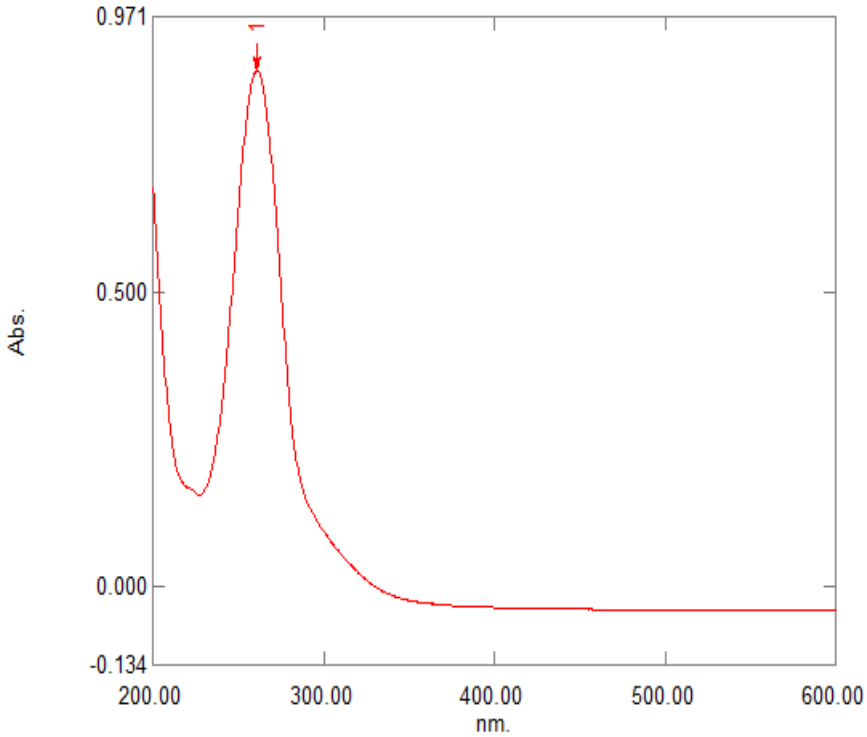

APPENDIX 7: UV/VIS spectrum of CuL1

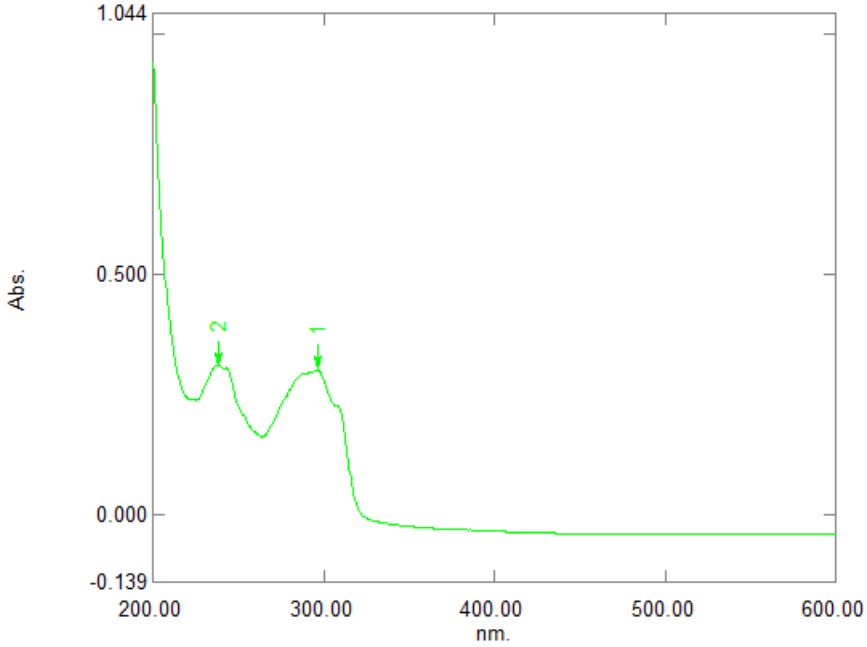

APPENDIX 8: UV/VIS spectrum of CuL2

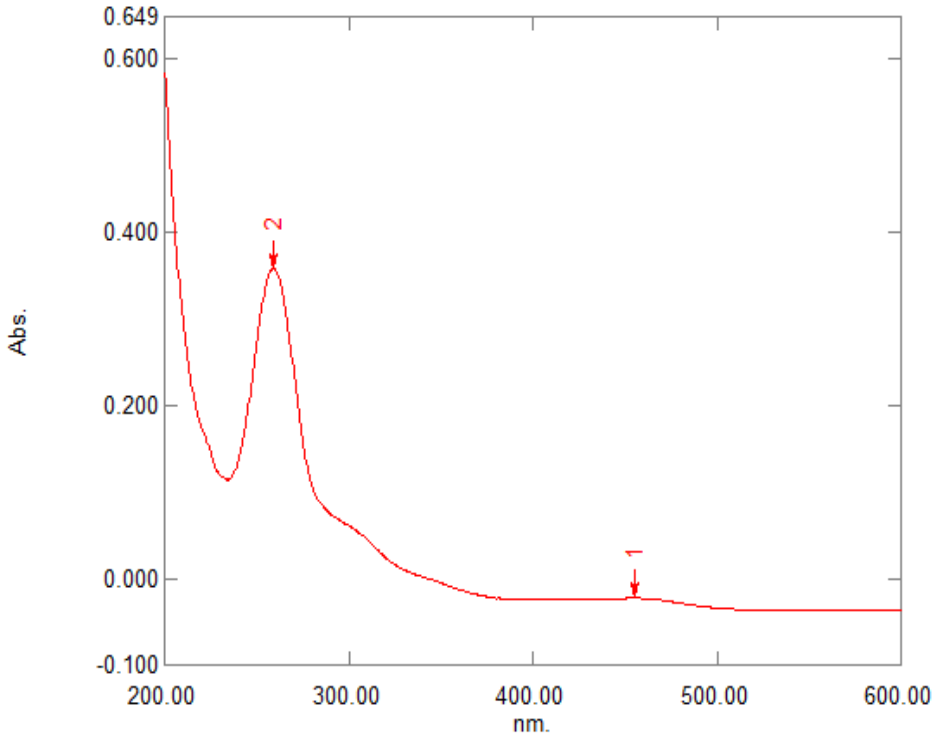

APPENDIX 9: UV/VIS spectrum of CuL3

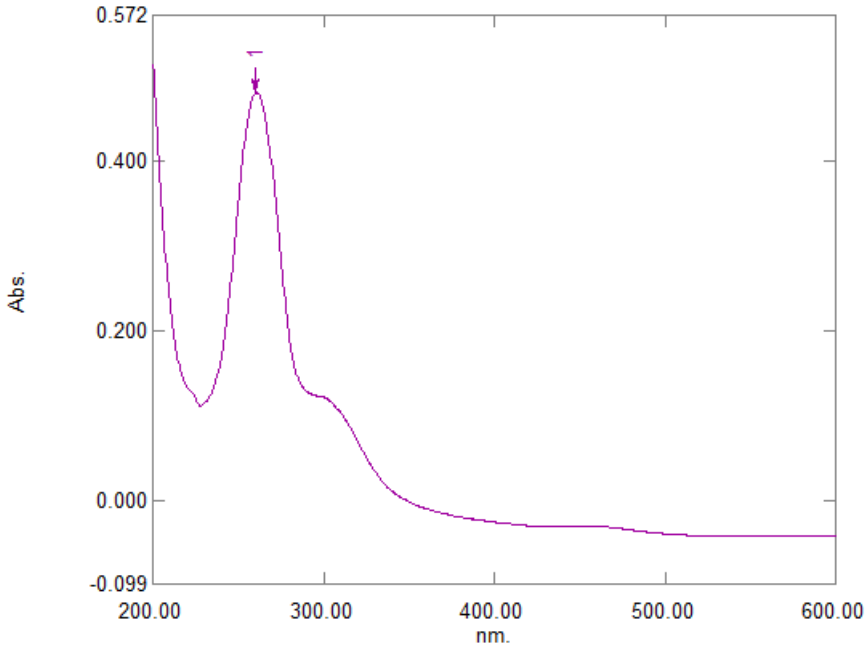

APPENDIX 10: FTIR spectrum of L1

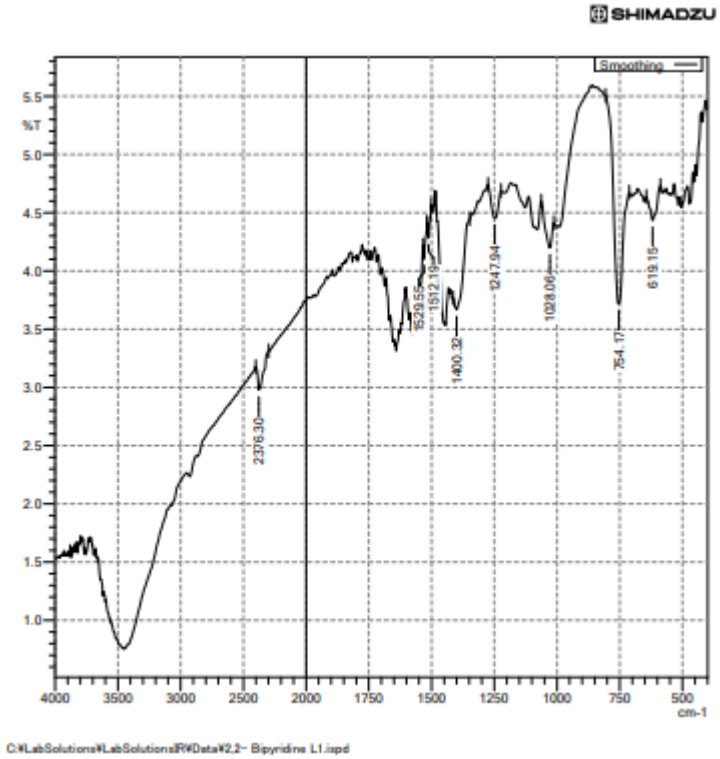

APPENDIX 11: FTIR spectrum of L2

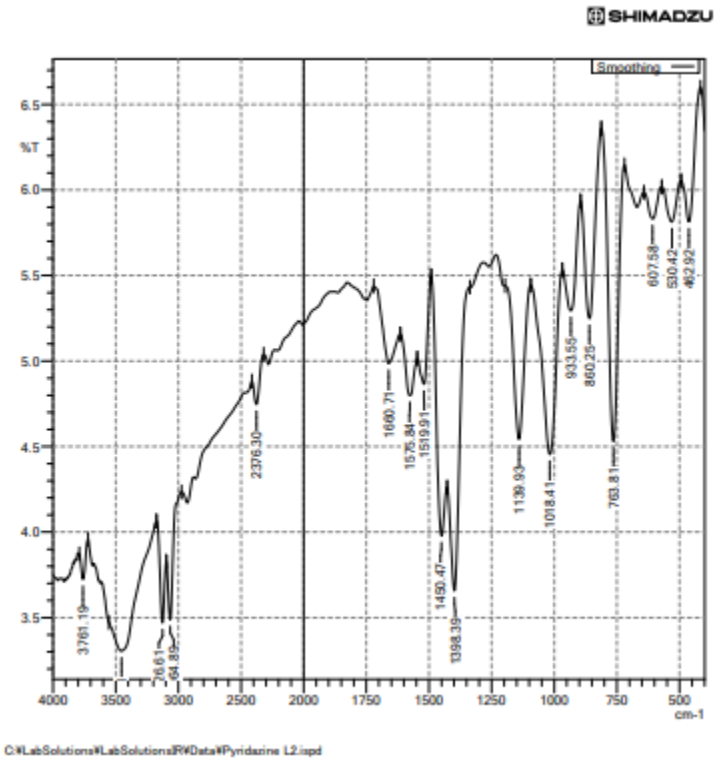

APPENDIX 12: FTIR spectrum of L3

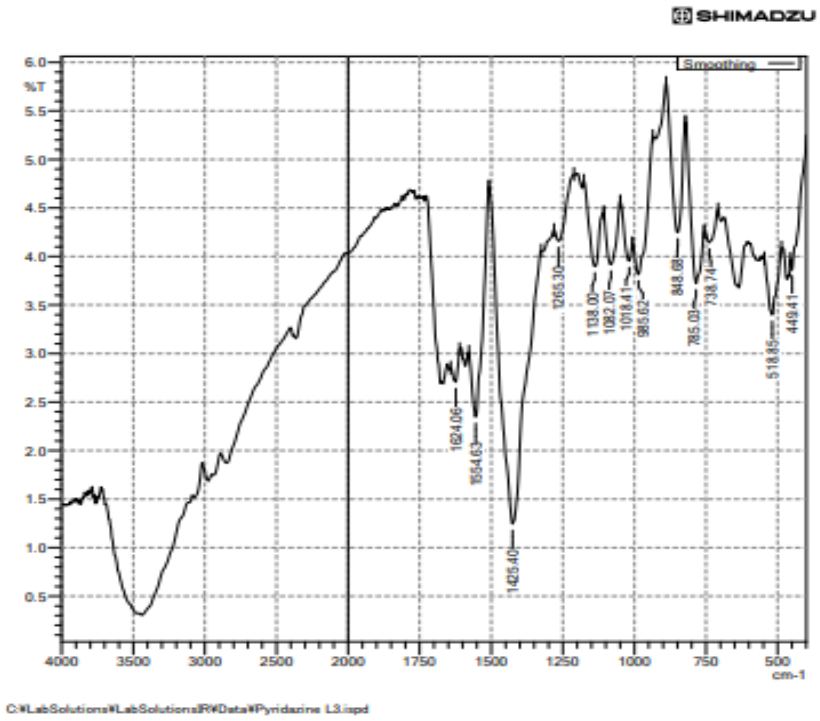

APPENDIX 13: FTIR spectrum of CuL1

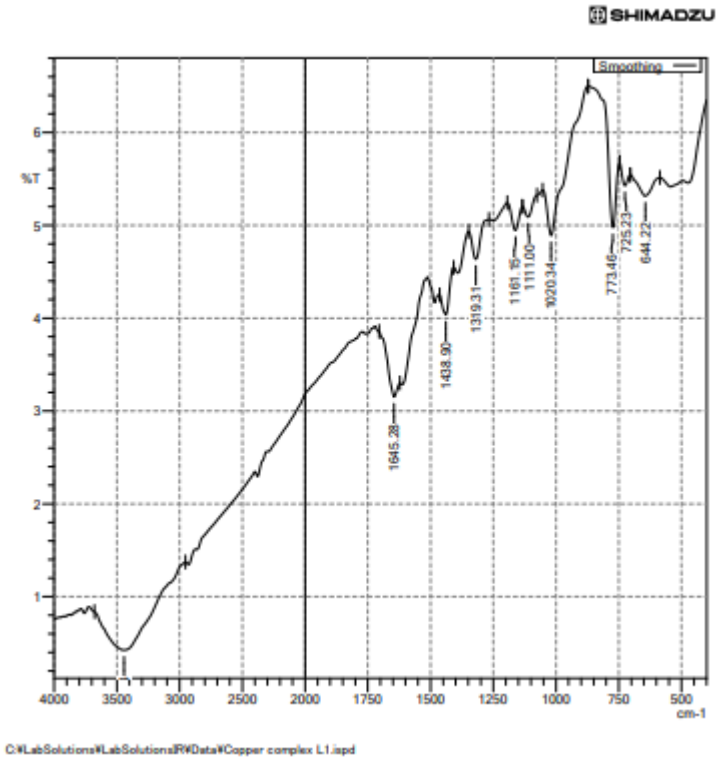

APPENDIX 14: FTIR spectrum of CuL2

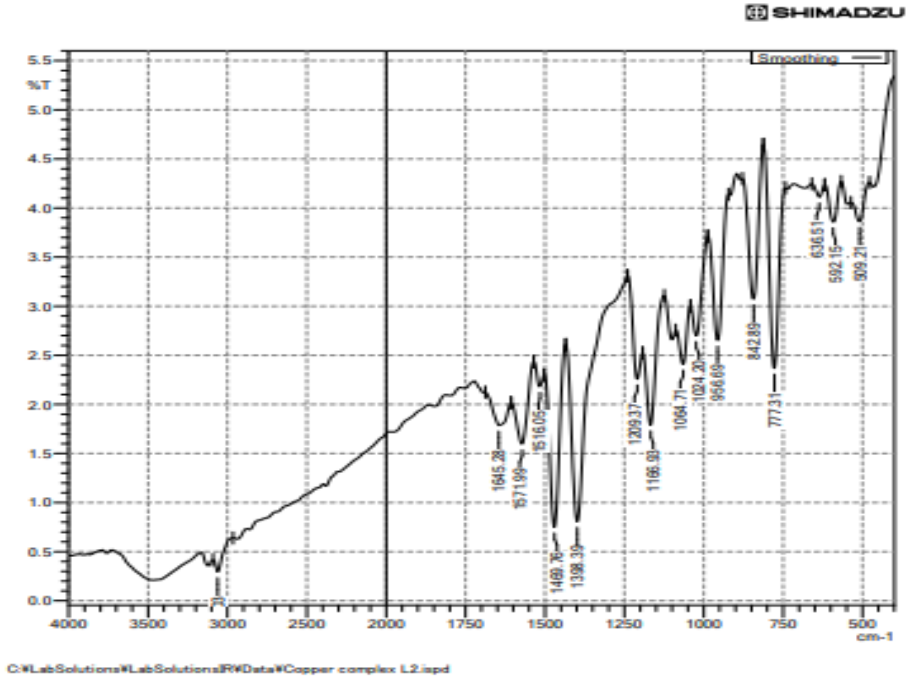

APPENDIX 15: FTIR spectrum of CuL3

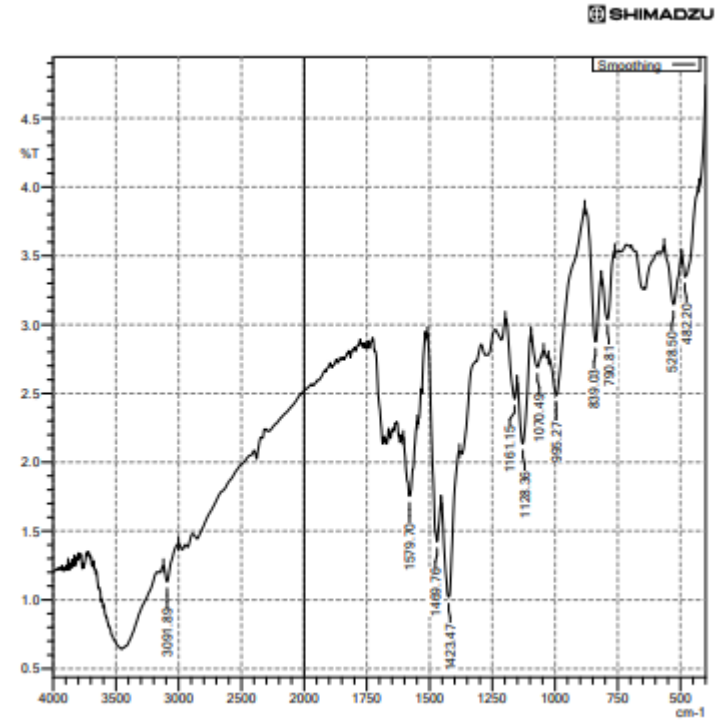

APPENDIX 16: FTIR spectrum of ZnL1

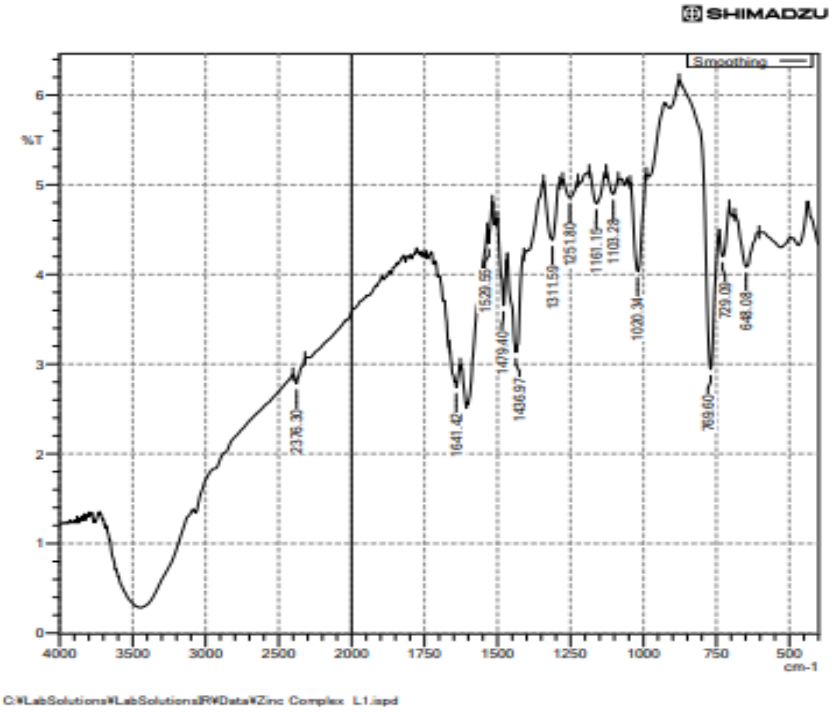

APPENDIX 17: FTIR spectrum of ZnL2

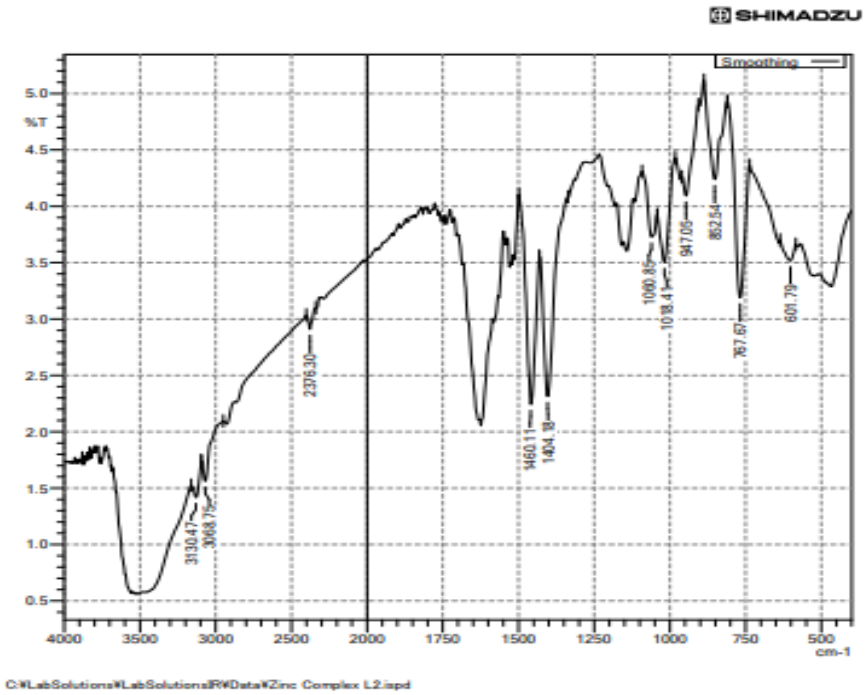

APPENDIX 18: FTIR spectrum of ZnL3

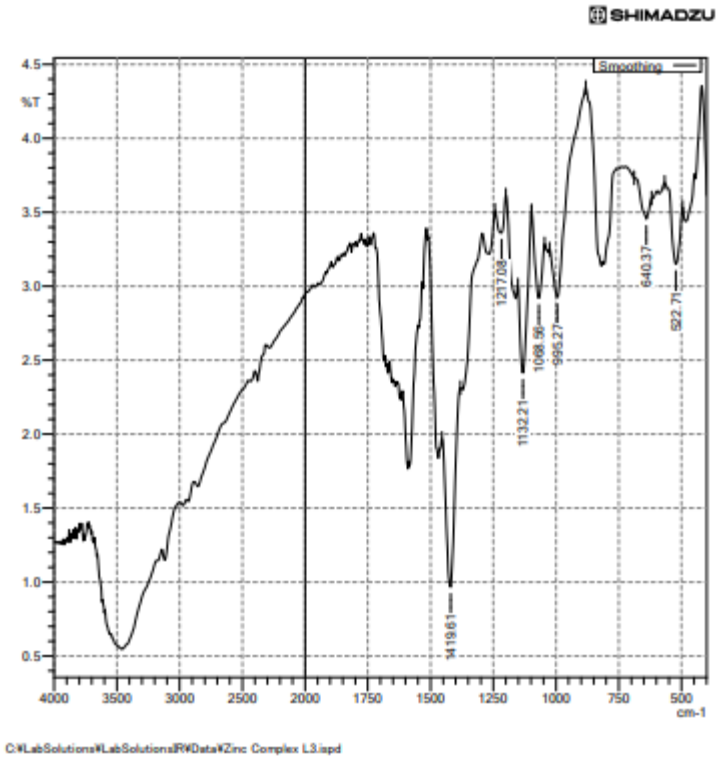

APPENDIX 19: ^{1}H-NMR spectrum of CuL1

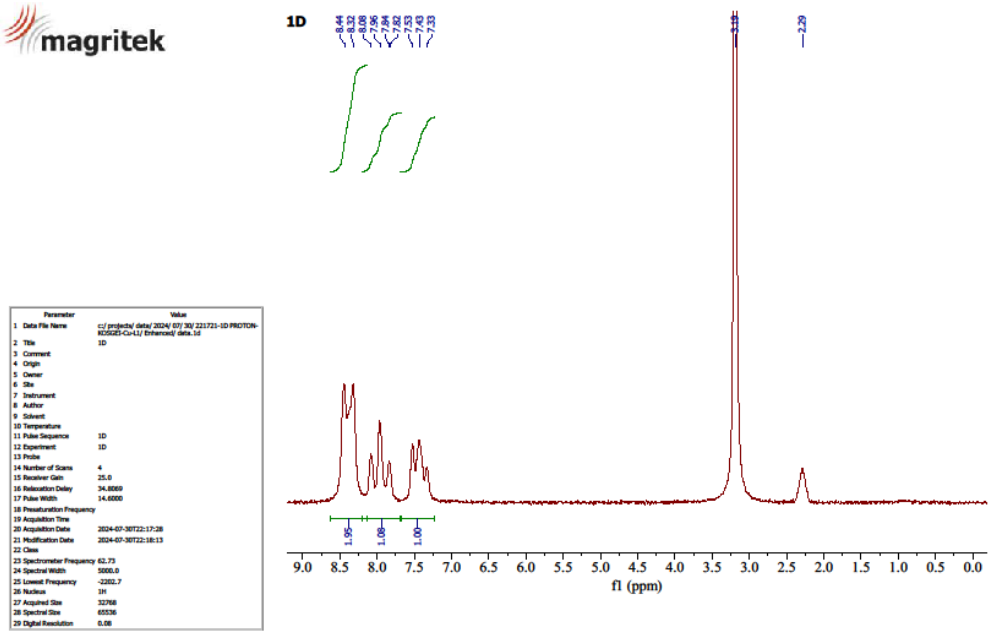

	Parameter	Value
1	Data File Name	c:/ projects/ data/ 2024/ 07/ 30/ 221721-1D PROTON-KDSGE5-Cu-L1/ Enhanced/ data.1d
2	Title	1D
3	Comment	
4	Origin	
5	Owner	
6	Site	
7	Instrument	
8	Author	
9	Solvent	
10	Temperature	
11	Pulse Sequence	1D
12	Experiment	1D
13	Probe	
14	Number of Scans	4
15	Receiver Gain	25.0
16	Relaxation Delay	34.8069
17	Pulse Width	14.6000
18	Presaturation Frequency	
19	Acquisition Time	
20	Acquisition Date	2024-07-30T22:17:28
21	Modification Date	2024-07-30T22:18:13
22	Class	
23	Spectrometer Frequency	62.73
24	Spectral Width	5000.0
25	Lowest Frequency	-2202.7
26	Nucleus	1H
27	Acquired Size	32768
28	Spectral Size	65536
29	Digital Resolution	0.08

APPENDIX 20: ^{1}H-NMR spectrum of CuL2

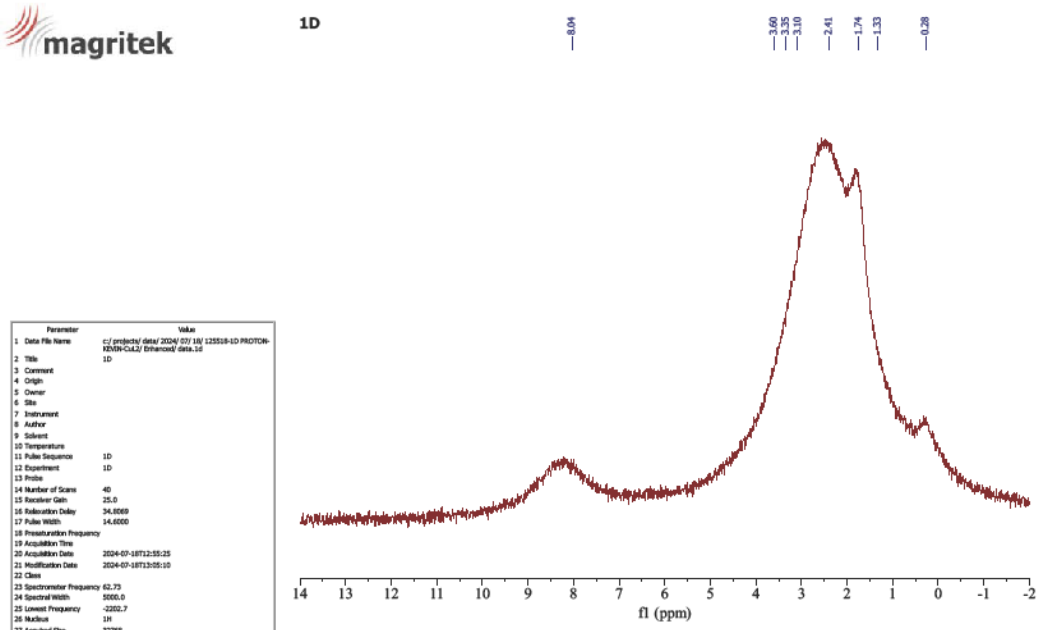

	Parameter	Value
1	Data File Name	c:/ projects/ data/ 2024/ 07/ 18/ 125518-1D PROTON-KEN5H-CuL2/ Enhanced/ data.1d
2	Title	1D
3	Comment	
4	Origin	
5	Owner	
6	Site	
7	Instrument	
8	Author	
9	Solvent	
10	Temperature	
11	Pulse Sequence	1D
12	Experiment	1D
13	Probe	
14	Number of Scans	40
15	Receiver Gain	25.0
16	Relaxation Delay	34.8069
17	Pulse Width	14.6000
18	Presaturation Frequency	
19	Acquisition Time	
20	Acquisition Date	2024-07-18T12:55:25
21	Modification Date	2024-07-18T13:05:10
22	Class	
23	Spectrometer Frequency	62.73
24	Spectral Width	5000.0
25	Lowest Frequency	-2202.7
26	Nucleus	1H
27	Acquired Size	32768
28	Spectral Size	65536
29	Digital Resolution	0.08

APPENDIX 21: ^{1}H-NMR spectrum of CuL3

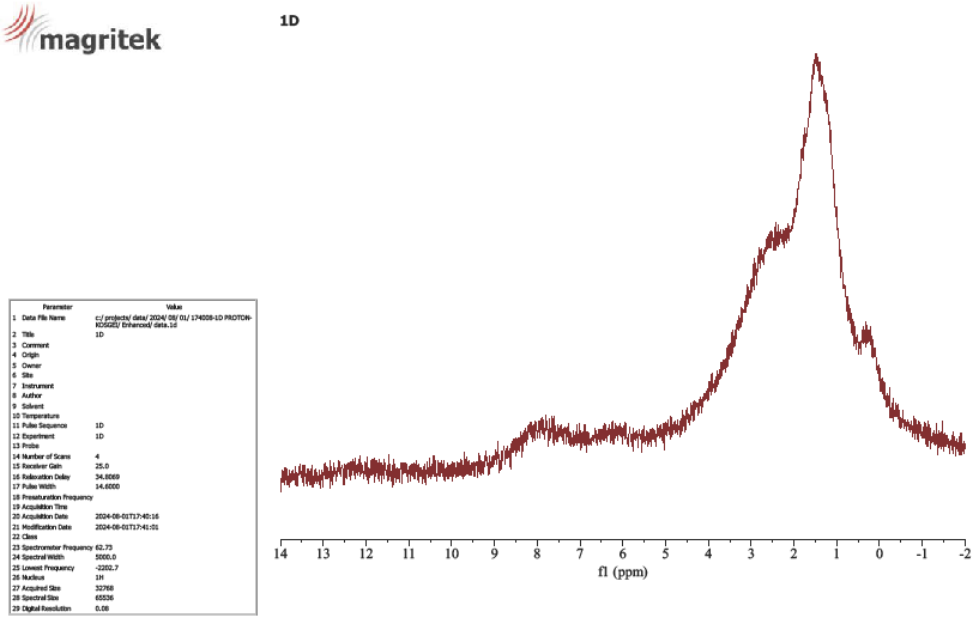

Parameter	Value
1 Data File Name	c:/ projects/ data/ 2024/ 08/ 01/ 174008-1D PROTON-KDSGE5/ Enhanced/ data.1d
2 Title	1D
3 Comment	
4 Origin	
5 Owner	
6 Site	
7 Instrument	
8 Author	
9 Solvent	
10 Temperature	
11 Pulse Sequence	1D
12 Experiment	1D
13 Probe	
14 Number of Scans	4
15 Receiver Gain	25.0
16 Relaxation Delay	34.8069
17 Pulse Width	14.6000
18 Presaturation Frequency	
19 Acquisition Time	
20 Acquisition Date	2024-08-01T17:40:16
21 Modification Date	2024-08-01T17:41:01
22 Class	
23 Spectrometer Frequency	62.73
24 Spectral Width	5000.0
25 Lowest Frequency	-2202.7
26 Nucleus	1H
27 Acquired Size	32768
28 Spectral Size	65536
29 Digital Resolution	0.08

APPENDIX 22: ^{1}H-NMR spectrum of ZnL1

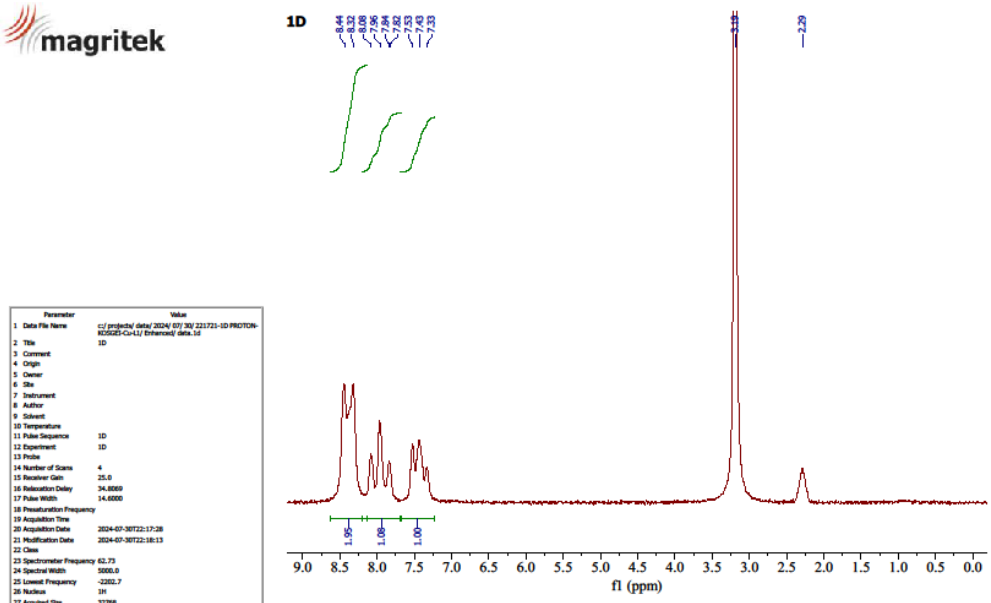

Parameter	Value
1 Data File Name	c:/ projects/ data/ 2024/ 07/ 30/ 221721-1D PROTON-KDSGE5-Cu-L1/ Enhanced/ data.1d
2 Title	1D
3 Comment	
4 Origin	
5 Owner	
6 Site	
7 Instrument	
8 Author	
9 Solvent	
10 Temperature	
11 Pulse Sequence	1D
12 Experiment	1D
13 Probe	
14 Number of Scans	4
15 Receiver Gain	25.0
16 Relaxation Delay	34.8069
17 Pulse Width	14.6000
18 Presaturation Frequency	
19 Acquisition Time	
20 Acquisition Date	2024-07-30T22:17:28
21 Modification Date	2024-07-30T22:18:13
22 Class	
23 Spectrometer Frequency	62.73
24 Spectral Width	5000.0
25 Lowest Frequency	-2202.7
26 Nucleus	1H
27 Acquired Size	32768
28 Spectral Size	65536
29 Digital Resolution	0.08

APPENDIX 23: ^{1}H-NMR spectrum of ZnL2

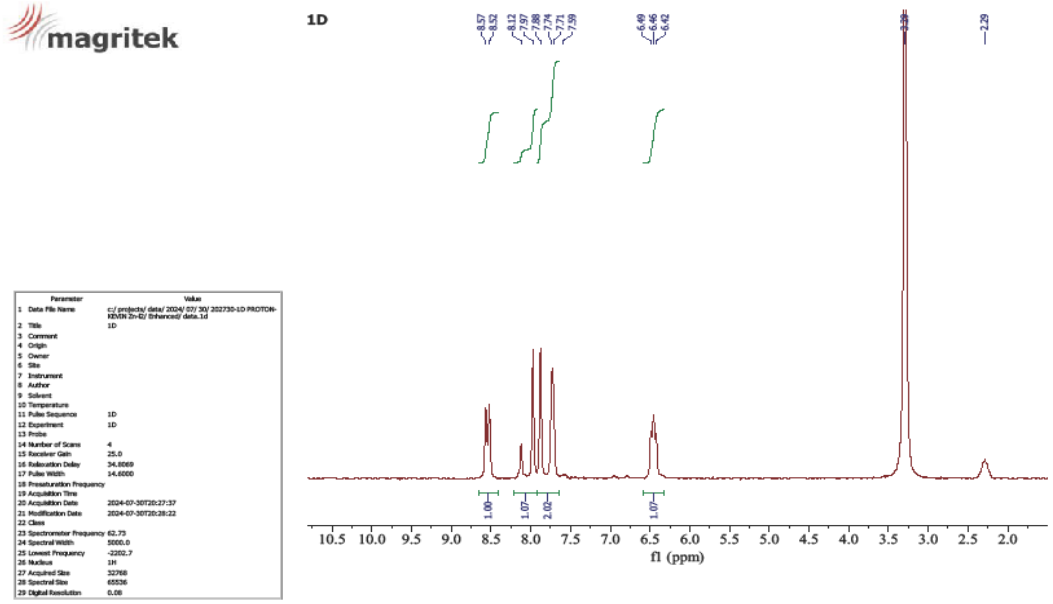

	Parameter	Value
1	Data File Name	c:/ projects/ data/ 2024/ 07/ 30/ 202730-1D PROTON-KEVIN Zn-E/ Enhanced/ data.1d
2	Title	1D
3	Comment	
4	Origin	
5	Owner	
6	Site	
7	Instrument	
8	Author	
9	Solvent	
10	Temperature	
11	Pulse Sequence	1D
12	Experiment	1D
13	Probe	
14	Number of Scans	4
15	Receiver Gain	25.0
16	Relaxation Delay	34.8069
17	Pulse Width	14.6000
18	Presaturation Frequency	
19	Acquisition Time	
20	Acquisition Date	2024-07-30T20:27:37
21	Modification Date	2024-07-30T20:28:22
22	Class	
23	Spectrometer Frequency	62.73
24	Spectral Width	5000.0
25	Lowest Frequency	-2202.7
26	Nucleus	1H
27	Acquired Size	32768
28	Spectral Size	65536
29	Digital Resolution	0.08

APPENDIX 24: ^{1}H-NMR spectrum of ZnL3

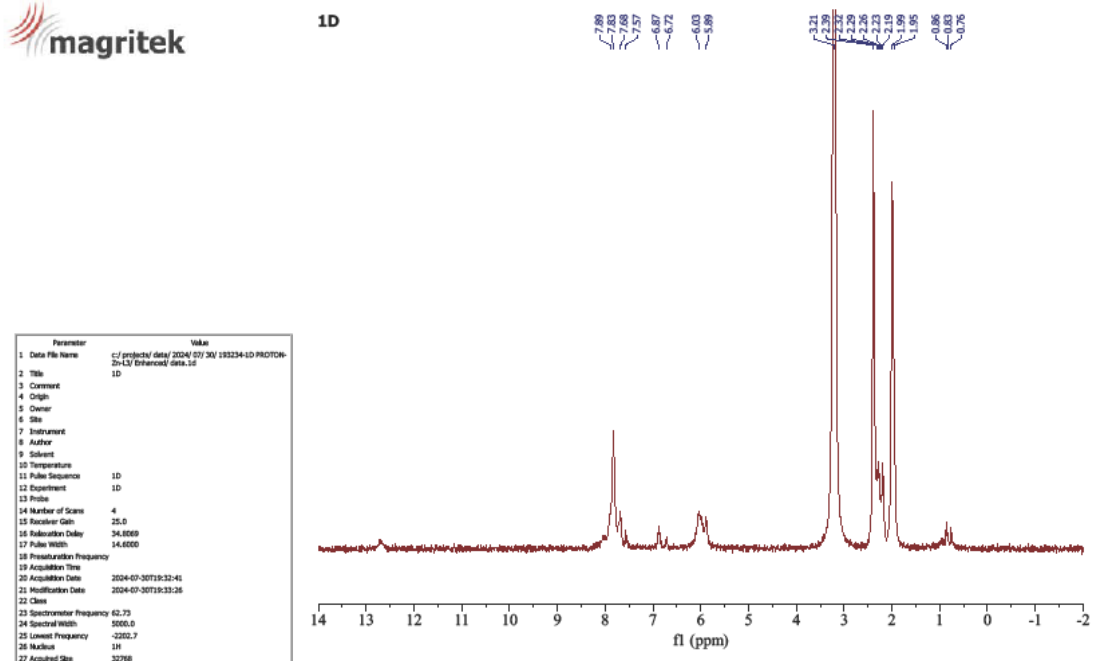

	Parameter	Value
1	Data File Name	c:/ projects/ data/ 2024/ 07/ 30/ 193234-1D PROTON-Zn-L3/ Enhanced/ data.1d
2	Title	1D
3	Comment	
4	Origin	
5	Owner	
6	Site	
7	Instrument	
8	Author	
9	Solvent	
10	Temperature	
11	Pulse Sequence	1D
12	Experiment	1D
13	Probe	
14	Number of Scans	4
15	Receiver Gain	25.0
16	Relaxation Delay	34.8069
17	Pulse Width	14.6000
18	Presaturation Frequency	
19	Acquisition Time	
20	Acquisition Date	2024-07-30T19:32:41
21	Modification Date	2024-07-30T19:33:26
22	Class	
23	Spectrometer Frequency	62.73
24	Spectral Width	5000.0
25	Lowest Frequency	-2202.7
26	Nucleus	1H
27	Acquired Size	32768
28	Spectral Size	65536
29	Digital Resolution	0.08

APPENDIX 25: Diameters of Inhibition in the Selected Microbial Strains

Compound		Diameter of inhibition (mm) in:								
	Concentration	Staphylococcus aureus			Escherichia coli			Candida albicans		
		R1	R2	R3	R1	R2	R3	R1	R2	R3
L1	400 µg/ml	11.2	11.5	10.9	-	-	-	11.4	11.8	11.8
	600 µg/ml	11.1	11.8	12.0	11.5	11.7	11.5	11.4	12.2	11.9
	800 µg/ml	11.4	11.8	12.0	12.2	12.4	12.0	12.5	12.7	12.8
	1000 µg/ml	13.7	14.1	14.0	13.5	13.8	13.9	13.3	13.1	13.4
L2	400 µg/ml	11.9	11.8	12.2	-	-	-	12.8	13.4	12.9
	600 µg/ml	12.4	12.1	12.5	11.0	11.8	12.1	13.3	12.7	13.5
	800 µg/ml	12.2	12.9	13.3	11.8	12.5	12.8	14.7	14.9	14.1
	1000 µg/ml	14.3	14.6	14.8	13.9	14.2	14.4	14.9	15.0	14.7
L3	400 µg/ml	14.4	13.8	14.1	13.0	13.7	13.9	14.8	15.1	14.9
	600 µg/ml	14.0	14.6	14.8	13.5	13.5	14.2	16.1	15.8	15.2
	800 µg/ml	14.9	15.7	15.9	14.3	14.6	14.5	17.1	16.8	16.5
	1000 µg/ml	16.6	16.2	16.1	15.1	15.4	15.5	16.8	17.4	17.2
CuL1	400 µg/ml	13.9	14.2	14.5	12.9	13.2	13.3	13.4	13.8	13.9
	600 µg/ml	14.1	14.9	15.1	13.5	13.7	13.5	13.4	14.1	13.9
	800 µg/ml	15.6	15.8	15.1	14.2	14.4	14.0	14.5	14.9	14.8
	1000 µg/ml	15.7	16.1	16.0	15.5	16.0	15.9	15.3	15.1	15.4
CuL2	400 µg/ml	15.9	15.8	16.2	12.8	12.5	13.1	16.8	17.4	16.9
	600 µg/ml	16.4	16.1	16.5	13.0	13.8	14.1	17.3	16.7	17.5
	800 µg/ml	16.5	16.9	17.1	13.8	14.5	14.8	18.7	18.9	18.1
	1000 µg/ml	18.5	18.6	18.9	14.9	14.2	14.4	18.9	19.0	19.2
CuL3	400 µg/ml	19.4	18.8	19.1	17.0	17.7	17.9	19.8	20.1	19.9
	600 µg/ml	19.0	19.6	19.8	17.9	17.5	18.2	20.1	19.8	19.2
	800 µg/ml	19.9	20.7	20.9	18.3	17.9	18.4	21.1	20.7	20.9
	1000 µg/ml	21.6	21.2	21.1	19.1	19.4	19.6	20.9	21.7	21.2
ZnL1	400 µg/ml	13.6	14.0	14.2	12.6	12.9	13.1	13.6	13.9	13.4
	600 µg/ml	14.2	14.8	15.3	13.7	13.9	13.5	13.7	14.1	13.8
	800 µg/ml	15.4	15.5	15.4	14.6	14.7	14.0	14.7	14.8	14.5
	1000 µg/ml	15.4	16.5	16.0	15.7	16.2	16.3	15.5	15.3	15.9
ZnL2	400 µg/ml	16.1	16.0	16.4	13.1	12.8	13.2	16.9	17.5	17.0
	600 µg/ml	16.7	16.4	16.6	13.3	13.5	14.6	17.5	16.9	17.2

		800 µg/ml	16.8	16.7	17.0	13.6	14.7	14.9	18.3	18.7	18.0
		1000 µg/ml	18.8	18.4	18.2	14.7	14.1	14.2	18.7	19.4	19.5
ZnL3		400 µg/ml	18.8	18.2	18.5	16.4	17.1	17.3	19.2	19.5	19.3
		600 µg/ml	19.5	20.1	20.3	18.4	18.0	18.7	20.6	20.3	19.7
		800 µg/ml	20.5	21.2	21.4	18.8	18.4	18.7	21.5	21.2	21.1
		1000 µg/ml	21.9	21.5	21.4	19.5	19.7	19.9	21.2	22.0	21.5
Standard (ampicillin)	**1**	400 µg/ml	25.4	25.0	25.1	23.1	23.0	23.4	-	-	-
		600 µg/ml	26.2	26.0	26.5	24.1	24.3	24.1	-	-	-
		800 µg/ml	26.6	26.9	26.9	24.3	24.8	24.8	-	-	-
		1000 µg/ml	27.4	27.9	27.9	25.4	25.9	25.1	-	-	-
Standard (fluconazole)	**2**	400 µg/ml	-	-	-	-	-	-	24.5	24.3	24.3
		600 µg/ml	-	-	-	-	-	-	24.6	24.8	24.0
		800 µg/ml	-	-	-	-	-	-	24.7	24.8	24.7
		1000 µg/ml	-	-	-	-	-	-	25.0	25.3	24.7
DMSO		400 µg/ml	0	0	0	0	0	0	0	0	0
		600 µg/ml	0	0	0	0	0	0	0	0	0
		800 µg/ml	0	0	0	0	0	0	0	0	0
		1000 µg/ml	0	0	0	0	0	0	0	0	0

APPENDIX 26: RESEARCH PERMIT

REPUBLIC OF KENYA

NATIONAL COMMISSION FOR SCIENCE,TECHNOLOGY & INNOVATION

Ref No: 208977

Date of Issue: 14/March/2024

RESEARCH LICENSE

This is to Certify that Mr.. KEVIN NYARANGO OTAO of Chuka University, has been licensed to conduct research as per the provision of the Science, Technology and Innovation Act, 2013 (Rev.2014) in Tharaka-Nithi on the topic: SYNTHESIS, CHARACTERIZATION AND ANTIMICROBIAL PROPERTIES OF HETEROCYCLIC N, N- BIDENTATE LIGANDS AND THEIR TRANSITION METAL (ii) COMPLEXES for the period ending : 14/March/2025.

License No: NACOSTI/P/24/33721

208977

Applicant Identification Number

Director General
NATIONAL COMMISSION FOR SCIENCE,TECHNOLOGY & INNOVATION

Verification QR Code

NOTE: This is a computer generated License. To verify the authenticity of this document, Scan the QR Code using QR scanner application.

See overleaf for conditions